

CFAR DETECTION IN K-DISTRIBUTED SEA CLUTTER

A THESIS SUBMITTED TO
THE GRADUATE SCHOOL OF NATURAL AND APPLIED SCIENCES
OF
MIDDLE EAST TECHNICAL UNIVERSITY

BY

AYŞİN ÇETİN

IN PARTIAL FULLFILLMENT OF THE REQUIREMENTS
FOR
THE DEGREE OF MASTER OF SCIENCE
IN
ELECTRICAL AND ELECTRONICS ENGINEERING

SEPTEMBER 2008

Approval of the thesis:

CFAR DETECTION IN K-DISTRIBUTED SEA CLUTTER

submitted by **AYŞİN ÇETİN** in partial fulfillment of the requirements for the degree of **Master of Science in Electrical and Electronics Engineering Department, Middle East Technical University** by,

Prof. Dr. Canan Özgen
Dean, Graduate School of **Natural and Applied Sciences**

Prof. Dr. İsmet Erkmn
Head of Department, **Electrical and Electronics Engineering**

Prof. Dr. Altuncan Hızal
Supervisor, **Electrical and Electronics Engineering Dept., METU**

Assoc. Prof. Dr. Şimşek Demir
Co-Supervisor, **Electrical and Electronics Engineering Dept., METU**

Examining Committee Members:

Prof. Dr. Gülbin Dural
Electrical and Electronics Engineering Dept.,
METU

Prof. Dr. Altuncan Hızal
Electrical and Electronics Engineering Dept.,
METU

Assoc. Prof. Dr. Şimşek Demir
Electrical and Electronics Engineering Dept.,
METU

Prof. Dr. Erdem Yazgan
Electrical and Electronics Engineering Dept., HU

Assist. Prof. Dr. Çağatay Candan
Electrical and Electronics Engineering Dept.,
METU

Date: (02.09.2008)

I hereby declare that all information in this document has been obtained and presented in accordance with academic rules and ethical conduct. I also declare that, as required by these rules and conduct, I have fully cited and referenced all material and results that are not original to this work.

Name, Last Name : Ayşin, Çetin

Signature :

ABSTRACT

CFAR DETECTION IN K-DISTRIBUTED SEA CLUTTER

Çetin, Ayşin

M. Sc., Department of Electrical and Electronics Engineering

Supervisor: Prof. Dr. Altunkan Hızal

Co-Supervisor: Assoc. Prof. Dr. Şimşek Demir

September 2008, 119 pages

Conventional fixed threshold detectors set a fixed threshold based on the overall statistical characteristics of the spatially uniform clutter over all ranges to give a specific probability of false alarm and detection. However, in radar applications clutter statistics are not known a priori. Constant False Alarm Rate (CFAR) techniques provide an adaptive threshold to estimate the clutter statistics and to distinguish targets from clutter. In Cell Averaging CFAR (CA-CFAR) the threshold is controlled by averaging the fixed size CFAR cells surrounding the cell under test.

In this thesis, radar detection of targets in sea clutter modelled by compound K-distribution is examined from a statistical detection viewpoint by Monte Carlo simulations. The performance of CA-CFAR processors is analysed under varying conditions of sea clutter spatial correlation and spikiness for several cases of false alarm probability, the length of cell size used in the CFAR processor and the number of pulses integrated prior to CA-CFAR processor.

The detection performance of CA-CFAR is compared with the performance of fixed threshold detection. The performance evaluations are quantified by CFAR loss. CFAR loss is defined as the increase in average signal to clutter ratio compared to that of fixed threshold, required to achieve a given probability of detection and probability of false alarm. Curves for CFAR loss to the spikiness and spatial correlation of clutter, number of pulses integrated and the length of cell size are presented.

Keywords: K-Distribution, CA-CFAR, CFAR Gain, Sea Clutter, Radar Detection

ÖZ

K-DAĞILIMLI DENİZ KARGAŞASI ORTAMINDA SABİT HATALI ALARM SIKLIĞI (SHAS) İLE TESPİT

Çetin, Ayşin

Yüksek Lisans, Elektrik ve Elektronik Mühendisliği Bölümü

Tez Danışmanı: Prof. Dr. Altunkan Hızal

Ortak Tez Danışmanı: Doç. Dr. Şimşek Demir

Eylül 2008, 119 sayfa

Geleneksel sabit eşik tespit ediciler, belirli hatalı alarm ve tespit olasılıkları sağlayabilmek için çevre kargaşasının tüm menzilde sahip olduğu istatistiksel özellikleri kullanarak sabit bir eşik değeri belirler. Ancak radar uygulamalarında çevre kargaşasının istatistiksel özellikleri önceden bilinmemektedir. Sabit Hatalı Alarm Sıklığı (SHAS) teknikleri çevre kargaşası istatistiklerini kestirebilmek ve hedefleri çevre kargaşasından ayırt edebilmek amacıyla uyarlanabilir bir eşik değeri belirler. Hücre Ortalamalı SHAS (HO-SHAS) da ise eşik değeri test edilen hücreyi çevreleyen sınırlı sayıdaki hücrenin ortalaması alınarak kontrol edilir.

Bu tezde, K-dağılımlı deniz kargaşası ortamındaki radar hedeflerinin tespiti istatistiksel bir bakış açısıyla Monte Carlo benzetimler kullanılarak incelenmektedir. HO-SHAS işlemcinin başarımı deniz kargaşasının değişen uzaysal ilintisi ve şekilsel yapısı için farklı hatalı alarm olasılıkları, HO-SHAS işlemcinin hücre uzunlukları ve HO-SHAS öncesinde toplanan darbe sayılarına

göre incelenmektedir.

HO-SHAS'ın tespit başarımı sabit eşik tespit edicinin başarımıyla karşılaştırılmaktadır. Başarım değerlendirmeleri SHAS kaybı niceliğiyle ifade edilmektedir. SHAS kaybı verilen bir hatalı alarm ve tespit olasılığı için ortalama sinyal kargaşa oranının sabit eşik tespit edicide elde edilen değere göre artışı ile tanımlanmaktadır. SHAS kaybının deniz kargaşasının şekilsel yapısına, deniz kargaşasının uzaysal ilintisine, toplanan darbe sayısına ve SHAS hücre uzunluğuna göre değişimini gösteren eğriler sunulmaktadır.

Anahtar Kelimeler: K-Dağılımı, CA-CFAR, CFAR Kazancı, Deniz Kargaşası, Radarlarda Tespit

To my mom and dad, for their encouragement

and

To Gökberk, for his endless love and patience

ACKNOWLEDGMENTS

I am very pleased to express my gratitude and indebtedness to my advisor, Prof. Dr. Altuncan Hızal for his valuable guidance and genial criticism. I have benefited greatly from his extensive technical knowledge and fatherly advices.

I also appreciate to my colleagues from TÜBİTAK UEKAE İLTAREN for their discussions and heartening words.

I am extremely grateful to my parents and little sister Selin whose support and encouragement have been invaluable. I feel very lucky to be their daughter and to have a little sister like her.

Finally and most importantly, I wish to express my deepest gratitude to my husband, Gökberk, without whose support this work would not have been possible.

TABLE OF CONTENTS

ABSTRACT.....	iv
ÖZ.....	vi
ACKNOWLEDGMENTS.....	ix
TABLE OF CONTENTS	x
LIST OF TABLES	xiii
LIST OF FIGURES	xiv
TABLE OF ABBREVIATIONS	xx
CHAPTERS	
1. INTRODUCTION	1
1.1. LITERATURE SURVEY	1
1.2. GOAL OF THE THESIS	8
1.3. THESIS ORGANIZATION	8
2. BACKGROUND	10
2.1. SEA CLUTTER.....	10
2.2. COMPOUND K-DISTRIBUTION CLUTTER MODEL.....	11
2.2.1. <i>K-Distribution of Voltage</i>	11
2.2.2. <i>K-Distribution of Power</i>	18
2.2.3. <i>An Emprical Model For Shape Parameter</i>	21
2.2.4. <i>Spatial Correlation in Sea Clutter</i>	22
2.2.4.1. Generation of Exponentially Correlated Gaussian Random Numbers.....	24

2.2.4.2. Generation of Correlated Gamma Distributed Random Numbers.....	26
2.2.4.3. Generation of Correlated K-Distributed Clutter	30
2.3. RADAR DETECTION	32
2.3.1. <i>Fixed Threshold Detection</i>	34
2.3.1.1. Fixed Threshold Detection in Rayleigh Noise.....	35
2.3.1.2. Fixed Threshold Detection in K-Distributed Clutter	37
2.3.2. <i>Cell Averaging CFAR (CA-CFAR) Detection</i>	42
2.3.2.1. CA-CFAR Detection in Rayleigh Noise	45
2.3.3. <i>CFAR Loss</i>	49
2.3.4. <i>Ideal CFAR Detection</i>	53
3. PERFORMANCE ANALYSIS	60
3.1. ASSUMPTIONS MADE	60
3.2. SIMULATION STEPS	62
3.3. VERIFICATION OF APPROACHES	63
3.4. CA-CFAR DETECTION IN SPATIALLY UNCORRELATED (SU) K-DISTRIBUTED CLUTTER	66
3.4.1. <i>Single Pulse Detection</i>	66
3.4.2. <i>Multiple Pulse Detection</i>	77
3.5. CA-CFAR DETECTION IN SPATIALLY CORRELATED (SC) K-DISTRIBUTED CLUTTER	86
4. PRACTICAL POINT OF VIEW	99
4.1. ESTIMATION OF THE K-DISTRIBUTION SHAPE PARAMETER	100
4.2. EFFECT OF INCORRECT ESTIMATION OF THE SHAPE PARAMETER	101
5. CONCLUSION.....	105
5.1. FUTURE WORK.....	109
REFERENCES.....	110

APPENDICES

A. CHANGE OF VARIABLES AND JACOBIAN CALCULATION	113
A.1. <i>Obtaining Rayleigh Distributed Envelope from Two Complex Gaussian Component.....</i>	<i>114</i>
A.2. <i>Generalised Distributed Voltage to Gamma Distributed Power.....</i>	<i>116</i>
A.3. <i>Rayleigh Distributed Voltage to Exponentially Distributed Power..</i>	<i>116</i>
B. CHARACTERISTIC FUNCTIONS OF RANDOM VARIABLES	118

LIST OF TABLES

Table 1-1 Four cases in which detection decision may result	2
Table 1-2 Swerling fluctuating target models	4
Table 2-1 Spatial correlation lengths of sea clutter, [18]	23
Table 2-2 Ideal CFAR gains over fixed threshold detection	58
Table 3-1 Comparison of analytic and simulation results for $\nu = 0.5$	64
Table 3-2 CFAR loss in dB for sample values of ν and M when $P_{fa} = 10^{-4}$ and $N = 1$	70

LIST OF FIGURES

Figure 2-1 The K-distribution of voltage for various values of ν	16
Figure 2-2 The K-distribution of power for various values of ν	21
Figure 2-3 Amplitude variation with range of gamma distributed data for $\nu = 5$ and spatial correlation length $R = 1$	29
Figure 2-4 Amplitude variation with range of gamma distributed data for $\nu = 5$ and spatial correlation length $R = 30$	29
Figure 2-5 ACF of correlated gamma data set.....	30
Figure 2-6 Simulation scheme	31
Figure 2-7 Normalised histogram of simulated compound K data for shape parameter $\nu = 5$ and correlation length $R = 30$ compared with the analytical definition of the K distribution PDF.....	32
Figure 2-8 K-distributed samples and fixed threshold.....	34
Figure 2-9 $\log_{10} P_{fa}$ vs. α graph for single and multiple pulse fixed threshold detection of Rayleigh noise.....	37
Figure 2-10 $\log_{10} P_{fa}$ vs. fixed threshold for a single pulse SU K-distributed clutter	39
Figure 2-11 $\log_{10} P_{fa}$ vs. fixed threshold for 3 pulse integration of SU K- distributed clutter.....	40
Figure 2-12 $\log_{10} P_{fa}$ vs. fixed threshold for 10 pulse integration of SU K- distributed clutter.....	40
Figure 2-13 $\log_{10} P_{fa}$ vs. fixed threshold for 20 pulse integration of SU K- distributed clutter.....	41
Figure 2-14 $\log_{10} P_{fa}$ vs. fixed threshold for 30 pulse integration of SU K- distributed clutter.....	41

Figure 2-15 CA-CFAR configuration	43
Figure 2-16 K-distributed samples and CA-CFAR threshold	44
Figure 2-17 $\log_{10} P_{fa}$ vs. α graph of closed form (represented by solid lines) and simulated results for single pulse CA-CFAR detection of Rayleigh noise	46
Figure 2-18 $\log_{10} P_{fa}$ vs. α for 3 pulse CA-CFAR detection of Rayleigh noise ...	47
Figure 2-19 $\log_{10} P_{fa}$ vs. α for 10 pulse CA-CFAR detection of Rayleigh noise .	48
Figure 2-20 $\log_{10} P_{fa}$ vs. α for 20 pulse CA-CFAR detection of Rayleigh noise .	48
Figure 2-21 $\log_{10} P_{fa}$ vs. α for 30 pulse CA-CFAR detection of Rayleigh noise .	49
Figure 2-22 True CFAR loss calculation from P_d vs. SCR of single pulse detection for SU clutter with $\nu = 0.5$, SW-II target, $P_{fa} = 10^{-4}$ and $M = 16$	50
Figure 2-23 CFAR loss calculation from $\log_{10} P_{fa}$ vs. α of single pulse detection for SU clutter with $\nu = 0.5$ and $M = 16$	52
Figure 2-24 P_d vs. SCR curves of ideal CFAR detection for SU clutter, SW-II target, $P_{fa} = 10^{-3}$ and $N = 1$	55
Figure 2-25 P_d vs. SCR curves of ideal CFAR detection, for SU clutter, SW-II target, $P_{fa} = 10^{-4}$ and $N = 1$	56
Figure 2-26 Conventional fixed threshold (dashed dotted curves) and ideal CFAR performance (solid curves), P_d vs. SCR curves for SU clutter, SW-II target, $P_{fa} = 10^{-4}$ and $N = 1$	57
Figure 2-27 P_d vs. SCR curves of ideal CFAR, CA-CFAR and fixed threshold detection for clutter with $\nu = 1.5$ for correlation lengths $R = 0$ and $R = 30$, $P_{fa} = 10^{-4}$ and $M = 16$	59
Figure 3-1 Approximate CFAR loss vs. $\log_{10} P_{fa}$ for SU clutter with $\nu = 0.2$ and $N = 1$	66
Figure 3-2 Approximate CFAR loss vs. $\log_{10} P_{fa}$ for SU clutter with $\nu = 0.5$ and $N = 1$	67

Figure 3-3 Approximate CFAR loss vs. $\log_{10} P_{fa}$ for SU clutter with $\nu = 1.5$ and $N = 1$	67
Figure 3-4 Approximate CFAR loss vs. $\log_{10} P_{fa}$ for SU clutter with $\nu = 10$ and $N = 1$	68
Figure 3-5 Approximate CFAR loss vs. M for SU clutter, $P_{fa} = 10^{-4}$ and $N = 1$..	69
Figure 3-6 P_d vs. SCR for SU clutter, $P_{fa} = 10^{-3}$, SW-II target, $M = 16$ and $N = 1$	70
Figure 3-7 P_d vs. SCR for SU clutter, $P_{fa} = 10^{-3}$, SW-II target, $M = 32$ and $N = 1$	71
Figure 3-8 P_d vs. SCR for SU clutter, $P_{fa} = 10^{-4}$, SW-II target, $M = 16$ and $N = 1$	71
Figure 3-9 P_d vs. SCR for SU clutter, $P_{fa} = 10^{-4}$, SW-II target, $M = 32$ and $N = 1$	72
Figure 3-10 True CFAR loss vs. M for SU clutter, SW-II target, $P_{fa} = 10^{-3}$, $P_d = 0.5$ and $N = 1$	73
Figure 3-11 True CFAR loss vs. M for SU clutter, SW-II target, $P_{fa} = 10^{-3}$, $P_d = 0.9$ and $N = 1$	73
Figure 3-12 True CFAR loss vs. M for SU clutter, SW-II target, $P_{fa} = 10^{-4}$, $P_d = 0.5$ and $N = 1$	74
Figure 3-13 True CFAR loss vs. M for SU clutter, SW-II target, $P_{fa} = 10^{-4}$, $P_d = 0.9$ and $N = 1$	74
Figure 3-14 A comparison of CFAR loss methods for SU clutter, SW-II target, $P_{fa} = 10^{-3}$, $P_d = 0.5$ and $N = 1$	76
Figure 3-15 A comparison of CFAR loss methods for SU clutter, SW-II target, $P_{fa} = 10^{-4}$, $P_d = 0.5$ and $N = 1$	76
Figure 3-16 A comparison of CFAR loss methods for SU clutter, SW-II target,	

$P_{fa} = 10^{-4}$, $P_d = 0.9$ and $N = 1$	77
Figure 3-17 $\log_{10} P_{fa}$ vs. α for SU clutter with $\nu = 1.5$ and $M = 32$	78
Figure 3-18 CFAR loss vs. N for SU clutter, SW-II target, $P_{fa} = 10^{-3}$ and $M = 16$	79
Figure 3-19 CFAR loss vs. N for SU clutter, SW-II target, $P_{fa} = 10^{-3}$ and $M = 32$	80
Figure 3-20 CFAR loss vs. N for SU clutter, SW-II target, $P_{fa} = 10^{-4}$ and $M = 16$	80
Figure 3-21 CFAR loss vs. N for SU clutter, SW-II target, $P_{fa} = 10^{-4}$ and $M = 32$	81
Figure 3-22 P_d vs. SCR curves for SU clutter with $\nu = 0.5$, SW-II target, $P_{fa} = 10^{-3}$ and $M = 32$	82
Figure 3-23 SCR vs. N curves for SU clutter, SW-II target, $P_{fa} = 10^{-3}$ and $M = 16$	83
Figure 3-24 SCR vs. N curves for SU clutter, SW-II target, $P_{fa} = 10^{-3}$ and $M = 32$	84
Figure 3-25 SCR vs. N curves for SU clutter, SW-II target, $P_{fa} = 10^{-4}$ and $M = 16$	84
Figure 3-26 SCR vs. N curves for SU clutter, SW-II target, $P_{fa} = 10^{-4}$ and $M = 32$	85
Figure 3-27 Approximate CFAR loss vs. M for SC clutter with $\nu = 1.5$, $N = 1$ & 10 and $P_{fa} = 10^{-3}$	87
Figure 3-28 Approximate CFAR loss vs. M for SC clutter with $\nu = 1.5$, $N = 1$ & 10 and $P_{fa} = 10^{-4}$	87
Figure 3-29 Approximate CFAR loss vs. M for SC clutter with $\nu = 10$, $N = 1$ & 10 and $P_{fa} = 10^{-3}$	88

Figure 3-30 Approximate CFAR loss vs. M for SC clutter with $\nu = 10$, $N = 1$ & 10 and $P_{fa} = 10^{-4}$	89
Figure 3-31 Approximate CFAR loss vs. M for SC clutter with $\nu = 0.5$, $N = 1$ & 10 and $P_{fa} = 10^{-3}$	90
Figure 3-32 Approximate CFAR loss vs. M for SC clutter with $\nu = 0.5$, $N = 1$ & 10 and $P_{fa} = 10^{-4}$	90
Figure 3-33 Approximate CFAR loss vs. M for SC clutter with $\nu = 0.2$, $N = 1$ & 10 and $P_{fa} = 10^{-3}$	91
Figure 3-34 Approximate CFAR loss vs. M for SC clutter with $\nu = 0.2$, $N = 1$ & 10 and $P_{fa} = 10^{-4}$	91
Figure 3-35 CFAR loss vs. M for SC clutter with $\nu = 0.2$, SW-II target, $N = 1$, $P_{fa} = 10^{-3}$ and $P_d = 0.5$	93
Figure 3-36 CFAR loss vs. M for SC clutter with $\nu = 0.5$, SW-II target, $N = 1$, $P_{fa} = 10^{-3}$ and $P_d = 0.5$	94
Figure 3-37 CFAR loss vs. M for SC clutter with $\nu = 1.5$, SW-II target, $N = 1$, $P_{fa} = 10^{-3}$ and $P_d = 0.5$	94
Figure 3-38 CFAR loss vs. M for SC clutter with $\nu = 10$, SW-II target, $P_{fa} = 10^{-3}$, $P_d = 0.5$ and $N = 1$	95
Figure 3-39 CFAR loss vs. M for SC clutter with $\nu = 0.2$, SW-II target, $P_{fa} = 10^{-3}$ and $N = 10$	96
Figure 3-40 CFAR loss vs. M for SC clutter with $\nu = 0.5$, SW-II target and $P_{fa} = 10^{-3}$ and $N = 10$	96
Figure 3-41 CFAR loss vs. M for SC clutter with $\nu = 1.5$, SW-II target, $P_{fa} = 10^{-3}$ and $N = 10$	97
Figure 3-42 CFAR loss vs. M for SC clutter with $\nu = 10$, SW-II target, $P_{fa} = 10^{-3}$ and $N = 10$	98

Figure 4-1 Approximate CFAR loss vs. ν for SU clutter, $N = 1$ and $M = 16$	102
Figure 4-2 Approximate CFAR loss vs. ν for SU clutter, $N = 1$ and $M = 32$...	102
Figure 4-3 α vs. ν for SU clutter and $M = 16$	103
Figure 4-4 α vs. ν for SU clutter and $M = 32$	104

TABLE OF ABBREVIATIONS

ACF	Auto Correlation Function
CA-CFAR	Cell Averaging Constant False Alarm Rate
CFAR	Constant False Alarm Rate
CUT	Cell Under Test
MC	Monte Carlo
MNLT	Memoryless NonLinear Transform
P_d	Probability of Detection
PDF	Probability Density Function
P_{fa}	Probability of False Alarm
RCS	Radar Cross Section
SC	Spatially Correlated
SCR	Signal to Clutter Ratio
SU	Spatially Uncorrelated
SW-II	Swerling type II

CHAPTER 1

INTRODUCTION

1.1. LITERATURE SURVEY

In radar detection, the usual case is that radar returns from a target are accompanied by unwanted returns, or interference, known as clutter. The detection of targets is then become a challenging task in the presence of clutter. Distinguishing targets has been the subject of research for decades. Understanding the statistical behavior of both clutter and targets is the first step in order to be able to develop successful detection strategies.

For detection of targets in clutter, a thresholding mechanism is necessary. Since the thresholding operation in any detector will be determined based on the distribution of the clutter echoes, the appropriate selection of probability distribution of radar clutter is crucial to achieve good performance results.

Since detection is a decision mechanism which decides whether or not target is present in the cell under test (CUT) by thresholding, the threshold needs to be decided. If the target signal plus the clutter signal or only the clutter signal exceeds the given threshold, detection decision is made, otherwise there will be no detection. As shown in Table 1-1 a detection decision may be a result of four cases.

Table 1-1 Four cases in which detection decision may result

Target Presence	Detection Decision	Result
YES	YES	Right decision
YES	NO	Error - Miss target
NO	YES	Error - False alarm
NO	NO	Right decision

Radars are often interested in complex man-made objects such as tanks, ships or airjets. The amplitude of radar targets depends on the aspect angle and the structure of the target. As [1] indicates most radar situations are often too complex and a method to assess the effects of fluctuating cross section is to postulate a reasonable model for the fluctuations and to analyze it mathematically. Thus, it is practical to provide a statistical measure of radar target strength. For radar performance analysis the Swerling models are commonly used. There are four statistical target models listed in Table 1-2. Each Swerling case corresponds to a set of conditions that approximate some real target.

When all the scatterers characterizing the radar target have approximately equal amplitude, the amplitude probability density function (PDF) is Rayleigh or Chi-square distribution of 2 degrees of freedom. This case is modelled by Swerling cases I and II. When a target comprises one dominant scatterer and several smaller amplitude scatterers, the amplitude PDF is Chi-square of 4 degrees of freedom. This case is modelled by Swerling cases III and IV. The Chi-square distribution of degree $2m$ that also describes the Swerling fluctuation models is

$$f(\sigma) = \frac{m}{(m-1)! \sigma_{av}} \left(\frac{m\sigma}{\sigma_{av}} \right)^{m-1} \exp\left(-\frac{m\sigma}{\sigma_{av}}\right), \quad \sigma > 0 \quad (1.1)$$

where σ_{av} is the average radar cross section (RCS) over all target fluctuations.

Table 1-2 Swerling fluctuating target models

Target Model	Amplitude PDF	Amplitude PDF (Other definitions)	m	Structure	Fluctuations Rate
Swerling I	Chi-square distribution of degree 2	Exponential, Rayleigh-power	1	Large number of independent scatterers	Scan to scan
Swerling II	Chi-square distribution of degree 2	Exponential, Rayleigh-power	1	Large number of independent scatterers	Pulse to pulse
Swerling III	Chi-square distribution of degree 4	-	2	Large dominant scatterer + a collection of small independent scatterers	Scan to scan
Swerling IV	Chi-square distribution of degree 4	-	2	Large dominant scatterer + a collection of small independent scatterers	Pulse to pulse

The assumption used in Swerling cases I and III is that the echo pulses received from a target on any one scan are of constant amplitude throughout the entire scan but are independent (uncorrelated) from scan to scan. An echo fluctuation of this type is referred as scan to scan fluctuation [1]. In Swerling cases II and IV the fluctuations are more rapid than in cases I and III and are taken to be independent

from pulse to pulse. The steady target which has no fluctuation is called as Swerling type 0.

In this thesis, the main concern is the performance of maritime surveillance radars which is inevitably limited by the presence of sea clutter, the unavoidable but unwanted radar returns from the sea surface. Realistic modeling of this clutter process is thus a prerequisite for any reliable assessment of systems. As [2] indicates, under certain conditions the nature of the backscatterer from sea surface is well known to depart from the Rayleigh voltage form. Especially when a radar has a spatial resolution high enough to resolve structure on the sea surface, the sea clutter received by the system is not well modelled by a Gaussian process [3]. A number of candidate distributions such as log-normal (e.g. [4]) and Weibull (e.g. [5]) have been shown to describe accurately the amplitude fluctuations observed in experimental measurements although they have no physical to the scattering process they describe. High resolution sea clutter is represented by compound K-distribution model first by Ward [6] . The compound K-distribution model for sea clutter amplitude statistics has received much attention, and it is now widely accepted that this provides a good phenomenological description of sea clutter [6]-[8]. Some physical justification for this model has also been proposed [7],[9],[10]. In [11] it is shown that the compound form of K-distribution provides an excellent description for measurements made at S, X and J bands for all the range resolutions employed.

The compound K-distribution representation of sea clutter is based on the assumption that sea clutter in a given range bin exhibits Rayleigh voltage fluctuations (termed the speckle), the variance of which varies in time and space according to a gamma distribution. This compound form of K-distribution has the particular advantage of permitting the correlation properties of the clutter to be properly modelled, including the effects of radar frequency agility [2]. In [3] it is implied that the sea clutter amplitude statistics are best described in terms of the compound K-distribution. Hence, the K-distribution provides a much improved statistical clutter model and is now incorporated in many radar performance

calculations.

The main task of the radar detection processors is to determine an appropriate threshold in order to automatically detect targets against noise and/or clutter background. The implications of the K-distribution on detection performance have been analysed in some detail for the cases of fixed threshold detection [12] and K-distributed clutter plus noise [13].

In this thesis two main processors are analysed and compared. First one is the conventional fixed threshold detector, which sets a fixed threshold based on the known overall characteristics of the clutter to give a specific probability of false alarm (P_{fa}).

Second one is the Cell Averaging Constant False Alarm Rate (CA-CFAR) detector. If the prior knowledge of clutter statistics is not available which is usually the case in radar applications, Constant False Alarm Rate (CFAR) techniques are used. In [14], CFAR is defined as a property of threshold control devices that maintain an approximately constant rate of false target detections when the noise and/or clutter levels, and/or electronic countermeasures into the detector are variable. A well known practical method for setting such a threshold is the Cell Averaging Constant False Alarm Rate (CA-CFAR) processor [15]. CA-CFAR is a CFAR technique in which the threshold is controlled by the average of received amplitudes in cells surrounding the CUT, as a means of controlling the false alarm rate [14]. Hence an adaptive means to control P_{fa} in non-stationary clutter is provided by CA-CFAR detection.

Radars may increase detection sensitivity by adding returns from successive transmissions. This process is called integration. Integration may be accomplished in the radar receiver either before or after the detector. Integration after the detector is called post detection or noncoherent integration which is used in this thesis. The effects of post detection integration of several pulses against K-distributed background have been adressed by [11], [16].

Since the CA-CFAR processor sets the threshold by estimating the clutter mean level within a finite CA-CFAR window, there is an inherent loss of detection probability in a CA-CFAR processor compared with the fixed threshold detection performance in homogeneous noise and/or clutter background. The fixed threshold detection, on the other hand, sets a fixed threshold under the assumption that the clutter statistics are known a priori. This relative performance loss of a CA-CFAR processor is called the CFAR loss. There are two different methods that may be employed to measure the CFAR loss. First one defines this loss by the increase in the mean SCR needed for the CA-CFAR processor scheme achieve a certain probability of detection (P_d) and P_{fa} relative to the fixed threshold detection. (In the following sections by SCR mean SCR is meant.) This true CFAR loss will be a function of the particular CFAR scheme, the target type and probability of detection, P_d as well as the clutter statistics and the probability of false alarm, P_{fa} [16]. Alternatively, another method called threshold multiplier method uses the CA-CFAR threshold multiplying factor, α as a measure. α is used in CA-CFAR configurations to set the false alarm rate constant. Threshold multiplier method results in approximate CFAR loss values and this approximate CFAR loss values are independent of P_d , hence the target type.

If the clutter exhibits significant spatial correlation the CA-CFAR may be able to follow the local fluctuations giving an improvement in performance, or CFAR gain, compared to so-called ideal fixed threshold. Examples of this are given in [17]. The limit of such improvement is described by the concept of the ideal CFAR detector [11]. The quantitative measurement of performance of three types of CFAR processors including CA-CFAR in different spatially correlated (SC) clutter conditions has been addressed for single pulse detection in [2]. A more physical analysis based partly on simulation is presented in [18]. In [16] for three different data recordings of different autocorrelation functions are used in order to explore the performance of CA-CFAR in correlated sea clutter, using the compound K-distribution clutter model and pulse to pulse integration.

1.2. GOAL OF THE THESIS

In this thesis the performance of CA-CFAR processor is aimed to be explored in K-distributed clutter background when Swerling type II (SW-II) target is present in CUT, under various conditions of clutter spatial correlation and over a range of CA-CFAR processor parameters.

The behaviour of CA-CFAR processor against sea clutter which exhibit significant spatial correlation is attractive, since CA-CFAR may follow the local fluctuations and this may give a performance improvement to CA-CFAR processor compared to fixed threshold detector. In this thesis, the purpose is to obtain and analyse this improvement. To do this, firstly the uncorrelated K-distributed background is to be understood well and be analysed in detail. Then when the spatial correlation effect is introduced into the background, the performance results may be compared. It is also desired to investigate under which CA-CFAR condition the best detection performance is achieved.

In addition to the CA-CFAR parameters, the post detection integration may give some improvement to the detection performance. Different number of pulses are integrated and the effect of integration is modelled to understand the performance achievements against both spatially uncorrelated (SU) and spatially correlated (SC) K-distributed sea clutter.

1.3. THESIS ORGANIZATION

This thesis is divided into five chapters:

Chapter 2 presents theoretical background of radar detection in sea clutter. Section 2.1 defines the sea clutter and gives information about its nature. Section 2.2 explains the representation of K-distributed sea clutter in detail and presents the

method used in the generation of spatially correlated K-distributed clutter samples. Afterwards, Section 2.3 mentions the fundamentals of radar detection. This section introduces both the detection procedures used in this thesis and the definition of CFAR loss which is the measure of the performance analysis. Moreover, the formulations and graphs for detection in noise are also given for comparison.

Chapter 3 covers simulation based radar detection performance analysis. Section 3.1 describes the assumptions made in analysis. Section 3.2 outlines the simulation steps. Section 3.3 explains the methods used for verification of simulation results. Section 3.4 and 3.5 present the simulation results for spatially uncorrelated and correlated clutter for both single and multiple pulse detection.

Chapter 4 provides the operational usage of simulation results in practice. Section 4.1 briefly defines an estimation method of the shape parameter of K-distribution. Section 4.2 gives results and assesses the effects of wrong estimation of the shape parameters.

Finally, Chapter 5 concludes the thesis with some remarks. Section 5.1 presents the possible future work in order to enhance this study.

CHAPTER 2

BACKGROUND

2.1. SEA CLUTTER

Sea clutter is defined as unavoidable and unwanted radar returns from the sea surface which makes the detection of wanted targets difficult. The nature of the radar echo from sea depends upon the shape of the sea surface. This shape, or the roughness, of the sea depends mainly on the wind. The sea clutter is also affected by the contaminants that change the water surface tension and the temperature of water relative to the air [1].

The sea may consist of two kind of waves; wind waves and swell waves. Generally waves result from the action of the wind blowing on the water surface. Such waves are called wind waves and cause a random appearing ocean height profile. However, swell is any system of water waves which has left the region where they were originally excited by the wind. Swell waves have less random structure than wind waves and they can travel great distances from the place where they originated.

2.2. COMPOUND K-DISTRIBUTION CLUTTER MODEL

2.2.1. K-Distribution of Voltage

High resolution sea clutter is represented by compound K-distribution model first by Ward [6]. In this compound model sea clutter consists of two components which specify the amplitude of the envelope of sea clutter returns.

The first component is a spatially varying mean level, often called the modulation process, and can be related to the surface profile of the sea. The mean level results from a bunching of scatterers associated with the long sea waves and swell structure [19]. This component has a longer correlation time, in other words varies only slowly with time and is unaffected by frequency agility [19].

The second is called the speckle component which occurs due to the multiple scatterer nature of the clutter in any range cell. This decorrelates over a few milliseconds due to the relative motion of the scatterers or through the use of frequency agility [19], [20]. For fixed frequency operation the speckle component of clutter returns will typically only decorrelate over periods of 5-10 ms [20].

So the sea clutter's complex envelope of compound K-distribution model can be given as a multiplication by these two components as given in (2.1).

$$\tilde{X} = Y \times \tilde{S} \quad (2.1)$$

In (2.1) \tilde{X} is the sea clutter's and \tilde{S} is the speckle component's complex envelope which is composed of in-phase and quadrature complex Gaussian random variables with zero mean and σ^2 variance as given in (2.2).

$$\begin{aligned}\tilde{S} &= S_I + S_Q \\ S_I &\sim N(0, \sigma^2) \text{ and } S_Q \sim N(0, \sigma^2)\end{aligned}\tag{2.2}$$

Local mean level, Y , has a distribution function $f_Y(y)$ modelled by generalised Chi distribution.

$$f_Y(y) = \frac{2b^{2\nu}}{\Gamma(\nu)} y^{2\nu-1} \exp(-b^2 y^2)\tag{2.3}$$

The amplitude of the sea clutter's complex envelope is given in (2.4).

$$|\tilde{X}| = Y \times |\tilde{S}|\tag{2.4}$$

Speckle component \tilde{S} 's amplitude has a Rayleigh amplitude distribution with a parameter of σ . The detailed information of how to obtain a Rayleigh amplitude distribution from the envelope of two complex Gaussian components is given in Appendix A.1.

The PDF of $|\tilde{S}|$ is given in (2.5).

$$f_s(s) = \frac{s}{\sigma^2} \exp\left(-\frac{s^2}{2\sigma^2}\right)\tag{2.5}$$

s can be written as given in (2.6).

$$s = \frac{x}{y}\tag{2.6}$$

If the variables are changed according to the (2.6), then joint probability density function, $f(x|y)$, will be as

$$\begin{aligned}
f_{x,y}(x|y) &= \frac{1}{\left| \frac{\partial x}{\partial y} \right|} f_s \left(\frac{x}{y} \right) \\
&= \frac{x}{y^2 \sigma^2} \exp \left(-\frac{x^2}{2y^2 \sigma^2} \right)
\end{aligned} \tag{2.7}$$

When the generalised Chi distributed local mean level in (2.3) is substituted into compound form, the overall amplitude distribution of K-distributed sea clutter's envelope $f_X(x)$ is given by;

$$\begin{aligned}
f_X(x) &= \int_0^{\infty} f_Y(y) f_{x,y}(x|y) dy \\
&= \int_0^{\infty} \frac{2b^{2\nu}}{\Gamma(\nu)} y^{2\nu-1} \exp(-b^2 y^2) \frac{x}{y^2 \sigma^2} \exp \left(-\frac{x^2}{2y^2 \sigma^2} \right) dy
\end{aligned} \tag{2.8}$$

In (2.8) the speckle component is averaged over all possible values of local mean level.

If y^2 and ν are changed by u and $\nu'+1$ in (2.8), then $f_X(x)$ will be written as in (2.9).

$$f_X(x) = \frac{b^{2(\nu'+1)} x}{\Gamma(\nu) \sigma^2} \int_0^{\infty} u^{\nu'-1} \exp \left(-b^2 u - \frac{x^2}{2u \sigma^2} \right) du \tag{2.9}$$

The integral in (2.9) is solved using (2.10) from [21].

$$\int_0^{\infty} \alpha^{t-1} \exp \left(-\left(\gamma \alpha + \frac{\beta}{\alpha} \right) \right) d\alpha = 2 \left(\frac{\beta}{\gamma} \right)^{\frac{t}{2}} K_t \left(2\sqrt{\beta\gamma} \right) \tag{2.10}$$

Here $K_t(\cdot)$ is a modified Bessel or K function. K-distribution name is originated from the use of modified Bessel function whose symbol is the letter K.

After writing $\sigma = \sqrt{\frac{2}{\pi}}$ and $b = \frac{2c}{\sqrt{\pi}}$ in (2.10), K-distribution PDF is obtained and given in (2.11).

$$f_X(x) = \frac{4c}{\Gamma(v)} (cx)^v K_{v-1}(2cx) \quad \text{where } c = \sqrt{\frac{\pi}{4}}b \quad (2.11)$$

Here b and c are scale parameters and v is the shape parameter which depends on sea conditions and the radar parameters.

The n th moments of y are given in (2.12),

$$E\langle y^n \rangle = \frac{1}{b^n} \frac{\Gamma\left(v + \frac{n}{2}\right)}{\Gamma(v)} \quad (2.12)$$

while the n th moments of the K-distribution can be found from (2.13).

$$\begin{aligned} E\langle x^n \rangle &= \int_0^{\infty} x^n f_X(x) dx \\ &= \int_0^{\infty} x^n \frac{4c}{\Gamma(v)} (cx)^v K_{v-1}(2cx) dx \end{aligned} \quad (2.13)$$

By using the integral equation in (2.14) from [21], the n th moments of the K-distribution can be calculated easily.

$$\int_0^{\infty} x^\mu K_\nu(\beta x) dx = 2^{\mu-1} \beta^{-\mu-1} \Gamma\left(\frac{1+\mu+\nu}{2}\right) \Gamma\left(\frac{1+\mu-\nu}{2}\right) \quad (2.14)$$

By changing the variables μ , ν and β into $v+n$, $v-1$ and $2c$, the n th moments of the K-distribution are given in (2.15).

$$E\langle x^n \rangle = \frac{1}{c^n} \frac{\Gamma\left(\nu + \frac{n}{2}\right)}{\Gamma(\nu)} \Gamma\left(\frac{n}{2} + 1\right) \quad (2.15)$$

The mean clutter level $E\langle x \rangle$ and the mean square clutter level $E\langle x^2 \rangle$ are calculated from (2.15) and given in (2.16).

$$E\langle x \rangle = \frac{\sqrt{\pi}}{c} \frac{\Gamma\left(\nu + \frac{1}{2}\right)}{2\Gamma(\nu)} \quad (2.16)$$

$$E\langle x^2 \rangle = \frac{\nu}{c^2}$$

The cumulative distribution probability of the K-distribution is given in (2.17).

$$F_X(x) = \int_{-\infty}^x \frac{4c}{\Gamma(\nu)} (ct)^\nu K_{\nu-1}(2ct) dt \quad (2.17)$$

$$= \frac{2c^\nu}{\Gamma(\nu)} x^\nu K_\nu(2cx)$$

Some plots of the K-distribution PDF of voltage are shown in Figure 2-1 for various values of shape parameter ν and with the scale parameter c set to give unity mean square value of the envelope, x . That is, the scale parameter is calculated by using (2.16) and given in (2.18).

$$c = \sqrt{\nu} \quad (2.18)$$

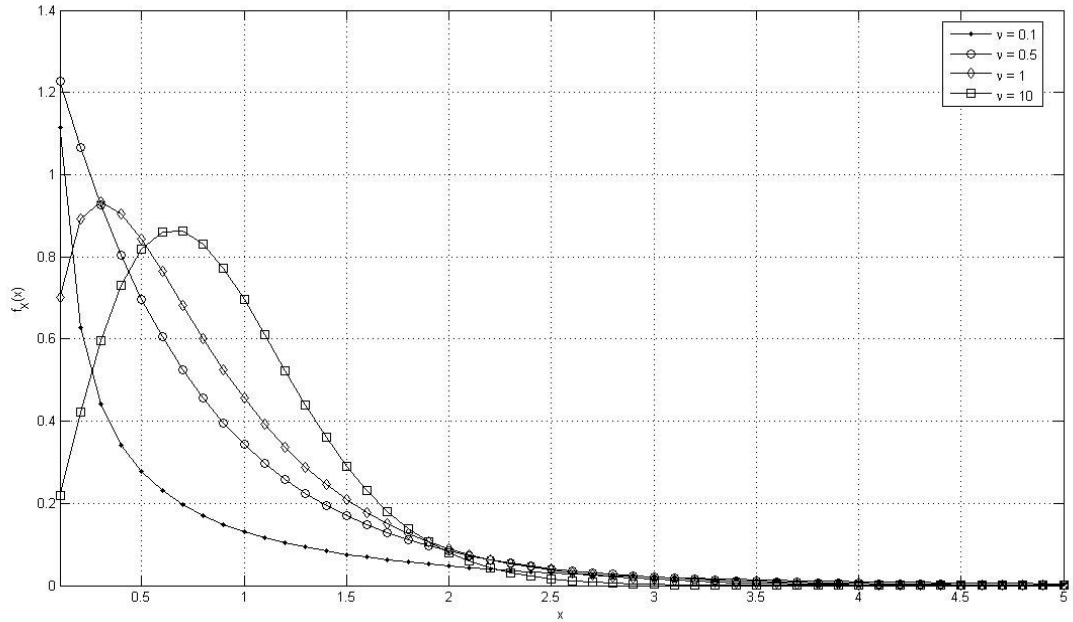


Figure 2-1 The K-distribution of voltage for various values of ν

Typically, the value of ν in sea clutter falls in the range $0.1 \leq \nu \leq \infty$. When $\nu \rightarrow \infty$ it reduces to the Rayleigh distribution, while small values of ν , say $\nu < 1$, correspond to spiky clutter [19].

If a second random variable θ is uniformly distributed over $(0, 2\pi)$ and statistically independent of the K-distributed X in (2.11), the characteristic function denoted by $C_Y(u; \nu)$ of a third random variable $Y = X \cos(\theta)$ is written as

$$\begin{aligned}
 C_Y(u; \nu) &= E_{X, \theta} \langle \exp(jXu \cos(\theta)) \rangle \\
 &= E_{X, \theta} \langle J_0(Xu) \rangle
 \end{aligned}
 \tag{2.19}$$

where $J_0(\cdot)$ is the zeroth order Bessel function and $E\langle \cdot \rangle$ is the expectation operator. Using the definition of characteristic function in Appendix B and (2.11), the characteristic function can be written as

$$E_{X,\theta} \langle J_0(Xu) \rangle = \frac{4c^{v+1}}{\Gamma(v)} \int_0^\infty x^v K_{v-1}(2cx) J_0(xu) dx \quad (2.20)$$

The equation above can be solved by the help of following equation from [21]

$$\int_0^\infty x^{\mu+w+1} J_\mu(ax) K_w(bx) dx = 2^{\mu+w} a^\mu b^w \frac{\Gamma(\mu+w+1)}{(a^2+b^2)^{\mu+w+1}} \quad (2.21)$$

Hence using (2.21), (2.20) yields to

$$C_Y(u; v, c) = \frac{(2c)^{2v}}{(u^2 + 4c^2)^v} \quad (2.22)$$

For convenience the shape parameter of the K-distribution v is set to $2c^2$ and (2.22) reduces to

$$C_Y(u; v) = \left(\frac{2v}{u^2 + 2v} \right)^v \quad (2.23)$$

In the limiting case when $v \rightarrow \infty$, the characteristic function will be

$$\lim_{v \rightarrow \infty} C_Y(u; v) = \exp\left(-\frac{u^2}{2}\right) \quad (2.24)$$

For convenience, if the limiting density of X is denoted as

$$\lim_{v \rightarrow \infty} f_X(x; a, v) \equiv f_X(x) \quad (2.25)$$

we have from (2.23) to (2.25),

$$E\langle J_0(Xu) \rangle = \int_0^\infty f_X(x) J_0(Xu) dx = \exp\left(-\frac{u^2}{2}\right) \quad (2.26)$$

Therefore,

$$\begin{aligned} f_X(x) &= x \int_0^\infty u \exp\left(-\frac{u^2}{2}\right) J_0(Xu) du \\ &= x \exp\left(-\frac{x^2}{2}\right) \end{aligned} \quad (2.27)$$

And so the limiting distribution ($\nu \rightarrow \infty$) of X is Rayleigh. For sufficiently large values of parameter ν , the K-distribution density in (2.11) serves as an approximation to Rayleigh density.

2.2.2. K-Distribution of Power

In Section 2.2.1 the sea clutter's complex envelope is modelled as compound K-distribution. In some radar applications the power of the K-distribution's complex envelope is desired since the square law detection is used. Again the power of K-distribution can be given as a multiplication by the two components, square of local mean level and speckle, as given in (2.28).

$$\begin{aligned} |\tilde{X}|^2 &= Y^2 \times |\tilde{S}|^2 \\ W &= Z \times R \end{aligned} \quad (2.28)$$

Local mean level, Y , has a density function $f_Y(y)$ given in (2.3). Using Jacobian calculation in Appendix A.2, the PDF of the underlying intensity Z can be found. In (2.29) the PDF of Z which is gamma distributed is given.

$$f_z(z) = \frac{b^{2\nu}}{\Gamma(\nu)} z^{\nu-1} \exp(-b^2 z) \quad (2.29)$$

Speckle component \tilde{S} 's amplitude has a Rayleigh PDF and its square R has an exponential PDF given in (2.30). The details of this conversion is given in Appendix A.3.

$$f_R(r) = \frac{1}{2\sigma^2} \exp\left(-\frac{r}{2\sigma^2}\right) \quad (2.30)$$

Similarly, r can be written as follows;

$$r = \frac{w}{z} \quad (2.31)$$

If the variables are changed according to the (2.31), then joint probability density function $f(x|y)$ will be as in (2.32).

$$f(w|z) = \frac{1}{2\sigma^2 z} \exp\left(-\frac{w}{2\sigma^2 z}\right) \quad (2.32)$$

The overall amplitude distribution of K-distributed sea clutter power is $f_w(w)$ and is given in (2.33).

$$\begin{aligned} f_w(w) &= \int_0^{\infty} f_z(z) f_{w,z}(w|z) \\ &= \int_0^{\infty} \frac{b^{2\nu}}{\Gamma(\nu)} z^{\nu-1} \exp(-b^2 z) \frac{1}{2\sigma^2 z} \exp\left(-\frac{w}{2\sigma^2 z}\right) dz \end{aligned} \quad (2.33)$$

Here if ν is changed by $\nu'+1$, then $f_w(w)$ can be written as in (2.34).

$$f_w(w) = \frac{b^{2(v'+1)} x}{\Gamma(v) 2\sigma^2} \int_0^\infty z^{v'-1} \exp\left(-b^2 z - \frac{w}{2\sigma^2 z}\right) dz \quad (2.34)$$

The integral in (2.34) can be calculated using the equation in (2.10). After writing $\sigma = \sqrt{\frac{2}{\pi}}$ and $b = \frac{2c}{\sqrt{\pi}}$, the PDF of K-distributed sea clutter power is obtained as in (2.35).

$$f_w(w) = \frac{2c^{v+1}}{\Gamma(v)} w^{\frac{v-1}{2}} K_{v-1}(2c\sqrt{w}) \quad \text{where } c = \frac{\sqrt{\pi}}{2} b \quad (2.35)$$

Here b and c are scale parameters and v is the shape parameter.

The n th moments of the K-distribution of power is calculated from (2.36).

$$\begin{aligned} E\langle w^n \rangle &= \int_0^\infty w^n f_w(w) dw \\ &= \int_0^\infty w^n \frac{2c^{v+1}}{\Gamma(v)} w^{\frac{v-1}{2}} K_{v-1}(2c\sqrt{w}) dw \end{aligned} \quad (2.36)$$

By using the integral equation in (2.14) the n th moments of the K-distribution of power can be calculated. Similar calculations as in Section 2.2.1 yield (2.37).

$$E\langle w^n \rangle = \frac{1}{c^{2n}} \frac{\Gamma(v+n)}{\Gamma(v)} \Gamma(n+1) \quad (2.37)$$

The mean clutter power level $E\langle w \rangle$ and the mean square clutter power level $E\langle w^2 \rangle$ are calculated from (2.37) and given in (2.38).

$$E\langle w \rangle = \frac{\nu}{c^2}$$

$$E\langle w^2 \rangle = \frac{4}{c^4}(\nu + 1)$$
(2.38)

Some plots of the K-distribution PDF of power are shown in Figure 2-2 for various values of shape parameter ν and with the scale parameter c set to give unity mean value of the envelope, x . That is, the scale parameter is taken as in (2.39).

$$c = \sqrt{\nu}$$
(2.39)

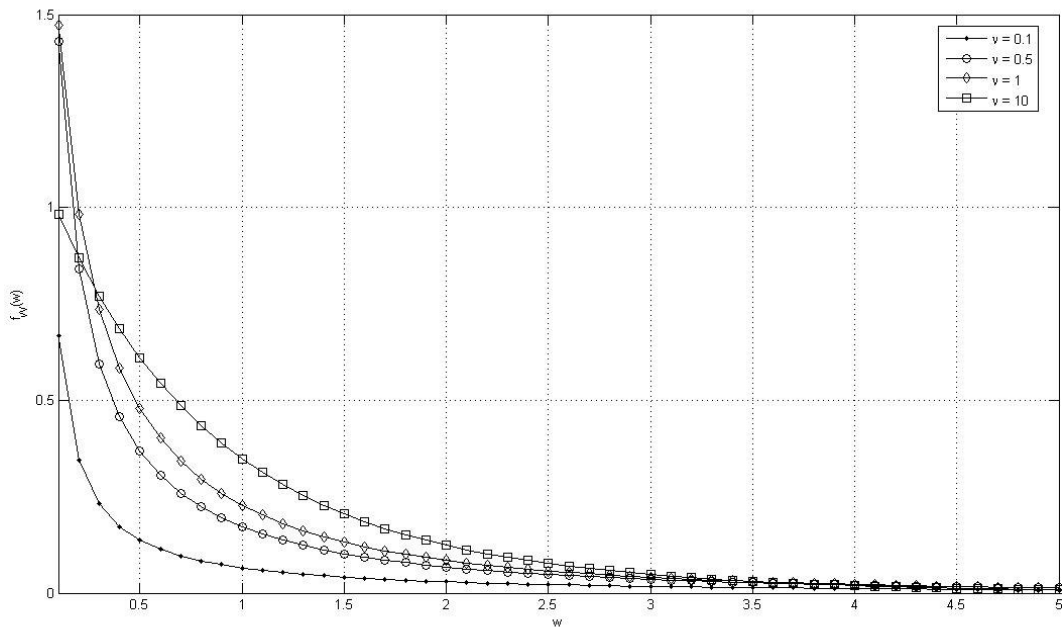


Figure 2-2 The K-distribution of power for various values of ν

2.2.3. An Empirical Model For Shape Parameter

The parametrization of the shape parameter of the K-distribution, ν , has been

achieved by matching the spread of results to simple functional forms. In this way an empirical model has been developed at I-Band (9-10 GHz) for the dependence of ν on radar, environmental and geometric parameters. The model has been derived [22] as

$$\log_{10}(\nu) = \frac{2}{3} \log_{10}(\varphi) + \frac{5}{8} \log_{10}(L) - p - \frac{\cos(2\theta)}{3} \quad (2.40)$$

where ν is the estimated value of the shape parameter of the K-distribution, L is the across range resolution in meters $100 < L < 800$, φ is the grazing angle in degrees $0.1^\circ < \varphi < 10^\circ$, p describes the polarisation effects with $p = 1.39$ for vertical and $p = 2.09$ for horizontal polarization and θ is the aspect angle with respect to the swell direction in radians. This last term can be omitted if there is no swell.

This empirical model does not include the variation of shape parameter with range resolution, ΔR . The dependence of range resolution is complex but a good guide to performance can be obtained by assuming a dependence of $\Delta R^{\frac{5}{8}}$. As [20] mentions this approximation is supported by some experimental measurements in [11].

2.2.4. Spatial Correlation in Sea Clutter

The spatial correlation of sea clutter returns are strongly related to the structure of sea wave. This exhibition of significant spatial correlation is often associated with the sea swell [18]. As given in [18], the correlation length ρ of sea surface in the range direction is taken to be a length characteristic of wind waves, given in terms of wind velocity W in m/s and g , acceleration due to gravity ($\sim 9.81 \text{ m/s}^2$). It is found that

$$\rho = \frac{\pi W}{2g} (3 \cos^2 \theta + 1)^{1/2} \quad (2.41)$$

where θ is the angle between the line of sight and the wind direction.

The correlation length ρ may be written in terms of the radar range resolution ΔR . The correlation length R expressed in range samples is given in (2.42).

$$R = \frac{\rho}{\Delta R} \quad (2.42)$$

Some values of R for different sea states are given in Table 2-1 for ΔR is equal to 2 m and 15 m and $\theta = 0$. In Table 2-1 the term sea state is used in order to describe the roughness of the sea as a measure of wave height.

Table 2-1 Spatial correlation lengths of sea clutter, [18]

Sea state	Wind speed, W (m/s)	Correlation length, ρ (m)	Correlation length, R	
			$\Delta R = 2$ m	$\Delta R = 15$ m
1	2.5	2.0	1	0
2	4.5	6.5	3	0
3	6.0	11.5	5	1
4	8.5	23.1	11	1
5	11.0	38.7	18	2
6	14.0	62.8	30	4

It can be seen that for high resolution radar the correlation length R , has values up

to 30 range samples for high sea states, in contrast to low resolution radar. Hence in this thesis the maximum spatial correlation length is chosen to be 30.

2.2.4.1. Generation of Exponentially Correlated Gaussian Random Numbers

Let g_n be a sequence of independent Gaussian deviates with zero mean, $E\langle g_n \rangle = 0$, and unit variance, $E\langle g_n^2 \rangle = 1$, i.e.

$$f_X(g_n = x) = \frac{1}{\sqrt{2\pi}} \exp\left(-\frac{x^2}{2}\right) \quad (2.43)$$

Let $\tau > 0$ be a real number and the correlation coefficient γ is as

$$\gamma \triangleq \exp\left(-\frac{1}{\tau}\right) \quad (2.44)$$

Now the sequence of numbers r_n is recursively defined via

$$r_0 \triangleq g_0; \quad r_{n+1} = \gamma r_n + \sqrt{1-\gamma^2} g_{n+1} \quad (2.45)$$

This can be written in a closed expression as

$$r_n = \gamma^n g_0 + \sqrt{1-\gamma^2} \sum_{i=1}^n g_i \gamma^{n-i} \quad (2.46)$$

Here the random numbers r_n are also Gaussian deviates with zero mean and unit variance since each r_n is the sum of Gaussian deviates, g_n . This statement can be proved by equations (2.47) and (2.48). Keeping in mind r_0 has a zero mean and unit variance, the equation in (2.47) can be obtained by taking the expectation of both sides of (2.45)

$$E\langle r_{n+1} \rangle = \gamma E\langle r_n \rangle + \sqrt{1-\gamma^2} E\langle g_{n+1} \rangle = 0; \quad E\langle r_n \rangle = 0, \quad E\langle g_{n+1} \rangle = 0 \quad (2.47)$$

Similarly in (2.48) variance of r_{n+1} is calculated. Here the cross term $E\langle r_n g_{n+1} \rangle$ vanishes because r_n and g_{n+1} are independent and thus uncorrelated.

$$E\langle r_{n+1}^2 \rangle = \gamma^2 E\langle r_n^2 \rangle + (1-\gamma^2) E\langle g_{n+1}^2 \rangle = 1; \quad E\langle r_n^2 \rangle = 1, \quad E\langle g_{n+1}^2 \rangle = 1 \quad (2.48)$$

The correlation coefficient is a normalized measure of the strength of the linear relationship between two variables. If the variables are same, it is named as autocorrelation coefficient. The autocorrelation coefficient $c(n;m)$ of the sequence r_n shall be defined by

$$c(n;m) = \frac{E\langle r_m r_{m+n} \rangle - E\langle r_m \rangle E\langle r_{m+n} \rangle}{E\langle (r_m - E\langle r_m \rangle)^2 \rangle^{1/2} E\langle (r_{m+n} - E\langle r_{m+n} \rangle)^2 \rangle^{1/2}} \quad (2.49)$$

Since r_n has zero mean and unit variance, therefore $c(n;m)$ reduces to $E\langle r_m r_{m+n} \rangle$.

Then it is simple to calculate

$$\begin{aligned} E\langle r_m r_{m+n} \rangle &= E\left\langle r_m \left(\gamma^n r_m + \sqrt{1-\gamma^2} \sum_{i=m+1}^{m+n} g_i f^{m+n-i} \right) \right\rangle \\ &= \gamma^n E\langle r_m^2 \rangle = \exp\left(-\frac{n}{\tau}\right) \end{aligned} \quad (2.50)$$

Here the Gaussian deviates g_i are not correlated with the number r_m , since $i > m$. Hence, the autocorrelation coefficient $c(n;m)$ is independent of m (i.e. the corresponding stochastic process is stationary) and is given by

$$c(n; m) \equiv c(n) = \gamma^n = \exp\left(-\frac{n}{\tau}\right) \quad (2.51)$$

2.2.4.2. Generation of Correlated Gamma Distributed Random Numbers

The simulation of a correlated gamma process takes a correlated Gaussian process of zero mean and unit variance as its starting point. This is then mapped on to the gamma process by memoryless nonlinear transform (MNLТ) generated by the solution of the equation in (2.52). Here by equating the cumulative distribution of a zero mean unit variance Gaussian process, evaluated at the value r taken by this process, with the cumulative distribution of the required process, thus determining the latter's value z [23]. So if the PDF of the values z of the required process is $f_{DIST}(z)$, the following expression is set.

$$\begin{aligned} \int_z^\infty f_{DIST}(z') dz' &= \frac{1}{\sqrt{2\pi}} \int_r^\infty \exp\left(-\frac{r'^2}{2}\right) dr' \\ &= \frac{1}{2} \operatorname{erfc}\left(\frac{r}{\sqrt{2}}\right) \end{aligned} \quad (2.52)$$

Here $\operatorname{erfc}(\cdot)$ is the complementary error function. The complementary quantile function $Q_{DIST}(\zeta)$ of the required distribution is now defined by

$$\int_{Q_{DIST}(\zeta)}^\infty f_{DIST}(z') dz' = \zeta \quad (2.53)$$

Using (2.53) the MNLТ that takes the input Gaussian random values into the corresponding values of the required non-Gaussian random variable is written as

$$z(r) = Q_{DIST} \left(\frac{1}{2} \operatorname{erfc} \left(\frac{r}{\sqrt{2}} \right) \right) \quad (2.54)$$

As previously stated, the locally Gaussian speckle and its gamma distributed randomly varying local power are brought together in the compound K model of sea clutter. In many circumstances it is the correlation properties of the more slowly varying gamma component of the clutter that affect radar performance [23]. Because of this, the generation of gamma distributed random processes with prescribed correlation properties is required.

So, the correlated Gaussian process of zero mean and unit variance is mapped onto a gamma distributed process Z by MNLT. The PDF of the gamma variable z , $f_z(z)$, is given in (2.29). Therefore, after replacing $f_{DIST}(z')$ with the equation of $f_z(z')$ in (2.52), the following equation is obtained.

$$\frac{b^{2\nu}}{\Gamma(\nu)} \int_z^\infty z'^{\nu-1} \exp(-b^2 z') dz' = \frac{1}{2} \operatorname{erfc} \left(\frac{r}{\sqrt{2}} \right) \quad (2.55)$$

The solution to (2.55) results in the correlated random gamma distributed variates z , having an autocorrelation function (ACF) of the form

$$E \langle z_m z_{m+n} \rangle = E \langle z^2 \rangle \exp \left(-\frac{n}{R} \right) \quad (2.56)$$

if the correlated Gaussian random variates r are generated using the recurrence in (2.46) and have an exponentially decaying ACF related in the following form [18].

$$E \langle r_m r_{m+n} \rangle = \gamma^n \quad (2.57)$$

As [18] states, it has been found empirically that to generate a gamma random variate with an ACF of the form (2.56), the Gaussian random variate must have an ACF related in the form

$$\gamma = \exp\left(-\frac{\nu^{0.7}}{R(\nu^{0.7} + 0.15)}\right) \quad (2.58)$$

In other words, a Gaussian process with an exponentially decaying ACF is transformed by the MNLT into a gamma process whose ACF also displays a seemingly exponential decay over several decades. The following formula has been devised to relate the observed characteristics decay times of the Gaussian, τ_G , and gamma, τ_γ , processes and the parameter ν of gamma distribution. [23]

$$\frac{\tau_G}{\tau_\gamma} = 1 + \frac{0.15}{\nu^{0.7}} \quad (2.59)$$

Remind that the variable R in (2.56) and (2.58) is the correlation length expressed as radar range samples and given in (2.42). Moreover, R is the number of samples after which the clutter may be said to be significantly decorrelated [18].

Examples of correlated gamma data for $\nu = 5$ are given in Figure 2-3 and Figure 2-4, for $R = 1$ and $R = 30$ respectively.

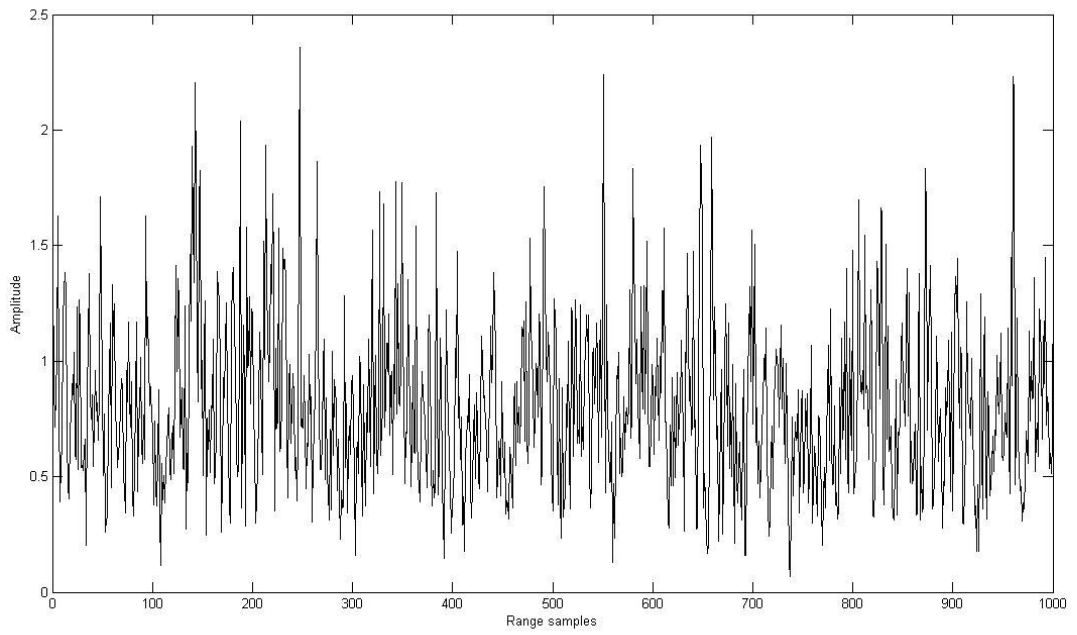


Figure 2-3 Amplitude variation with range of gamma distributed data for $\nu = 5$ and spatial correlation length $R = 1$

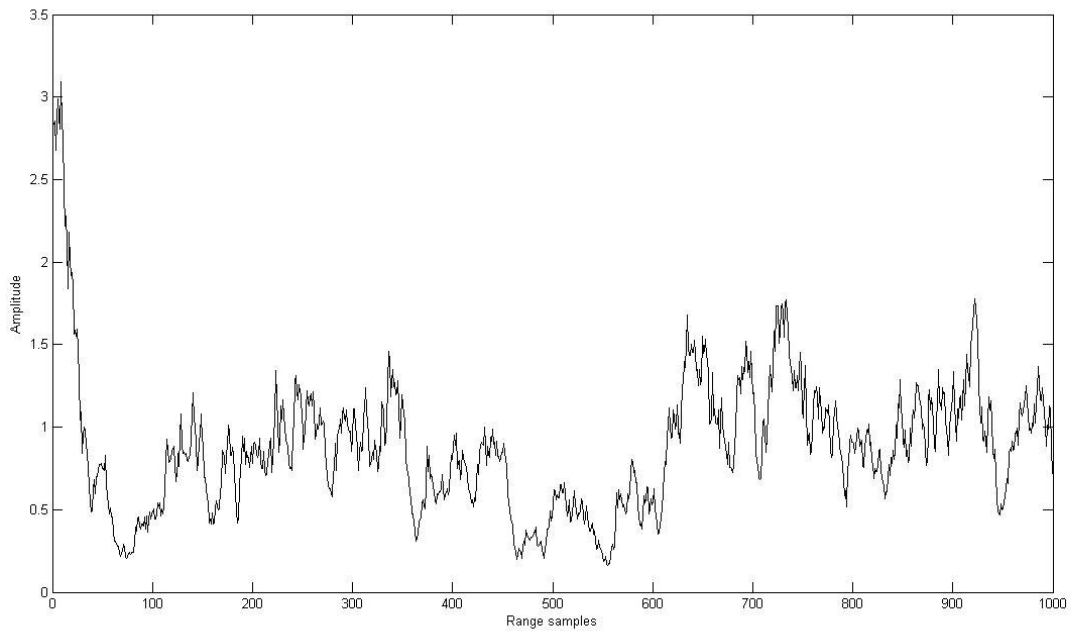


Figure 2-4 Amplitude variation with range of gamma distributed data for $\nu = 5$ and spatial correlation length $R = 30$

Figure 2-5 shows the ACF of both the simulated correlated gamma data set and the calculated from (2.56) when $R = 30$ and $\nu = 5$. Here the good agreement is noted.

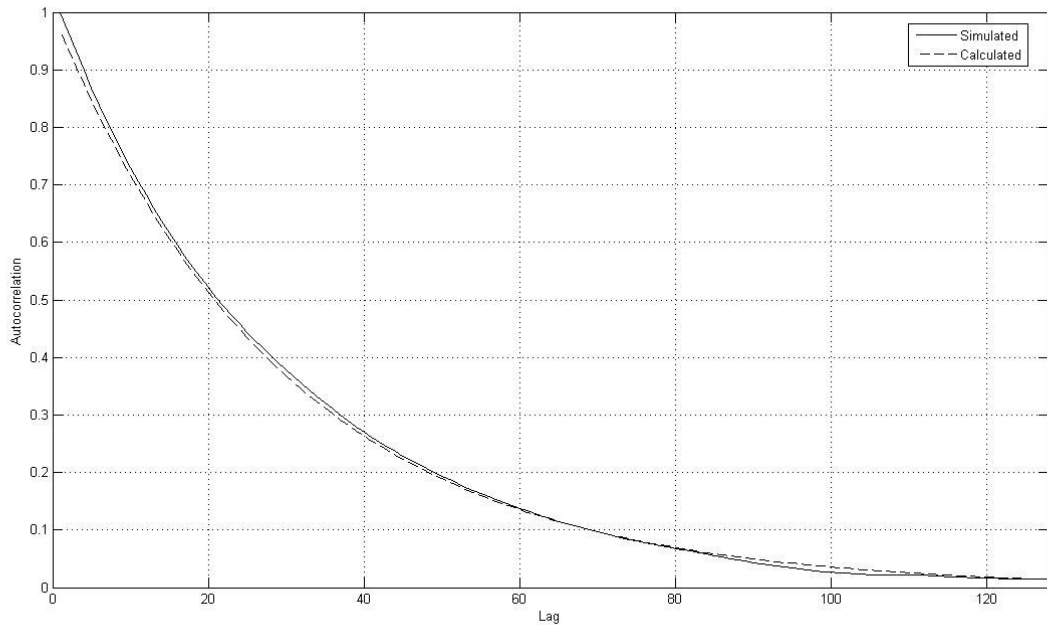


Figure 2-5 ACF of correlated gamma data set

2.2.4.3. Generation of Correlated K-Distributed Clutter

In order to generate correlated K-distributed clutter of voltage, the following steps are taken;

Correlated gamma random variables are generated by the MNLT approach using (2.55).

Uncorrelated Rayleigh variables are generated using (2.45).

Finally, the square root of the gamma variables and the Rayleigh variables are multiplied.

In this sense, if the square root of correlated Gamma variables are located on the diagonal of a Y matrix and uncorrelated Rayleigh variables form an array S , then correlated K-distributed random variable array X will be obtained from matrix multiplication $X = Y * S$ given by

$$Y = \sqrt{Z} = \begin{bmatrix} \sqrt{z_1} & 0 & 0 & 0 & 0 \\ 0 & \sqrt{z_2} & 0 & 0 & 0 \\ 0 & 0 & \sqrt{z_2} & 0 & 0 \\ 0 & 0 & 0 & \dots & 0 \\ 0 & 0 & 0 & 0 & \sqrt{z_N} \end{bmatrix} \quad (2.60)$$

$$S = [s_1 \ s_2 \ s_3 \ \dots \ s_N]^T$$

$$X = Y_{[N \times N]} * S_{[N \times 1]}$$

The simulation scheme for correlated K-distributed random variable generation is given in Figure 2-6.

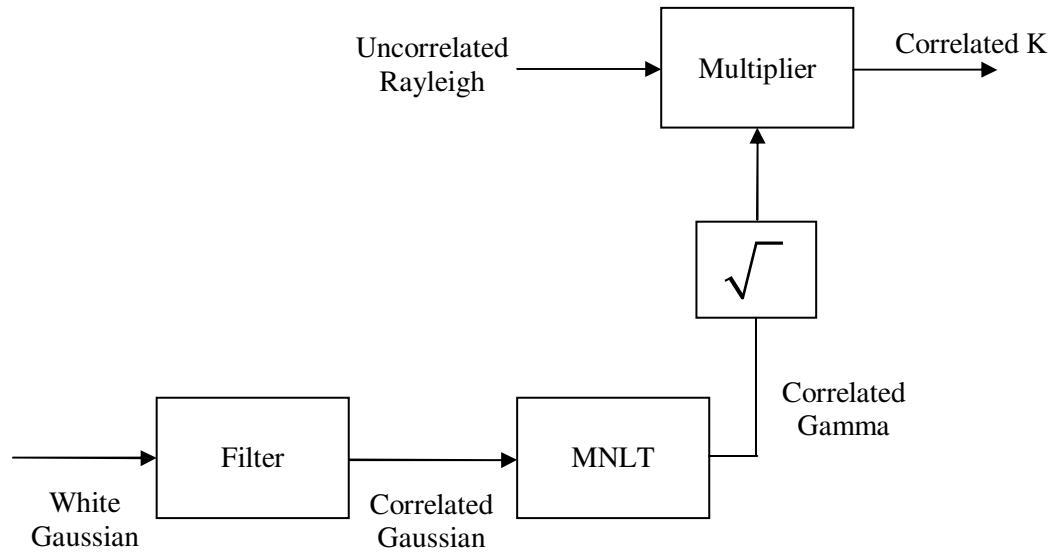


Figure 2-6 Simulation scheme

The resulting correlated K-distributed random variables have been tested by generating a K-distributed data set for $R=30$ and $\nu=5$. Figure 2-7 shows the comparison of the histogram of K data set with the PDF of K-distribution given in (2.11).

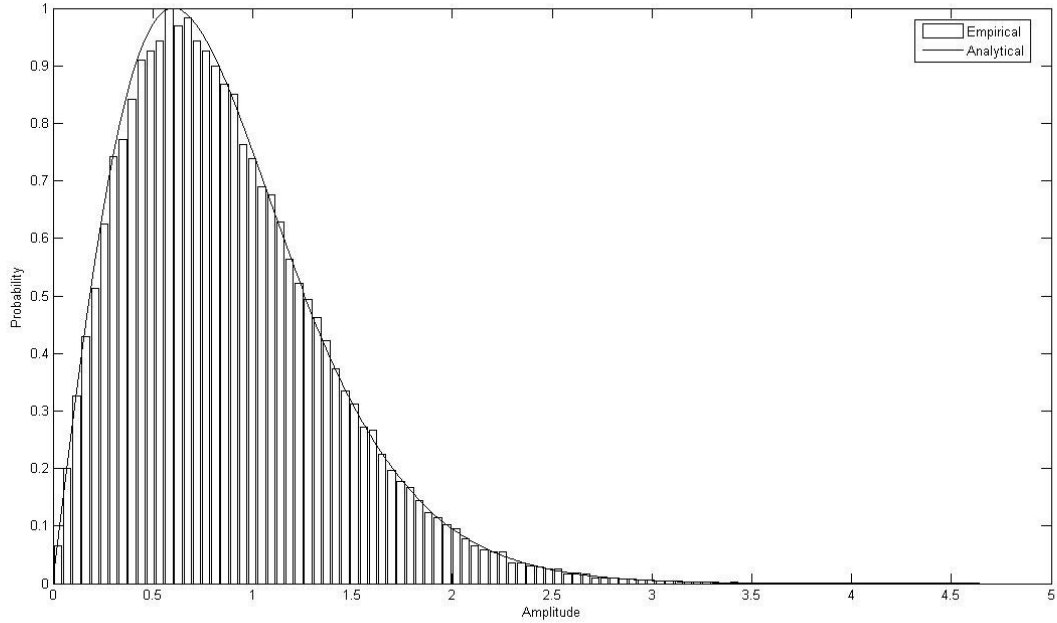


Figure 2-7 Normalised histogram of simulated compound K data for shape parameter $\nu = 5$ and correlation length $R = 30$ compared with the analytical definition of the K distribution PDF

2.3. RADAR DETECTION

The ability of a radar receiver to detect a weak echo signal is limited by the present noise that occupies the same part of the frequency spectrum as the signal. Detection of a radar signal is based on establishing a threshold at the output of the receiver. If the receiver output at the test cell is large enough to exceed threshold, a

target is said to be present. If the receiver output is not of sufficient amplitude to cross the threshold, only noise and/or clutter is said to be present. This comparison of whether or not the test cell amplitude exceeds the threshold can be defined with two hypothesis. Under the null hypothesis, H_0 , there is no target in the test cell; under the alternative hypothesis, H_1 , there is a target present in the test cell since the threshold T is exceeded.

$$\begin{aligned} X &\leq T \quad \text{under } H_0 \\ X &> T \quad \text{under } H_1 \end{aligned} \tag{2.61}$$

Here X is the sample in the test cell.

If the threshold level is set too low, noise and/or clutter may exceed the threshold and be mistaken for a target. This is called a false alarm. The probability that clutter returns exceed the threshold is given as probability of false alarm, P_{fa} and defined as

$$\begin{aligned} P_{fa} &= \Pr(X > T | H_0) \\ &= \int_T^{\infty} f_X(x | H_0) dx \end{aligned} \tag{2.62}$$

The solution of (2.62) results in the threshold for a given P_{fa} . The probability of detecting the signal, probability of detection (P_d), is the probability that the envelope of the sample X will exceed the threshold T which is set by the need to achieve some specified P_{fa} and defined as

$$\begin{aligned} P_d &= \Pr(X > T | H_1) \\ &= \int_T^{\infty} f_X(x | H_1) dx \end{aligned} \tag{2.63}$$

If the threshold is set too high, noise and/or clutter may not be large enough to

cause false alarms, but weak target echoes may not exceed the threshold and not be detected. When this occurs, it is called a missed detection.

2.3.1. Fixed Threshold Detection

If a radar has fixed the threshold in order to determine the existence of a target and give the required P_{fa} , then it is assumed that the clutter statistics, the overall shape and scale of the amplitude distribution, are known a priori. The form of this threshold is shown in Figure 2-8 for single pulse K-distributed clutter of $\nu = 0.5$ and $P_{fa} = 10^{-4}$.

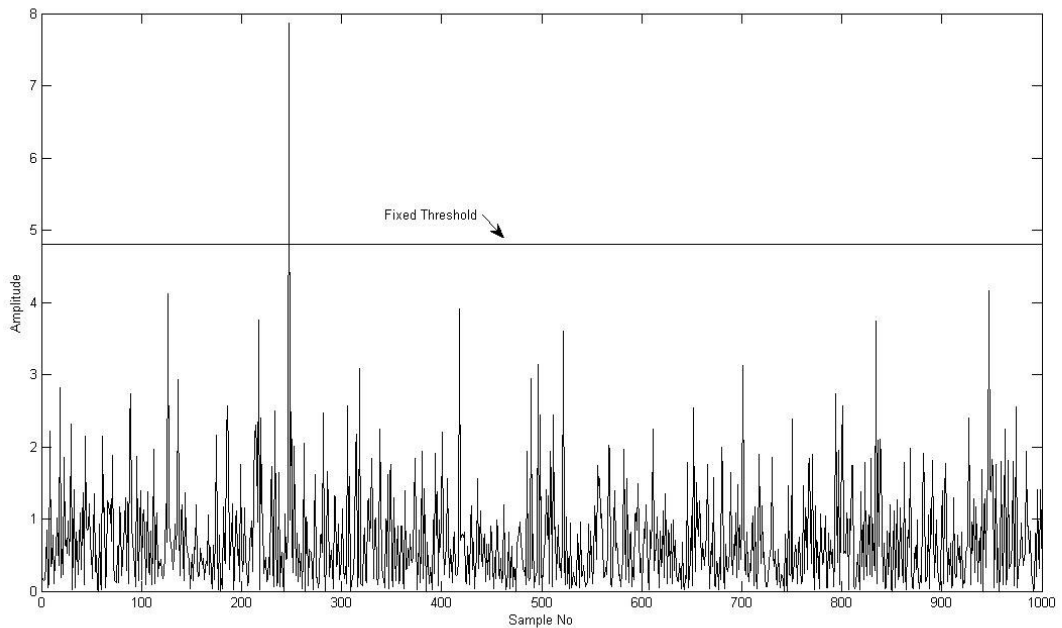


Figure 2-8 K-distributed samples and fixed threshold

It is evident that false alarms concentrate in areas of high clutter as a result of the effect of using a fixed threshold. In fixed threshold detection maximum detection appears in areas of high clutter where the target plus clutter return is maximum.

The fixed threshold, T_{fixed} is found from (2.64) as a function of clutter and/or noise PDF, $f_X(x)$ and P_{fa} .

$$P_{fa} = \int_{T_{fixed}}^{\infty} f_X(x) dx \quad (2.64)$$

2.3.1.1. Fixed Threshold Detection in Rayleigh Noise

The corresponding Rayleigh PDF of the envelope of the noise is expressed once again as below

$$f_R(r) = \frac{r}{\sigma^2} \exp\left(-\frac{r^2}{2\sigma^2}\right) \quad (2.65)$$

For a fixed threshold, T_{fixed} , the P_{fa} is given by

$$\begin{aligned} P_{fa} &= \int_{T_{fixed}}^{\infty} f_R(r) dr = \int_{T_{fixed}}^{\infty} \frac{r}{\sigma^2} \exp\left(-\frac{r^2}{2\sigma^2}\right) dr \\ &= \exp\left(-\frac{T_{fixed}^2}{2\sigma^2}\right) \end{aligned} \quad (2.66)$$

or T_{fixed} in terms of P_{fa}

$$T_{fixed} = \sigma \sqrt{2 \ln(P_{fa}^{-1})} \quad (2.67)$$

Rayleigh distribution raw moments are calculated from (2.68).

$$E\langle r^n \rangle = 2^{n/2} \sigma^n \Gamma\left(1 + \frac{n}{2}\right) \quad (2.68)$$

If $n = 1$, then the mean noise level is obtained from (2.68) and given in (2.69).

$$E\langle r \rangle = \sigma \sqrt{\frac{\pi}{2}} \quad (2.69)$$

Now since the threshold multiplier α is defined as $\alpha = \frac{T_{fixed}}{E\langle r \rangle}$, (2.67) can also written as

$$T_{fixed} = E\langle r \rangle \sqrt{\frac{4}{\pi} \ln(P_{fa}^{-1})} \quad (2.70)$$

For multiple pulse fixed threshold detection, (2.71) is needed to be solved.

$$P_{fa} = \int_{T_{fixed}}^{\infty} \frac{1}{2\pi} \int_{-\infty}^{\infty} \left[\int_0^{\infty} f_R(r) \exp(jtr) dr \right]^n \exp(-jtx) dt dx \quad (2.71)$$

where n represents the number of pulses used in fixed threshold detection. In the above equation the characteristic functions of random variables is used in order to obtain the PDF of sum of n Rayleigh distributed random variables. The detailed information of characteristic functions is given in Appendix B. It is also assumed that non-coherent detector sums envelope of n pulses.

(2.71) does not yield in a closed form, hence MC simulations are made in order to obtain P_{fa} for multiple pulse detection. Figure 2-9 shows the simulation results. Here the dotted line represents the results of (2.70) for verification purposes. Figure 2-9 shows that the closed form values of single pulse detection represented by dotted line are in close agreement with the simulation results. Furthermore, as N increases, threshold multiplier, α reduces for a given P_{fa} .

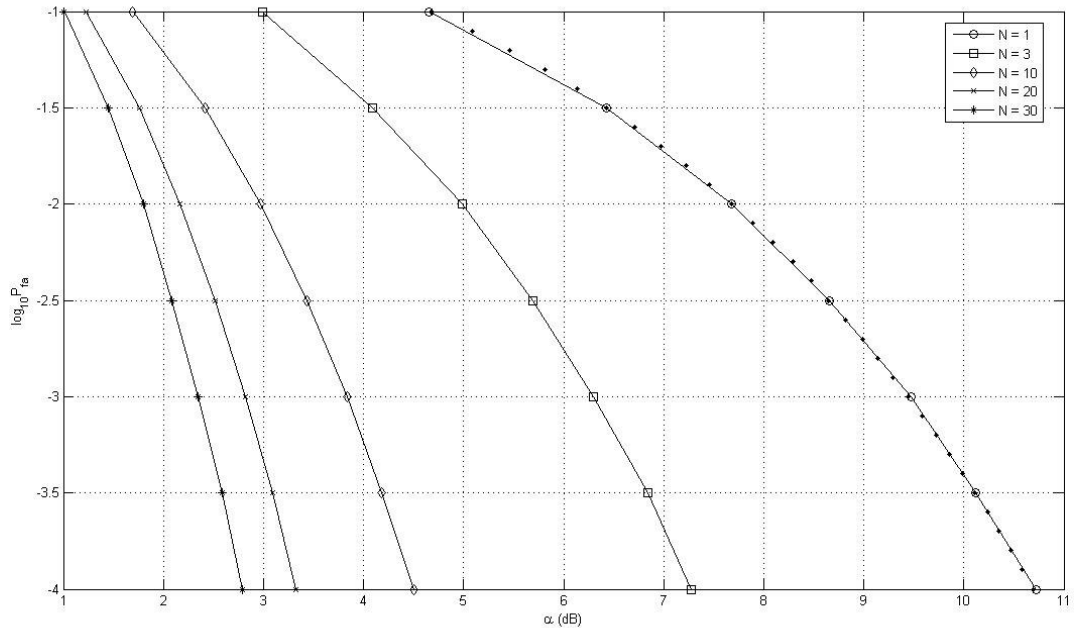


Figure 2-9 $\log_{10} P_{fa}$ vs. α graph for single and multiple pulse fixed threshold detection of Rayleigh noise

2.3.1.2. Fixed Threshold Detection in K-Distributed Clutter

If the test cell has K-distributed clutter, then the P_{fa} will be as follows;

$$P_{fa} = \int_{T_{fixed}}^{\infty} f_X(x) dx = \int_{T_{fixed}}^{\infty} \frac{4c}{\Gamma(v)} (cx)^v K_{v-1}(2cx) dx \quad (2.72)$$

After changing the variables as $c \rightarrow \frac{1}{2a}$ and $v-1 \rightarrow v'$, (2.73) is obtained as

$$\begin{aligned}
P_{fa} &= \int_{T_{fixed}}^{\infty} \frac{2}{a\Gamma(v+1)} \left(\frac{x}{2a}\right)^{v'+1} K_{v'}\left(\frac{x}{a}\right) dx \\
&= \frac{1}{2^{v'} a\Gamma(v'+1)} \int_{T_{fixed}}^{\infty} \left(\frac{x}{a}\right)^{v'+1} K_{v'}\left(\frac{x}{a}\right) dx
\end{aligned} \tag{2.73}$$

Noting the relation $K_u(z) = K_{-u}(z)$ and using the expressions given in (2.74) [21], P_{fa} results as in (2.75).

$$\int_z^{\infty} t^{-u} K_{u+1}(t) dt = z^{-u} K_u(z) \tag{2.74}$$

$$P_{fa} = \frac{1}{2^{v'} \Gamma(v'+1)} \left(\frac{T_{fixed}}{a}\right)^{v'+1} K_{v'+1}\left(\frac{T_{fixed}}{a}\right) \tag{2.75}$$

Changing the variables once again as $a \rightarrow \frac{1}{2c}$ and $v' \rightarrow v-1$, for fixed threshold detection of single pulse returns, the P_{fa} is given by

$$P_{fa} = \frac{2}{\Gamma(v)} (T_{fixed}c)^v K_v(2cT_{fixed}) \tag{2.76}$$

where now

$$\begin{aligned}
\alpha &= \frac{T_{fixed}}{E\langle x \rangle} \\
&= 2T_{fixed} \sqrt{\frac{b}{\pi}} \frac{\Gamma(v)}{\Gamma(v + 1/2)}
\end{aligned} \tag{2.77}$$

The detection threshold T_{fixed} normalised to the mean clutter level $E\langle x \rangle$ is expressed as α . If the clutter is known to be K-distributed and accurate estimates

of ν and c are available, then an appropriate threshold can be set from (2.76).

Using (2.76), the different curves are shown in Figure 2-10 for the different degrees of spikiness, i.e. shape parameter ν (0.2, 0.5, 1.5 and 10) and for single pulse detection.

Curves from Figure 2-11 to Figure 2-14 are given for multiple pulse detection (when 3, 10, 20 and 30 pulses integrated non-coherently) of spatially uncorrelated (SU) clutter. These curves are obtained by Monte Carlo (MC) simulation. The details about the simulation steps are given in Section 3.2. In these multiple pulse detection curves, it is assumed that the speckle component of clutter is independent from pulse to pulse and the modulation process is completely correlated.

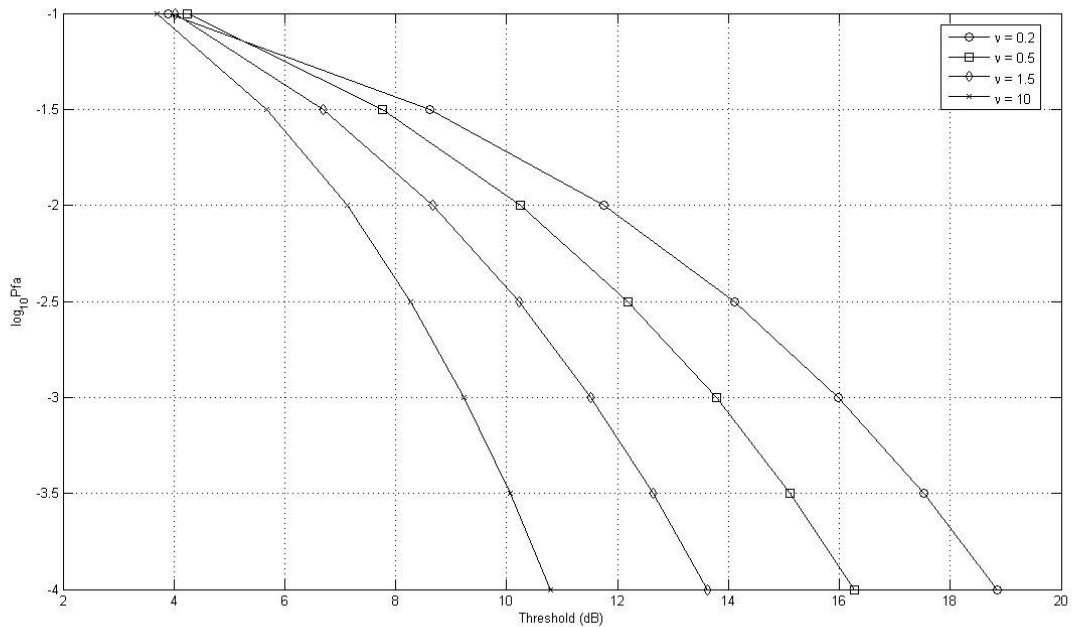


Figure 2-10 $\log_{10} P_{fa}$ vs. fixed threshold for a single pulse SU K-distributed clutter

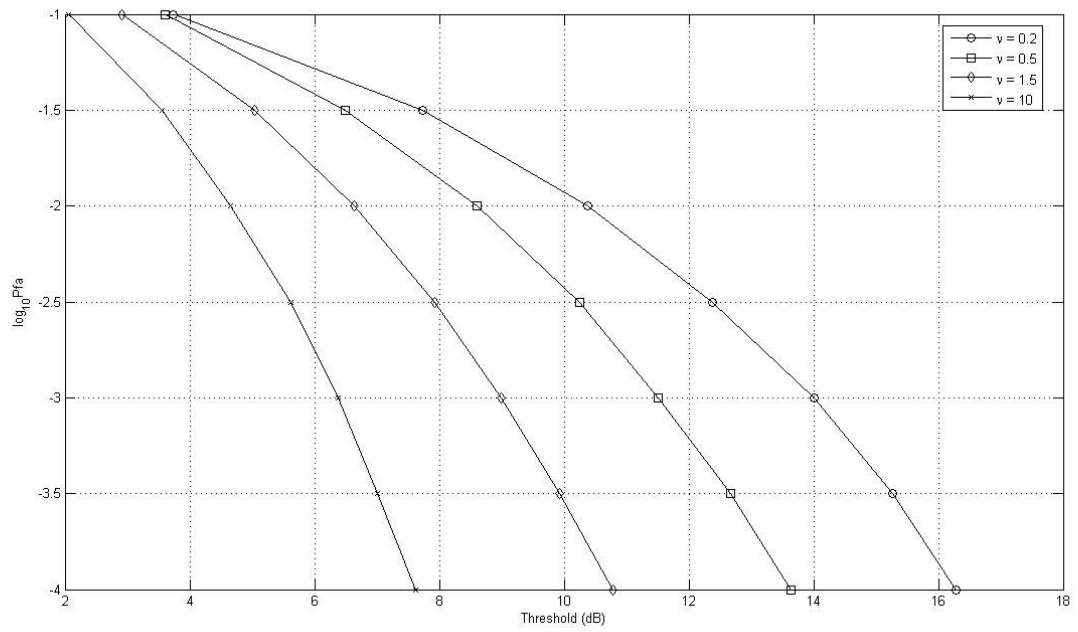


Figure 2-11 $\log_{10} P_{fa}$ vs. fixed threshold for 3 pulse integration of SU K-distributed clutter

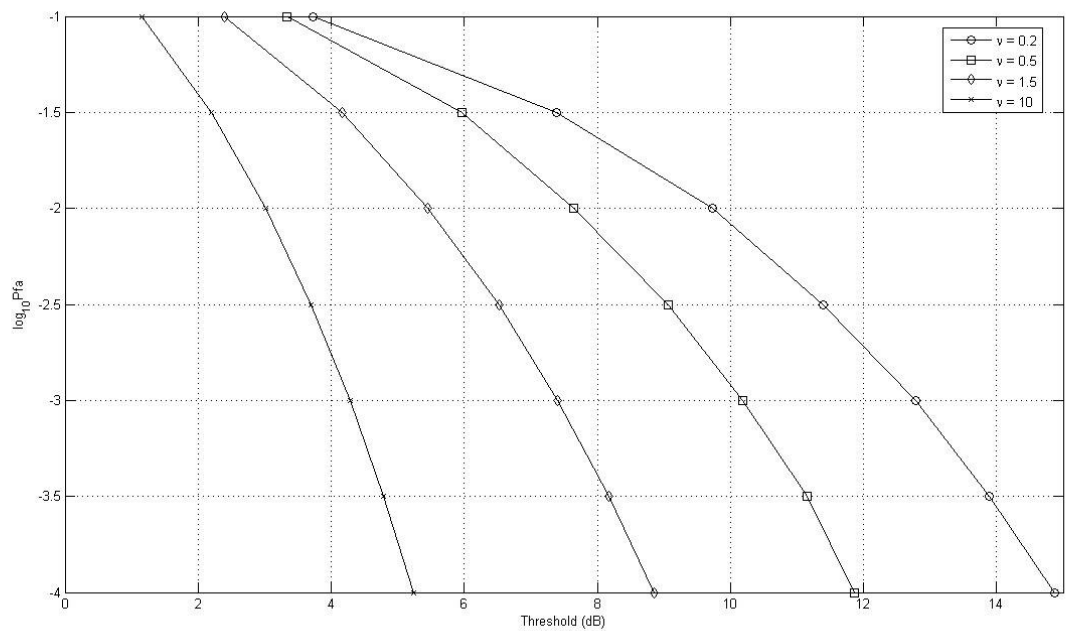


Figure 2-12 $\log_{10} P_{fa}$ vs. fixed threshold for 10 pulse integration of SU K-distributed clutter

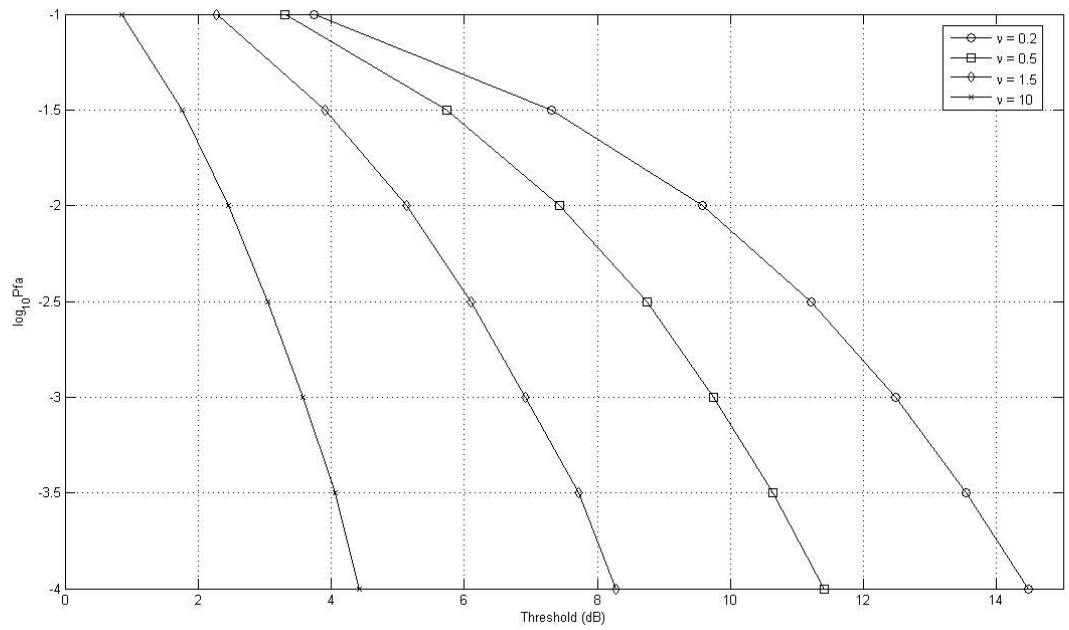


Figure 2-13 $\log_{10} P_{fa}$ vs. fixed threshold for 20 pulse integration of SU K-distributed clutter

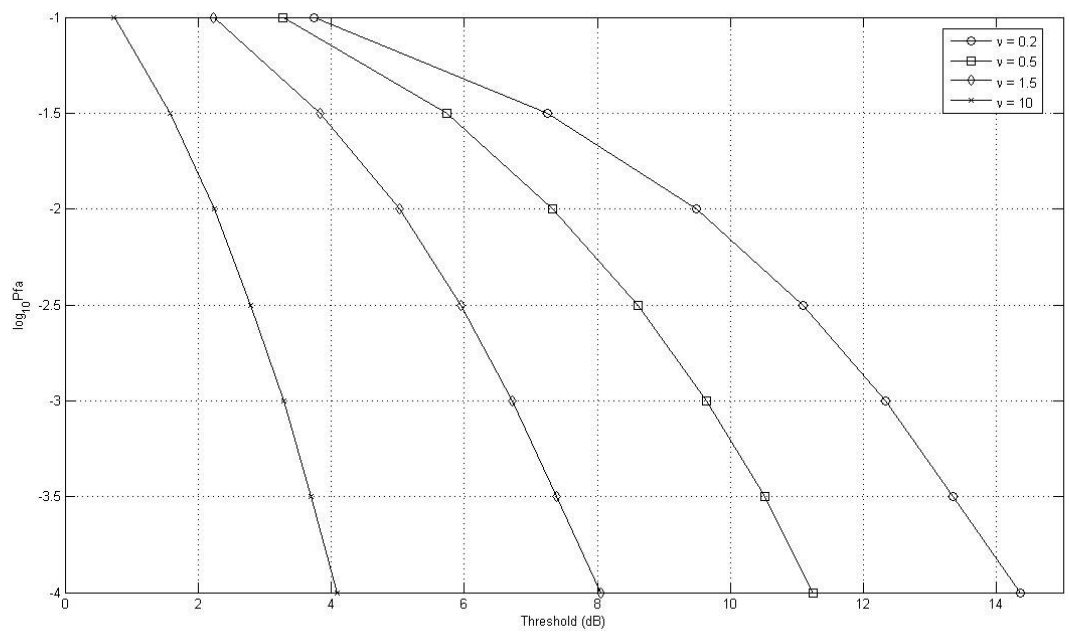


Figure 2-14 $\log_{10} P_{fa}$ vs. fixed threshold for 30 pulse integration of SU K-distributed clutter

From Figure 2-10 to Figure 2-14, as ν increases, the threshold required for any particular P_{fa} decreases. This means that the spikier clutter tends to obscure targets and thus tends to reduce detection performance. Furthermore, the results show that the effect of pulse to pulse integration is to make the curves steeper by moving them to the left. Hence, as the more pulses integrated P_{fa} at a given fixed threshold value reduces by averaging of the speckle fluctuations. However, as [3] also concludes, the spacing of curves remains approximately the same for single and multiple pulse detection. Thus, the performance due to spikiness of clutter is not affected.

2.3.2. Cell Averaging CFAR (CA-CFAR) Detection

In thermal noise or clutter an adaptive estimation of the mean level can be achieved by a CA-CFAR. Rather than relying on a knowledge of overall clutter statistics as in fixed threshold detection, by using CA-CFAR it should be possible to estimate the local variations of the mean clutter level when these are unknown. Figure 2-15 shows the operation of a double-sided CA-CFAR system.

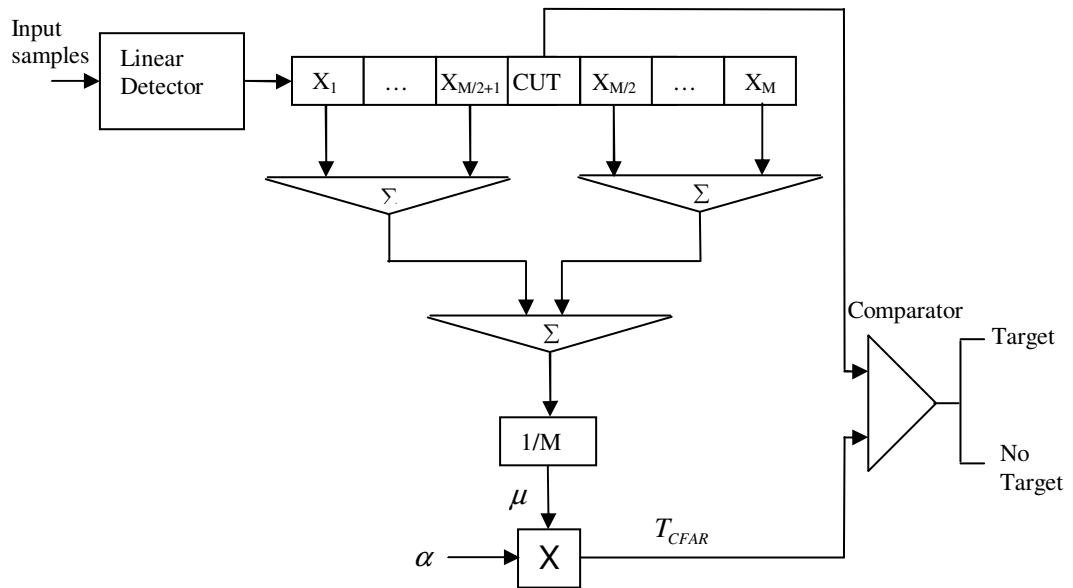


Figure 2-15 CA-CFAR configuration

The cell under test (CUT) is compared with a threshold T_{CFAR} , which is estimated from the mean level of the surrounding range cells, with clutter values x_i at either side of the CUT. In Figure 2-15, $M/2$ cells either side of the CUT are used to estimate the mean clutter level. The threshold multiplier, α is used to scale the estimate of the mean level. The appropriate value of α is chosen to achieve the desired value of P_{fa} in the absence of a target.

It is clear that in the CA-CFAR processor the threshold varies according to the local information about the total clutter level as shown in Figure 2-16 for single pulse K-distributed clutter of $\nu = 0.5$ and $P_{fa} = 10^{-3}$.

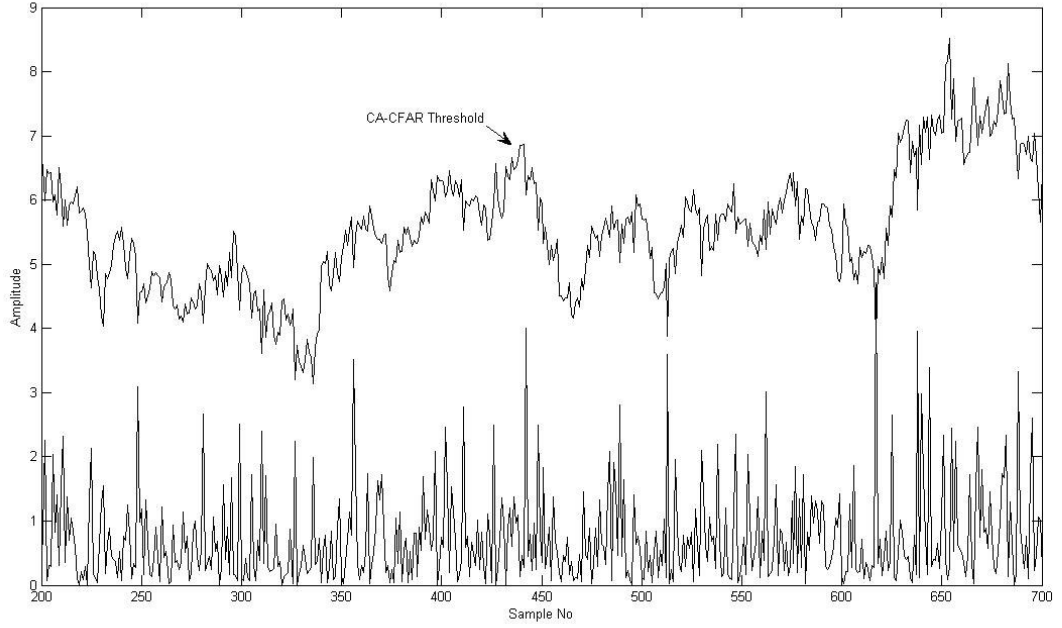


Figure 2-16 K-distributed samples and CA-CFAR threshold

The statistic μ in Figure 2-15 is a random variable whose distribution depends upon the particular CFAR scheme and the underlying distribution of each of the reference range samples. Thus the processor performance is determined by average detection and false alarm probabilities [24]. In other words, P_{fa} is determined in general by

$$P_{fa} = P(X > \alpha\mu \mid H_0), \quad \mu \geq 0 \quad (2.78)$$

which can also be written as

$$\begin{aligned} P_{fa} &= \int_0^{\infty} P(X > \alpha\mu \mid H_0) f_{\mu}(\mu) d\mu \\ &= E_{\mu} \langle P(X > \alpha\mu \mid H_0) \rangle \end{aligned} \quad (2.79)$$

Similarly the probability of detection P_d is given by

$$\begin{aligned}
P_d &= \int_0^{\infty} P(X > \alpha\mu | H_1) f_{\mu}(\mu) d\mu \\
&= E_{\mu} \langle P(X > \alpha\mu | H_1) \rangle
\end{aligned} \tag{2.80}$$

The CA-CFAR detection performance analysis in K-distributed clutter is given in Chapter 3 in detail.

There is an inherent loss of detection probability in a CFAR processor compared with the fixed threshold detection performance. This is because the CFAR processor sets the threshold by estimating the local clutter level within a finite reference window. This loss is explained in detail in Section 2.3.3.

In addition to the standart CA-CFAR, a large number of variants have been proposed to mitigate some of specific problems in practical scenerios. Some of the more common variants are Greater of CFAR (GO-CFAR), Smaller of CFAR (SO-CFAR), Order Statistics CFAR (OS-CFAR), Trimmed mean CFAR (TM-CFAR) and Censored Mean CFAR (CM-CFAR). The configuration of GO-CFAR uses the greater of mean level estimates either side of the test cell. In contrast, SO-CFAR uses the smaller of the mean level estimates either side of the CUT. In OS-CFAR the range cells in CFAR window is ranked to give ordered samples. The clutter power is estimated from the magnitude of the k th largest cell. In TM-CFAR the samples are ranked according to magnitude and T1 samples are trimmed from the lower end and T2 samples trimmed from upper end. Another approach is CM-CFAR in which the largest n samples of the window samples ranked according to the magnitude. The remaining $M - n$ samples are averaged to estimate the clutter mean level as the normal CA-CFAR. [19] Thus, the selection of particular CFAR technique depends mainly on the structure of background interference.

2.3.2.1. CA-CFAR Detection in Rayleigh Noise

For CA-CFAR detection of Rayleigh noise with linear detector, the equations

relating P_{fa} to α is not easy to calculate for both single and multiple pulse detection. Therefore the results are obtained again by MC simulations.

Figure 2-17 shows a plot of $\log_{10} P_{fa}$ as a function of threshold multiplier α for various sizes of CA-CFAR window, M . The solid lines are obtained both by MC simulation. A closed form expression in (2.81) suggested by [25] is also shown in Figure 2-17.

$$P_{fa} = \left[1 + \frac{\alpha^2}{M \left[c - (c-1) \exp(-m+1) \right]} \right] \quad (2.81)$$

where $c = 4/\pi$.

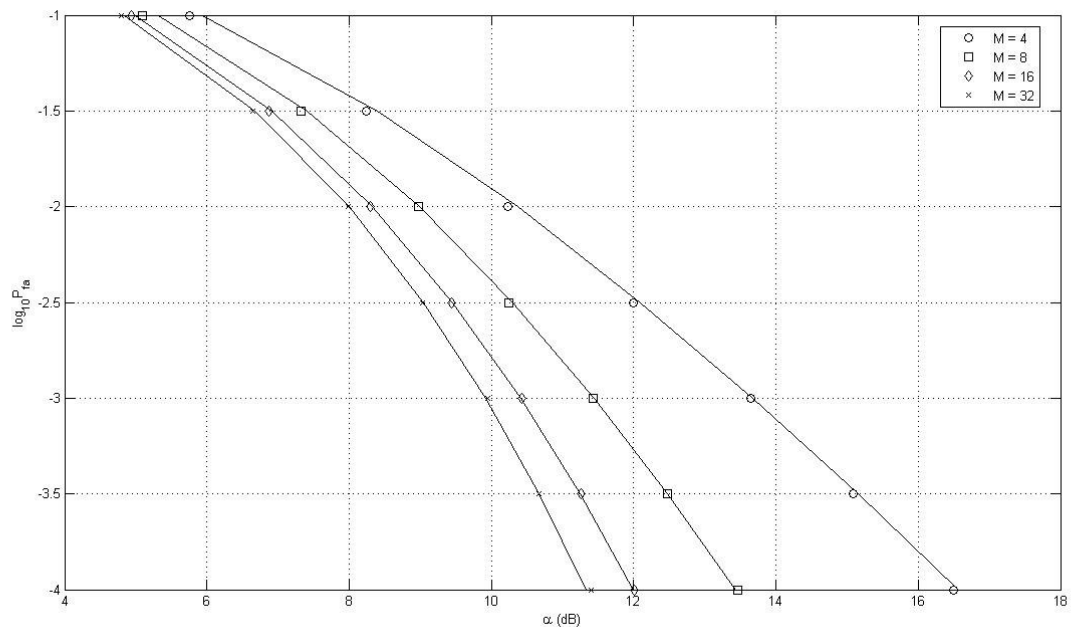


Figure 2-17 $\log_{10} P_{fa}$ vs. α graph of closed form (represented by solid lines) and simulated results for single pulse CA-CFAR detection of Rayleigh noise

It can be seen in Figure 2-17 that simulation results show good agreement with the

results obtained from (2.81).

In the following figures from Figure 2-18 to Figure 2-21, $\log_{10} P_{fa}$ is given as a function of α for multiple pulse CA-CFAR detection of Rayleigh noise.

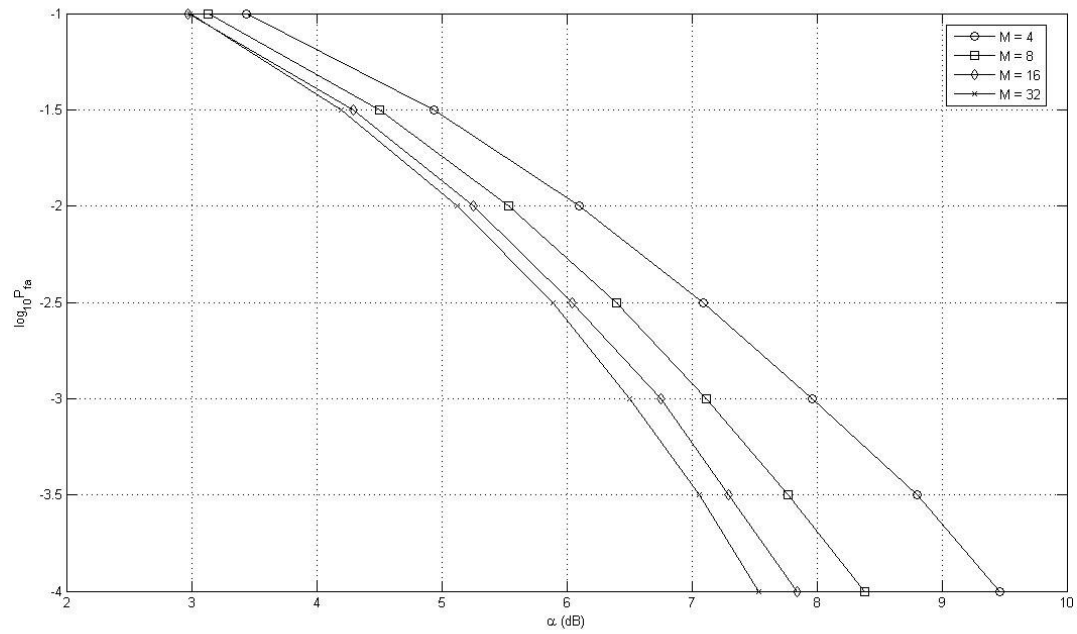


Figure 2-18 $\log_{10} P_{fa}$ vs. α for 3 pulse CA-CFAR detection of Rayleigh noise

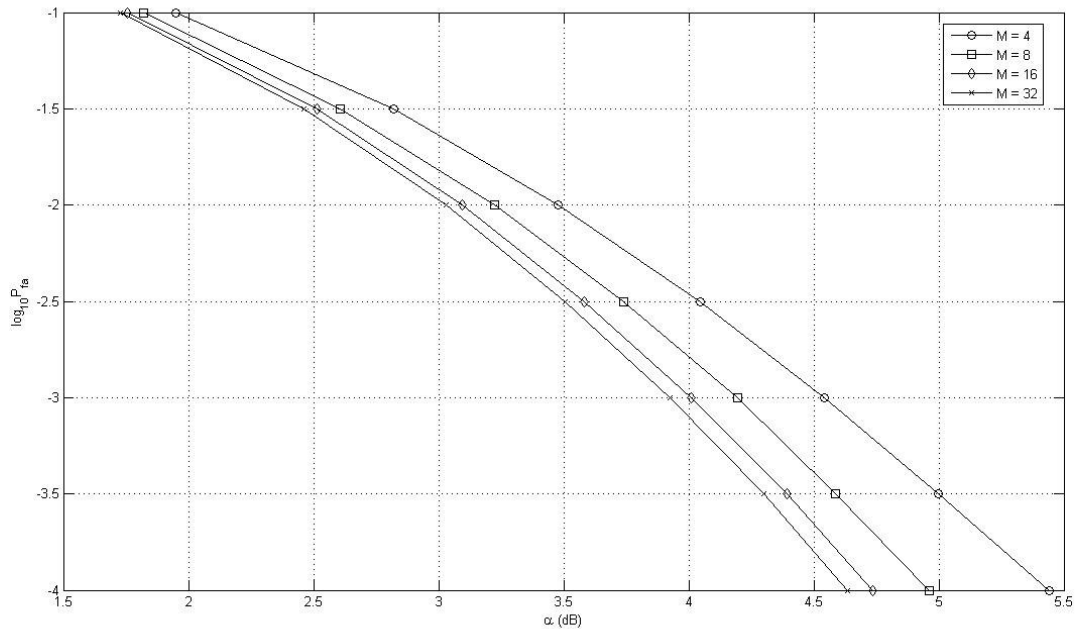


Figure 2-19 $\log_{10} P_{fa}$ vs. α for 10 pulse CA-CFAR detection of Rayleigh noise

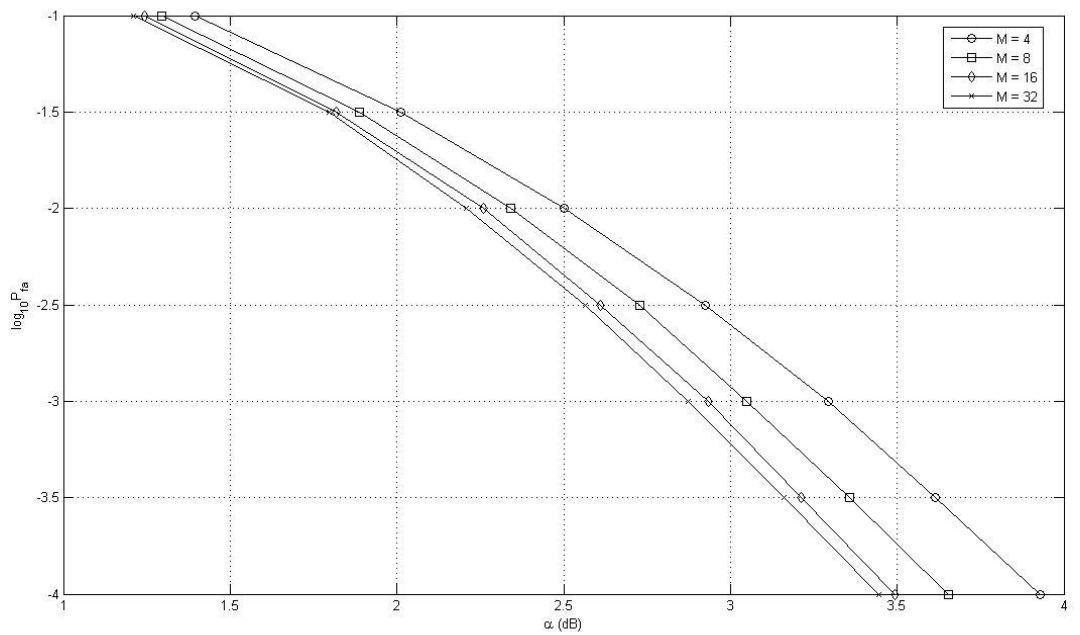


Figure 2-20 $\log_{10} P_{fa}$ vs. α for 20 pulse CA-CFAR detection of Rayleigh noise

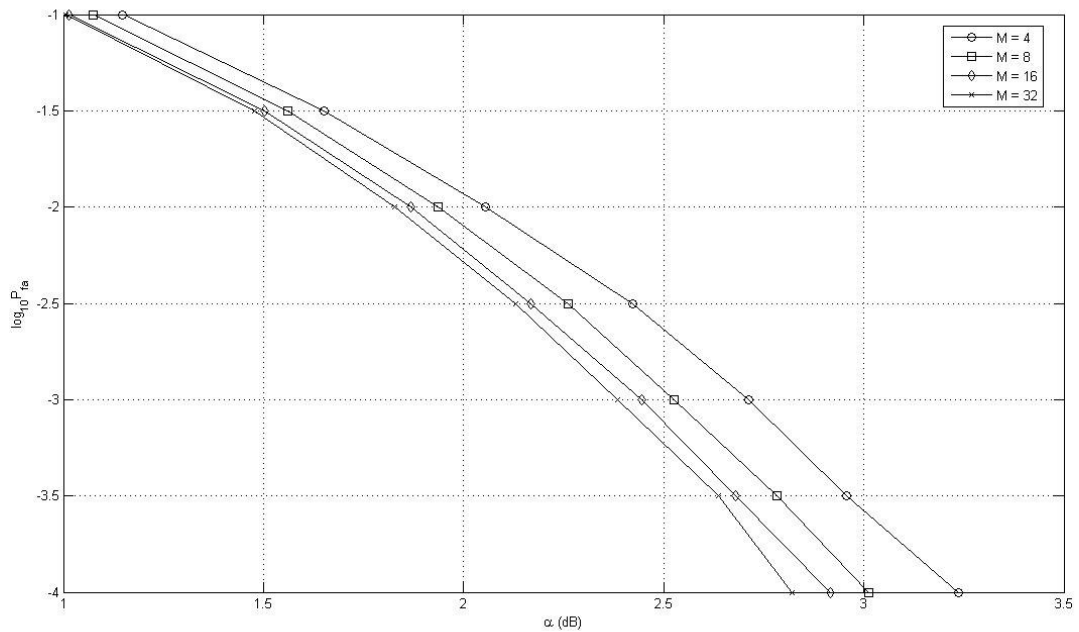


Figure 2-21 $\log_{10} P_{fa}$ vs. α for 30 pulse CA-CFAR detection of Rayleigh noise

From Figure 2-18 to Figure 2-21 it is seen that as M increases, the threshold multiplier, α decreases for any particular P_{fa} . Similarly, the increase in the number of pulses integrated, N reduces α . These conclusions means that the longer CA-CFAR window size and the more pulses integrated better detection performance is achieved.

2.3.3. CFAR Loss

There is an inherent loss of detection probability in a CA-CFAR processor compared with the fixed threshold detection performance in homogeneous noise and/or clutter background. This is because the CA-CFAR processor sets the threshold by estimating the clutter mean level within a finite CA-CFAR window. The fixed threshold detection, on the other hand, sets a fixed threshold under the assumption that the clutter statistics are known a priori. This relative performance loss of a CA-CFAR processor is called the CFAR loss.

There are two different methods that may be employed to measure the CFAR loss. It is generally quantified by the increase in the SCR needed for the CA-CFAR processor scheme to achieve a certain probability of detection and probability of false alarm relative to the fixed threshold detection. This true CFAR loss will be a function of the particular CFAR scheme, the target type and probability of detection, P_d as well as the clutter statistics and the probability of false alarm, P_{fa} [16].

A P_d versus SCR graph of Swerling type II (SW-II) target including the fixed detection threshold curve are given in Figure 2-22 for $P_{fa} = 10^{-4}$, $M = 16$ and $\nu = 0.5$. Here the CFAR loss calculation is also shown for sample values of P_d (0.5 and 0.9).

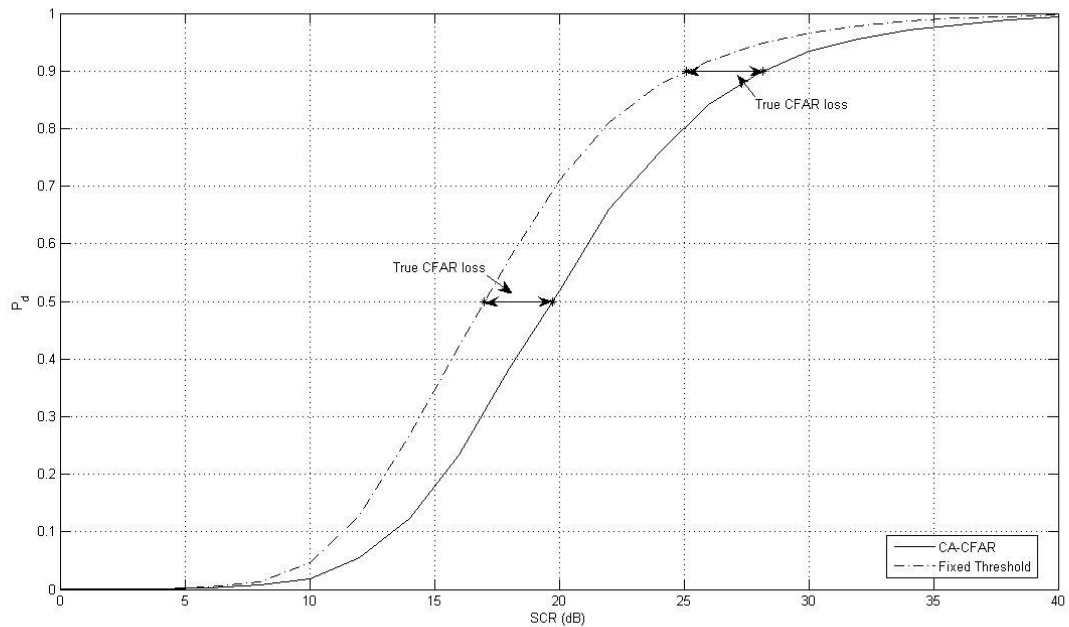


Figure 2-22 True CFAR loss calculation from P_d vs. SCR of single pulse detection for SU clutter with $\nu = 0.5$, SW-II target, $P_{fa} = 10^{-4}$ and $M = 16$

Alternatively, another method related to the threshold multiplier, α may be used. This one is based on the fact that the threshold, T_{CFAR} and P_d are closely related to each other. As T_{CFAR} increases, P_d decreases accordingly and vice versa. The increased value of T_{CFAR} means the increased value of α and for a given value of P_{fa} , the increased value of α implies that a higher value of SCR will be required to achieve a given value of P_d . Since the CFAR loss is defined as the increase in SCR relative to the fixed threshold detection, the increase in α can also be taken as a good guide to the CFAR loss [16]. For $P_d = 0.5$, this increase is very close to the true CFAR loss calculated from the change in SCR for a given P_{fa} [18]. This establishes a useful technique for measuring the CFAR loss which is independent of the detection probability. In this thesis this method is called as threshold multiplier method. Figure 2-23 shows this approximate CFAR loss from $\log_{10} P_{fa}$ versus α curves of fixed threshold and CA-CFAR detection for $\nu = 0.5$ and $M = 16$. As [16] implies, in most circumstances the change in α is a reliable guide to relative CFAR performance for P_d values of about 0.5.

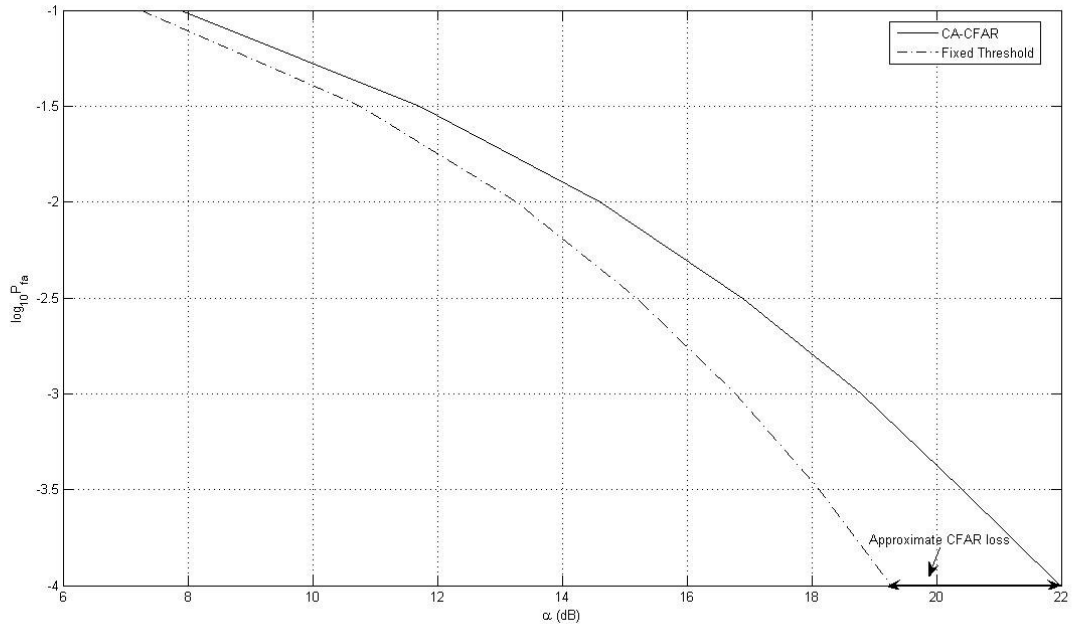


Figure 2-23 CFAR loss calculation from $\log_{10} P_{fa}$ vs. α of single pulse detection for SU clutter with $\nu = 0.5$ and $M = 16$

A significant difference between the two methods is that the threshold multiplier method calculates the CFAR loss using only the clutter from $\log_{10} P_{fa}$ versus α curves, however true CFAR loss calculation takes into account the target type since P_d versus SCR curves are used to set the true CFAR loss. As a result, CFAR loss results in threshold multiplier method is independent of target type.

If the clutter exhibits significant spatial correlation the CA-CFAR may be able to follow the local fluctuations, giving an improvement in performance or ‘CFAR gain’ compared to the fixed threshold [18]. The limit of such improvement is described by the concept of ideal CFAR detection.

2.3.4. Ideal CFAR Detection

As explained previously, it is possible to estimate the local mean level by using CA-CFAR. In the limiting case, where the threshold follows underlying mean level of K-distributed clutter exactly the best performance could be achieved. This type of detection is known as ideal CA-CFAR performance. However, as [16] mentions it may often not be practical to obtain the ideal CA-CFAR performance.

In order to achieve a threshold following underlying mean level, independent samples of the speckle component should be obtained and the modulation process should be assumed to be constant within the CA-CFAR window, but to vary widely between CA-CFAR window locations according to the overall generalised Chi-square PDF. The clutter is still assumed to be K-distributed, however the mean power of the locally Rayleigh clutter being modulated by a square root of gamma distributed variable over an extended area. Since the clutter in the CA-CFAR window is Rayleigh distributed, the CA-CFAR processor will perform as expected for Rayleigh noise except an additional source of fluctuation introduced by the modulation process.

Mathematically, the overall P_{fa} for fixed threshold detection can be also be written as

$$P_{fa} = \int_0^{\infty} P_{fa}(x|y) f_Y(y) dy \quad (2.82)$$

Here $f_Y(y)$ is the PDF of local clutter level of generalised Chi distribution given in (2.3) and $P_{fa}(x|y)$ is the P_{fa} of Rayleigh distributed speckle component which is written for given y as

$$\begin{aligned}
P_{fa}(x|y) &= \int_T^{\infty} f_{x,y}(x|y) dx \\
&= \int_T^{\infty} \frac{x}{y^2 \sigma^2} \exp\left(-\frac{x^2}{2y^2 \sigma^2}\right) dx \\
&= \exp\left(-\frac{T^2}{2y^2 \sigma^2}\right)
\end{aligned} \tag{2.83}$$

Here $\sigma = \sqrt{\frac{2}{\pi}}$.

The threshold is the multiplication of the threshold multiplier α and the overall mean clutter level. However, for ideal CFAR detection it is assumed that the threshold adapts exactly to the local mean intensity of the clutter level, y . The ideal CFAR threshold, T , is thus:

$$T = \alpha y \tag{2.84}$$

When this is substituted into (2.83), $P_{fa}(x|y)$ now becomes

$$P_{fa}(x|y) = \exp\left(-\frac{\pi\alpha^2}{4}\right) \tag{2.85}$$

Using (2.3) the overall P_{fa} will be averaged as follows

$$\begin{aligned}
P_{fa} &= \int_0^{\infty} P_{fa}(x|y) f_Y(y) dy \\
&= \frac{2b^{2v}}{\Gamma(v)} \exp\left(-\frac{\pi\alpha^2}{4}\right) \int_0^{\infty} y^{2v-1} \exp(-b^2 y^2) dy
\end{aligned} \tag{2.86}$$

When the equation of the overall P_{fa} in (2.86) can be solved using the integral equation given below from [21]

$$\int_0^{\infty} x^m \exp(-\beta x^n) dx = \frac{\Gamma(\gamma)}{n\beta^\gamma}, \quad \gamma = \frac{m+1}{n} \quad (2.87)$$

Finally the overall P_{fa} now becomes

$$P_{fa} = \exp\left(-\frac{\pi\alpha^2}{4}\right) \quad (2.88)$$

Since ideal CA-CFAR detection curves are useful guides to the bounds of possible performance, using the equation in (2.88), the P_d versus SCR graphs are evaluated by MC simulation for SW-II target. Figure 2-24 and Figure 2-25 show the P_d versus SCR curves for various ν and single pulse detection. The curves in Figure 2-24 is for $P_{fa} = 10^{-3}$ and the ones in Figure 2-25 is for $P_{fa} = 10^{-4}$.

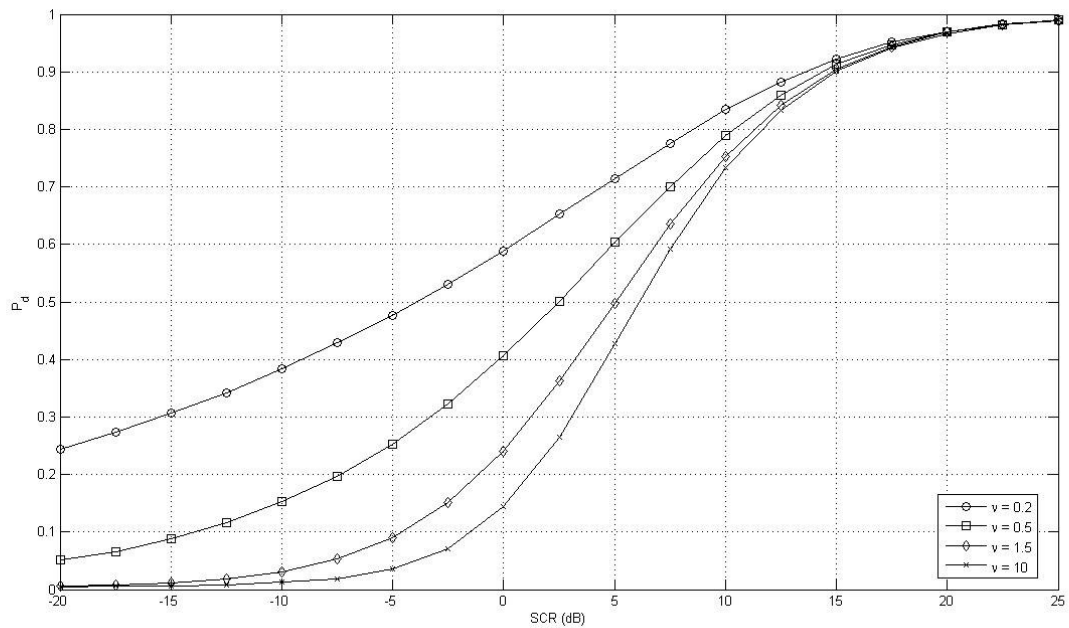


Figure 2-24 P_d vs. SCR curves of ideal CFAR detection for SU clutter, SW-II target,

$$P_{fa} = 10^{-3} \text{ and } N = 1$$

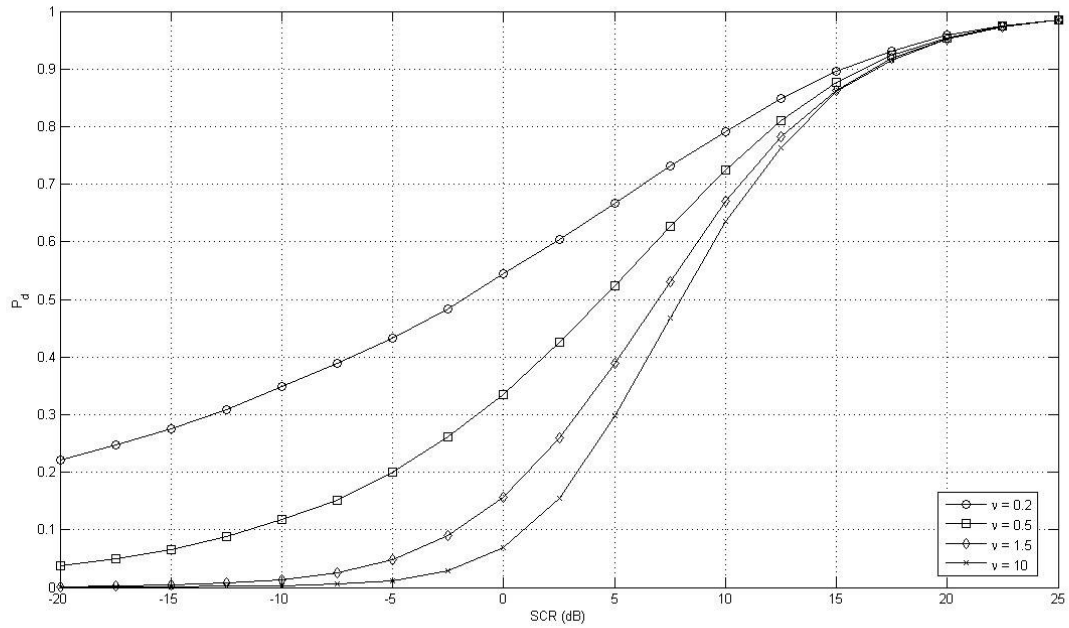


Figure 2-25 P_d vs. SCR curves of ideal CFAR detection, for SU clutter, SW-II target,

$$P_{fa} = 10^{-4} \text{ and } N = 1$$

As seen from Figure 2-24 and Figure 2-25, as might be expected if lower P_d or higher P_{fa} is to be achieved, the required SCR reduces. Moreover, for ideal CA-CFAR detection the best performance is achieved in the spikiest clutter. As [19] mentions, this is an expected result since as in very spiky clutter the clutter has very low local mean level between very large spikes. In these regions a target is more easily detected, provided that the threshold adapts appropriately.

Figure 2-26 shows a comparison for ideal CA-CFAR and fixed threshold detection curves. Here again true CFAR gain is represented as the difference in SCR between curves for a specific P_d .

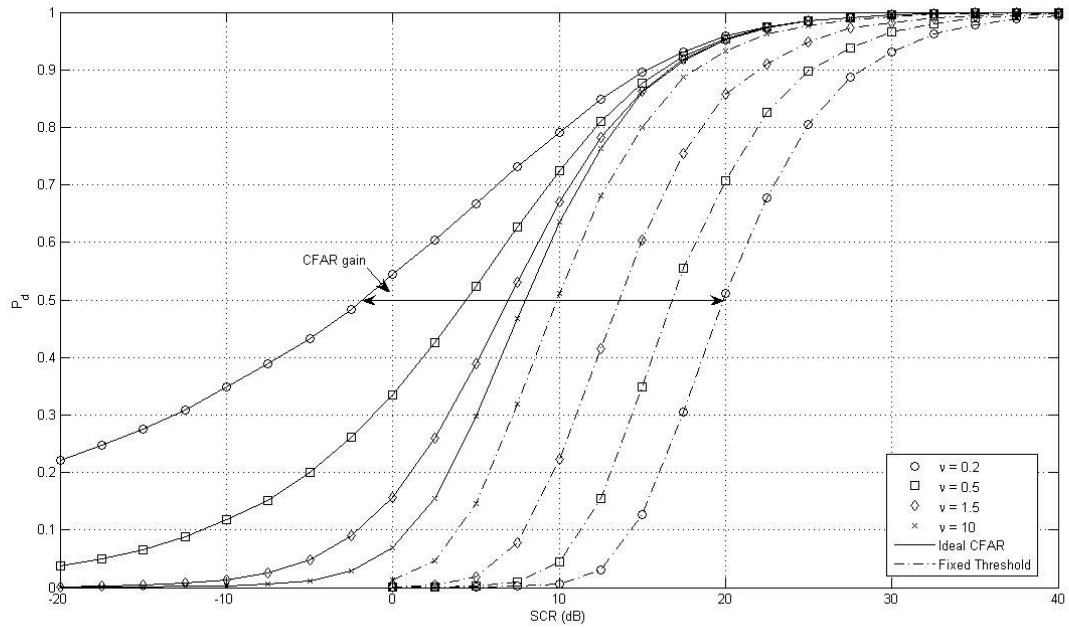


Figure 2-26 Conventional fixed threshold (dashed dotted curves) and ideal CFAR performance (solid curves), P_d vs. SCR curves for SU clutter, SW-II target,

$$P_{fa} = 10^{-4} \text{ and } N = 1$$

It can be seen that the CFAR gain is very large in spiky clutter, the ideal CFAR gain for $\nu = 0.2$ with $P_d = 0.6$ and $P_{fa} = 10^{-4}$ is ~ 20 dB. Table 2-2 shows the exact values of ideal CFAR gains for various shape parameters, P_{fa} values of 10^{-3} and 10^{-4} and P_d values of 0.5 and 0.9. Of course this ideal performance is predicated on knowing exactly the local mean level of the clutter.

Table 2-2 Ideal CFAR gains over fixed threshold detection

	$P_{fa} = 10^{-3}$		$P_{fa} = 10^{-4}$	
	$P_d = 0.5$	$P_d = 0.9$	$P_d = 0.5$	$P_d = 0.9$
$\nu = 0.2$	20.5167	11.5063	21.5683	12.7382
$\nu = 0.5$	11.5072	8.1108	12.3327	8.6940
$\nu = 1.5$	5.8186	4.5688	6.5374	5.1549
$\nu = 10$	1.3690	1.2281	1.7327	1.2586

It is unlikely that a CA-CFAR would be able to estimate the local mean level exactly. However, where significant correlation is present it may be possible to achieve some CFAR gain which is the main concern of this thesis and will be discussed with simulation results in the following chapter.

Before giving the detailed performance evaluations, it may be informative to comment on this CFAR gain with the help of Figure 2-27. In this figure P_d versus SCR curves for ideal CFAR, CA-CFAR and fixed threshold detection are shown for $\nu = 1.5$ and $P_{fa} = 10^{-4}$. The CA-CFAR window size is taken 16.

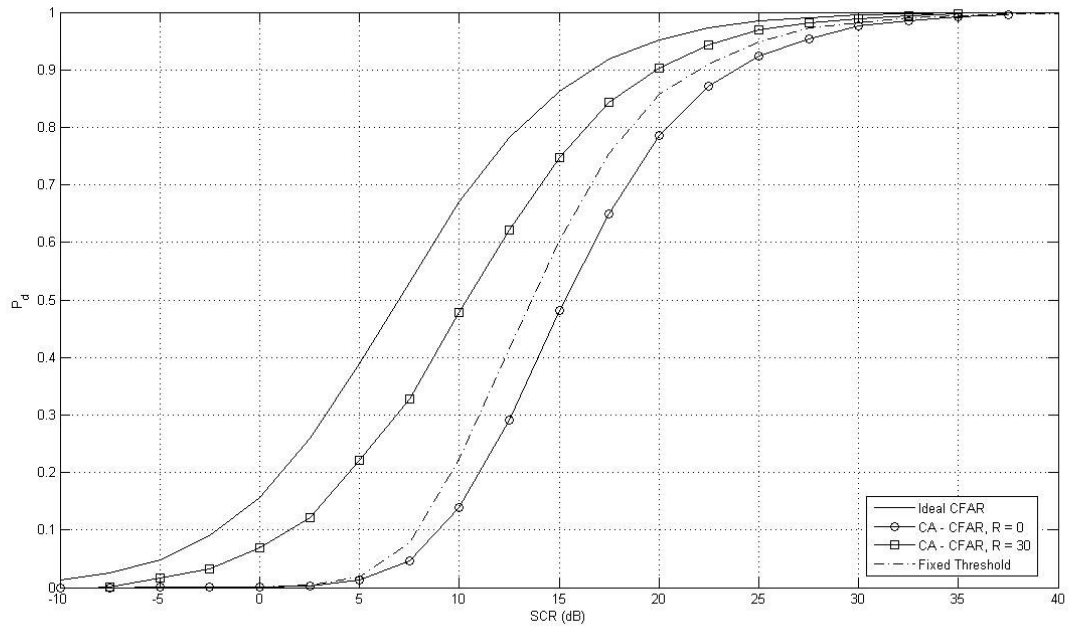


Figure 2-27 P_d vs. SCR curves of ideal CFAR, CA-CFAR and fixed threshold detection for clutter with $\nu = 1.5$ for correlation lengths $R = 0$ and $R = 30$,

$$P_{fa} = 10^{-4} \text{ and } M = 16$$

In Figure 2-27 the solid line represents the ideal CFAR detection, by which the upper bound of performance achievement relative to the fixed threshold detection shown by dashed dotted line is obtained. For uncorrelated clutter ($R = 0$) the CA-CFAR curve is at the left side of the fixed threshold curve which indicates that there is a CFAR loss. However, when clutter is highly correlated ($R = 30$) significant improvement in performance is seen, hence a CFAR gain is obtained.

CHAPTER 3

PERFORMANCE ANALYSIS

3.1. ASSUMPTIONS MADE

It is assumed in this thesis that the radar operates in a homogeneous background, in other words, no other target interfering the CFAR window and the background has the same clutter distribution with the cell under test (CUT). Also the target return locates in one single CA-CFAR cell, i.e., target is not extended. Therefore it is not necessary to use guard cells for CA-CFAR processing.

The simulated K-distributed clutter samples are assumed to have unity mean square.

In order to estimate the mean clutter level using CA-CFAR processor the samples are taken from the linear detector. In [26] the results of linear detector is compared with those of a square law detector for noise. It is shown there that there is a negligible difference between the expected performance of both types of detectors. Another similar conclusion that linear and square law CA-CFAR processors provide nearly the same detection performance is made for K-distributed clutter in [25].

The target in CUT has amplitude fluctuation of SW-II, which means the echo pulses received from the target fluctuates independently from one pulse to another

and the PDF for the radar cross section (RCS) of target is

$$p(\sigma) = \frac{1}{\sigma_{av}} \exp\left(-\frac{\sigma}{\sigma_{av}}\right) \quad (3.1)$$

where σ_{av} is the average over all values of target RCS. This exponential PDF represents the statistics of the square of a voltage which is described by a Rayleigh PDF. The details of changing variables from Rayleigh PDF of voltage to exponential PDF of power are explained in detail in Appendix A.3.

The independency of pulse to pulse is obtained by assuming the radar has pulse to pulse frequency agility, pulse to pulse change in frequency.

The signal to clutter ratio (SCR) is obtained using the mean square values for both Rayleigh distributed voltage signal of SW-II target, s and K-distributed clutter amplitude signal, c . Since the assumption of unity mean square K-distributed clutter is made, (3.2) gives the mean SCR.

$$\frac{S}{C} = \frac{E\langle s^2 \rangle}{E\langle c^2 \rangle} = \sigma_{av} \quad (3.2)$$

In this thesis by SCR, mean SCR is meant.

Integration of pulses before CA-CFAR processor is assumed to be performed over times short enough that target remains within a single cell resolvable by the radar.

While integrating pulses, it is always assumed that for pulse to pulse integration the speckle component of the clutter (equation in (2.7)) is fully decorrelated due to the use of frequency agility between pulses, whilst the underlying mean (equation in (2.3)) remains constant at a given range over the integration interval, as described in [11].

In order to obtain desired P_{fa} versus threshold multiplier graphs $100/\min(P_{fa})$ number of MC simulations are made. This simulation number is high enough to

result in accurate P_{fa} 's since the results are verified with the literature and the analytic solution for CA-CFAR detection with K-distributed clutter for $\nu = 0.5$. The detailed verification results are given in Section 3.3.

3.2. SIMULATION STEPS

In this thesis there are two main simulations;

- First one sets the threshold multiplier, α for a given P_{fa} and results in P_{fa} versus α curves.
- The other one determines the P_d versus SCR curves using α obtained in the previous simulation.

In order to obtain desired P_{fa} versus threshold multiplier, α , curves for every MC simulation step the following steps are taken:

1. For given shape parameter ν , number of pulses integrated, N and correlation length, R correlated or uncorrelated linearly detected K-distributed clutter samples are generated and integrated if multi pulse case is desired. The method used in generating K-distributed clutter samples is the same as given in Section 2.2.4.3. The Matlab 7.0's `randn(.)` function is used for generating uncorrelated Gaussian distributed random samples.
2. CA-CFAR algorithm in Section 2.3.2 runs for the given window size, M and zero guard cell size. In this thesis 4, 8, 16, and 32 window sizes are simulated.
3. CA-CFAR threshold is set for given α .
4. If clutter exceeds CA-CFAR threshold, false alarm number is incremented; otherwise not.

Then, in order to obtain P_d versus SCR curves for every MC simulation step the following steps are taken:

1. Threshold multiplier is selected from P_{fa} versus α curves for the given P_{fa} .
2. The SW-II target is modelled for the given SCR. The Matlab 7.0's raylrnd(.) function is used for generating target signal.
3. CA-CFAR algorithm in Section 2.3.2 runs for the given window size, M and zero guard cell size.
4. CA-CFAR threshold is set for given SCR.
5. If target plus clutter exceeds CA-CFAR threshold, detection number is incremented; otherwise not.

CFAR loss graphs are acquired from both of these two type of curves by also using the fixed threshold detection curves. The results related to the CFAR loss is explained in the following Sections 3.4 and 3.5 in detail.

3.3. VERIFICATION OF APPROACHES

In order to verify the approaches used in this thesis, some verification is made with the literature.

At first in order to obtain high enough MC simulation number the analytic solution for CA-CFAR detection with K-distributed clutter of $\nu = 0.5$ is compared with the simulation results of threshold multiplier. The comparison show that the results are close to each other as given in Table 3-1.

Table 3-1 Comparison of analytic and simulation results for $\nu = 0.5$

$\log_{10} P_{fa}$	Threshold multiplier, α (dB)	
	Analytic solution result	Simulation result
-1	8.2635	8.2696
-2	15.3415	15.2925
-3	19.9588	20.0150
-4	23.5904	23.6521

The analytic solution exists for $\nu = 0.5$ and the equation for P_{fa} of CA-CFAR detection is given in (3.3).

$$\begin{aligned}
 P_{fa} &= \int_0^{\infty} \left(\int_t^{\infty} P_X(x) dx \right) P_T(t) dt \\
 P_X(x) &= 2c \exp(-2cx) \\
 P_T(t) &= \frac{2cM}{\alpha \Gamma(M)} \left(\frac{2cMt}{\alpha} \right)^{M-1} \exp\left(-\frac{2cMt}{\alpha}\right)
 \end{aligned} \tag{3.3}$$

Here $P_X(x)$ is the PDF of the K-distribution of $\nu = 0.5$, $P_T(t)$ is the PDF of the CA-CFAR threshold and is assumed to be the PDF of the sum of M independent K-distributed samples and α is the threshold multiplier. (3.3) simply becomes the (3.4) which is solved by the help of an integral equation solution given in (3.5) from [21].

$$P_{fa} = \frac{1}{\Gamma(M)} \left(\frac{2cM}{\alpha} \right)^M \int_0^{\infty} t^{M-1} \exp\left(-2ct \left(1 + \frac{M}{\alpha}\right)\right) dt \tag{3.4}$$

$$\int_0^{\infty} \lambda^{\zeta-1} \exp(-\mu\lambda) d\lambda = \mu^{-\zeta} \Gamma(\zeta) \quad (3.5)$$

After changing the variables according to (3.5), overall P_{fa} yields;

$$P_{fa} = \left(\frac{M}{M + \alpha} \right)^M \quad (3.6)$$

Secondly, the results are compared with the CA-CFAR loss versus $-\log_{10}(P_{fa})$ figures for various shape parameters and cell sizes given for single pulse detection in linearly detected K-distributed clutter in [18]. It is seen that there is a good agreement between the simulation results of this thesis and [18].

Finally, the results are compared with the ones given in [2]. However, the loss curves presented in [2] have illustrated the overall detection loss, L_t . To determine the CFAR loss, L_{CFAR} , it is necessary to determine the loss that an ideal detector would suffer in the same spiky clutter environment and subtract this from the overall loss. This ideal detector loss is equivalent to $S_{50}(v)$ which is defined by the empirical formula in [20]. Thus,

$$L_{CFAR} = L_t - S_{50}(v) \quad (3.7)$$

where $S_{50}(v)$ is given as

$$S_{50}(v) = -\beta \log_{10} \left(\frac{v}{v + v_0} \right) \quad (3.8)$$

$$\beta = 3.450n^{0.4}, \quad v = 5.72n^{0.2}$$

3.4. CA-CFAR DETECTION IN SPATIALLY UNCORRELATED (SU) K-DISTRIBUTED CLUTTER

3.4.1. Single Pulse Detection

In this section single pulse is used for detecting targets in homogeneous K-distributed clutter.

Firstly, the detection performance of CA-CFAR processors has been analysed for various values of $\log_{10} P_{fa}$, ν (0.2, 0.5, 1.5 and 10) and CA-CFAR window size, M (4, 8, 16 and 32) using threshold multiplier method as explained in Section 2.3.3. Results are shown in from Figure 3-1 to Figure 3-4, which plots the CFAR loss relative to the fixed threshold detection as a function of $\log_{10} P_{fa}$.

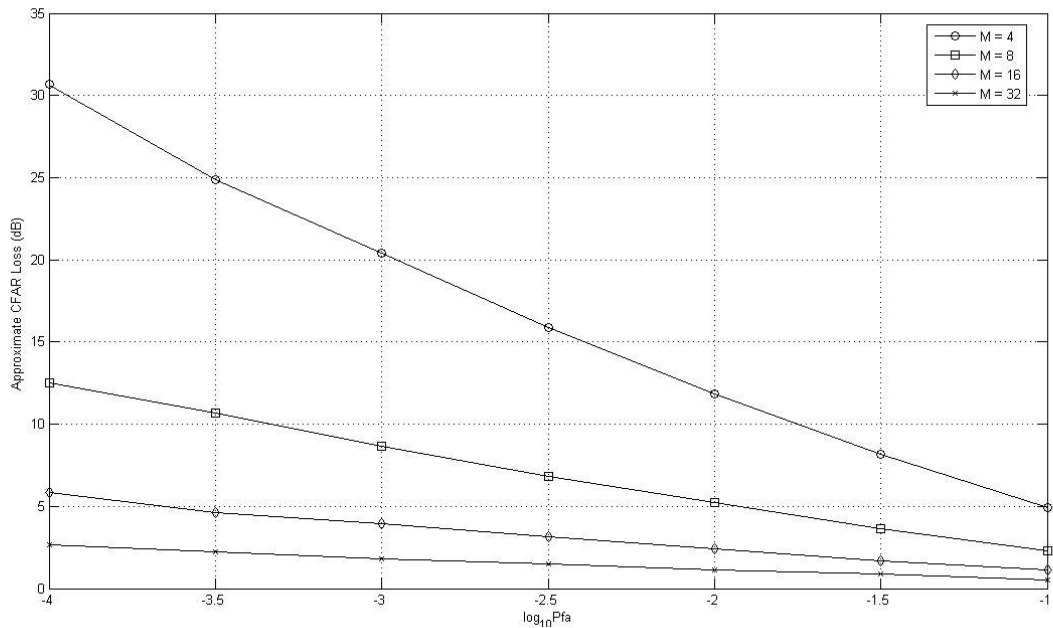


Figure 3-1 Approximate CFAR loss vs. $\log_{10} P_{fa}$ for SU clutter with $\nu = 0.2$ and

$$N = 1$$

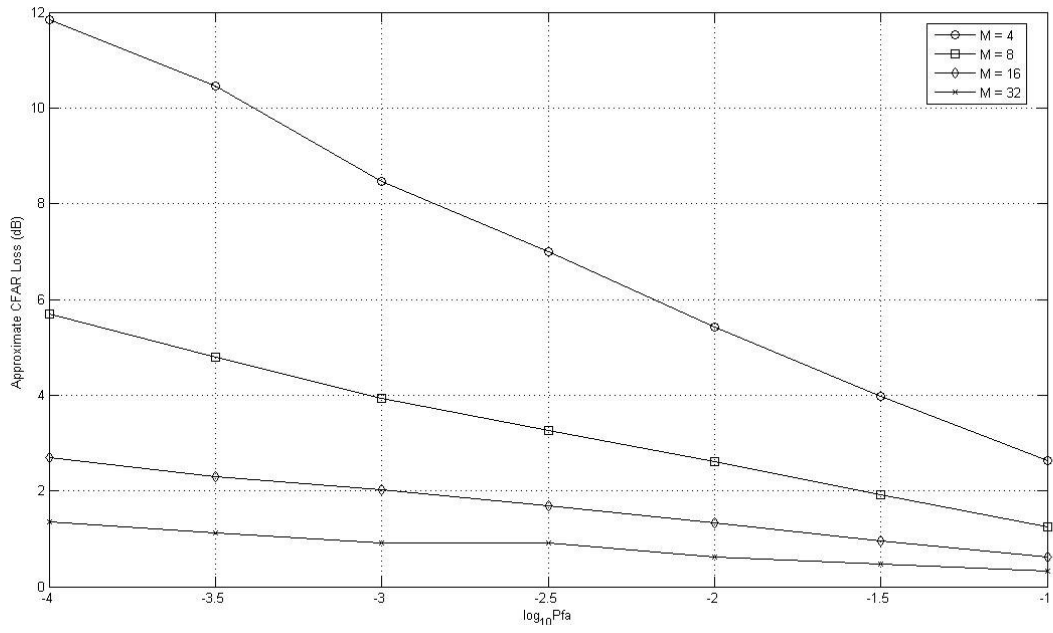


Figure 3-2 Approximate CFAR loss vs. $\log_{10} P_{fa}$ for SU clutter with $\nu = 0.5$ and $N = 1$

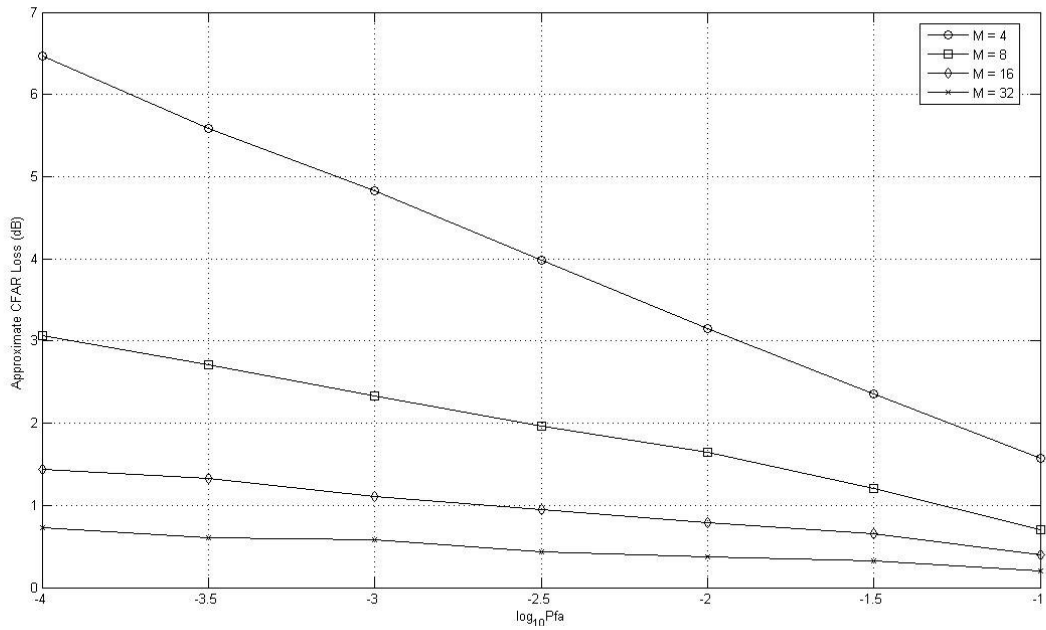


Figure 3-3 Approximate CFAR loss vs. $\log_{10} P_{fa}$ for SU clutter with $\nu = 1.5$ and $N = 1$

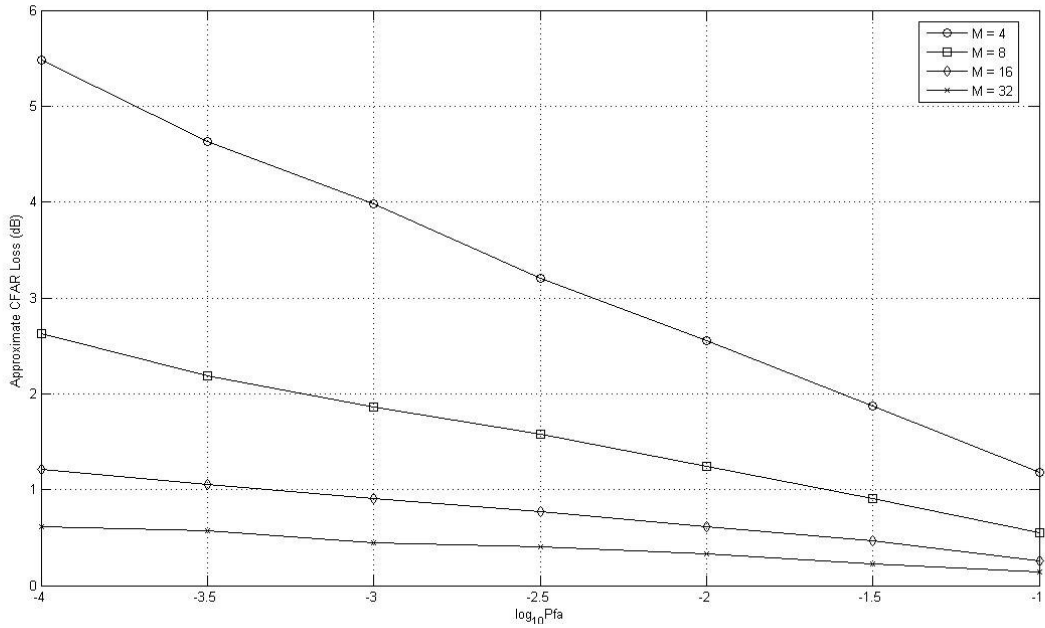


Figure 3-4 Approximate CFAR loss vs. $\log_{10} P_{fa}$ for SU clutter with $\nu = 10$ and $N = 1$

It is evident that the CFAR loss is strongly dependent on ν and is also fairly strongly dependent on CA-CFAR window size and the desired P_{fa} . For spiky clutter (e.g. $\nu = 0.2$) a CFAR loss of about almost 30 dB is possible for small CA-CFAR window size and low P_{fa} . The smaller the length of window size and the lower the desired P_{fa} , the CFAR loss increases and hence as [2] indicates, more sensitive the processor becomes to increasing clutter spikiness, i.e. lower values of ν .

Also the graphs of CFAR loss versus CA-CFAR window size M are given in Figure 3-5 for various shape parameter values and when P_{fa} is 10^{-4} . The dotted line in these figures represents the CFAR loss when Rayleigh distributed noise is present. As expected the values of noise are close to ones when K-distributed clutter of high shape parameter ($\nu = 10$).

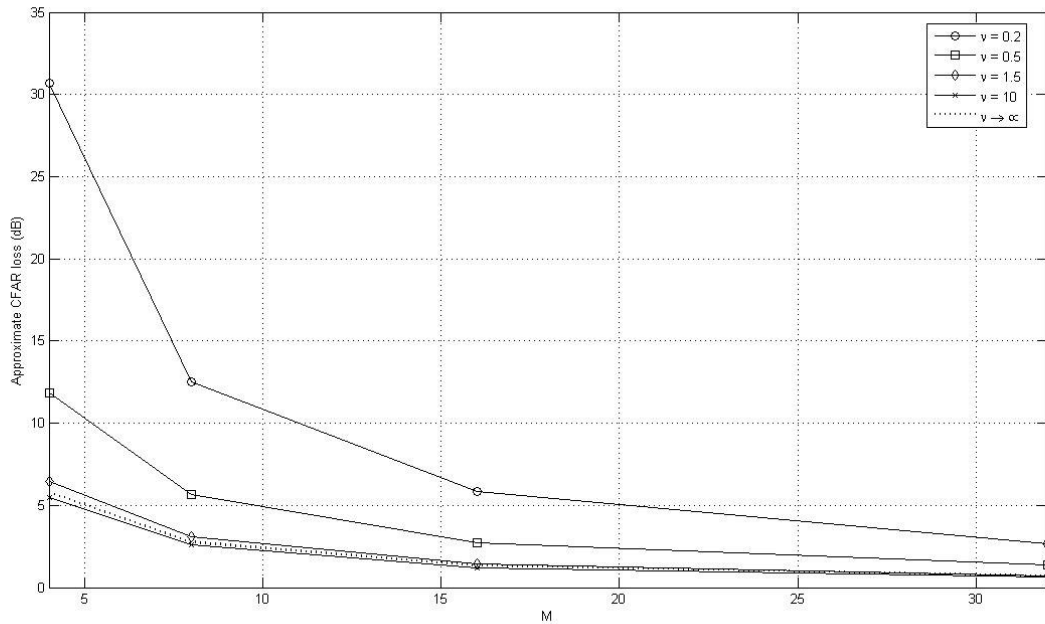


Figure 3-5 Approximate CFAR loss vs. M for SU clutter, $P_{fa} = 10^{-4}$ and $N = 1$

From Figure 3-5 the effect of window size is more evident. The longer the window size the less CFAR loss is obtained since better estimates are made with longer window size.

Table 3-2 provides a sample of data, giving the CFAR loss for CA-CFAR processor for ν (0.2, 0.5, 1.5 and 10) and M (4, 8, 16 and 32) for $P_{fa} = 10^{-4}$. It can be seen from Table 3-2 that a CFAR loss of greater than ~ 0.6 dB to ~ 5 dB can commonly be expected for decreasing values of M . The advantages of using large number of CA-CFAR cells can also be seen. The use of large number of CA-CFAR cells is more pronounced in spiky clutter. For instance the use of 16 as opposed to 32 CA-CFAR cells can introduce additional loss of ~ 0.6 dB to ~ 3.2 dB under from reasonable conditions and to more extreme, spiky cases.

Table 3-2 CFAR loss in dB for sample values of ν and M when $P_{fa} = 10^{-4}$ and $N = 1$

	$M = 4$	$M = 8$	$M = 16$	$M = 32$
$\nu = 0.2$	30.3700	12.5171	5.8457	2.6853
$\nu = 0.5$	11.8506	5.6881	2.7052	1.3530
$\nu = 1.5$	6.4703	3.0705	1.4417	0.7340
$\nu = 10$	5.4785	2.6248	1.2085	0.6126

P_d versus SCR graphs are also obtained using the previous simulation results for α . The resulting graphs with various ν are given in from Figure 3-6 to Figure 3-9 for the P_{fa} values of 10^{-3} and 10^{-4} and M values of 16 and 32 for SW-II target.

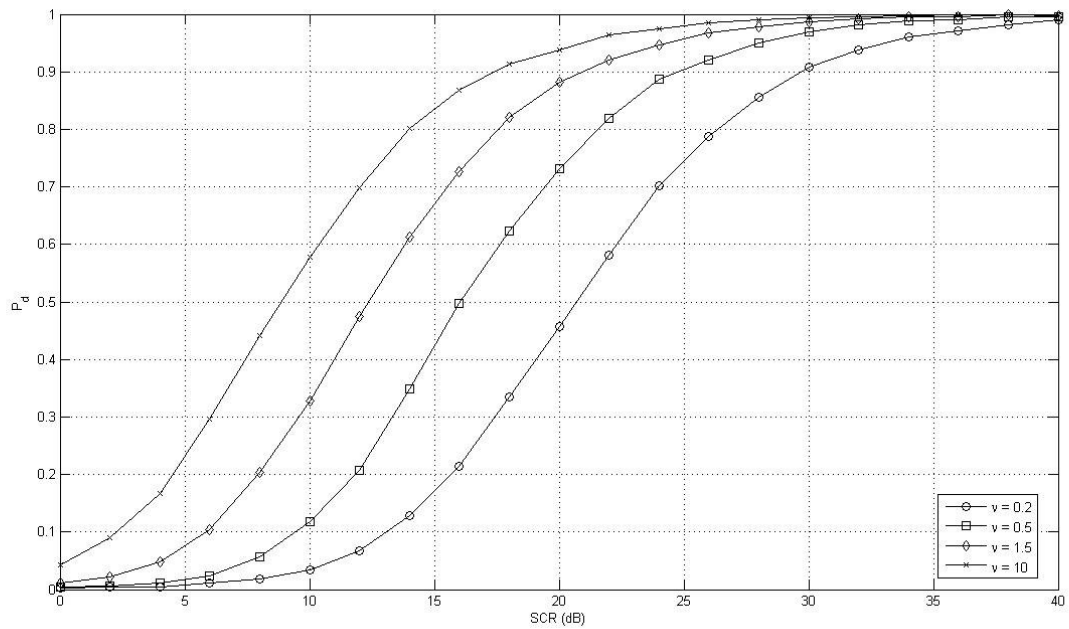


Figure 3-6 P_d vs. SCR for SU clutter, $P_{fa} = 10^{-3}$, SW-II target, $M = 16$ and $N = 1$

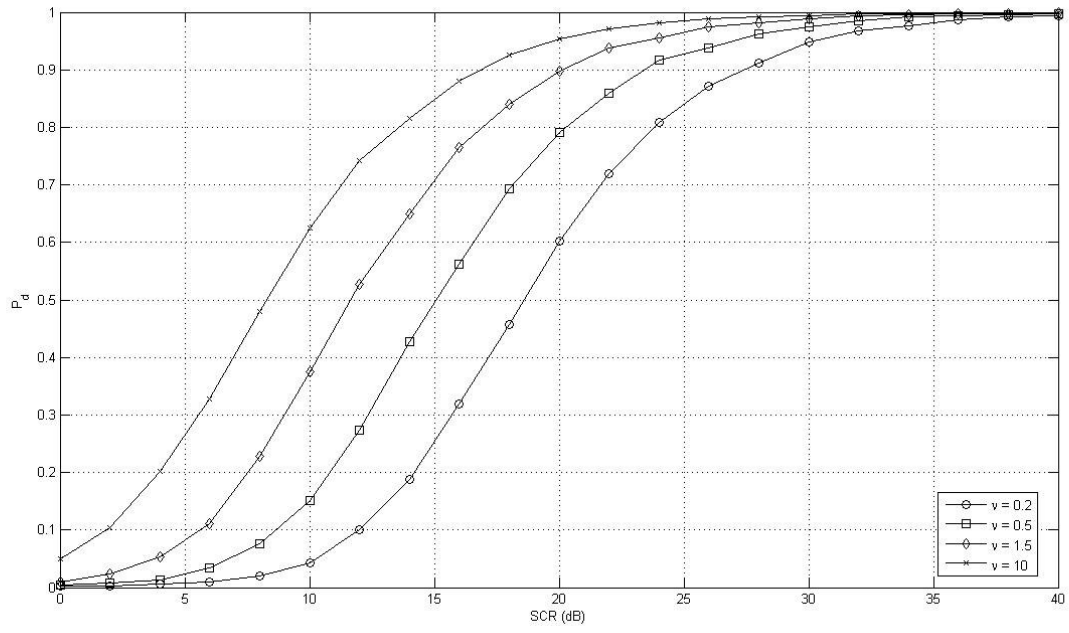


Figure 3-7 P_d vs. SCR for SU clutter, $P_{fa} = 10^{-3}$, SW-II target, $M = 32$ and $N = 1$

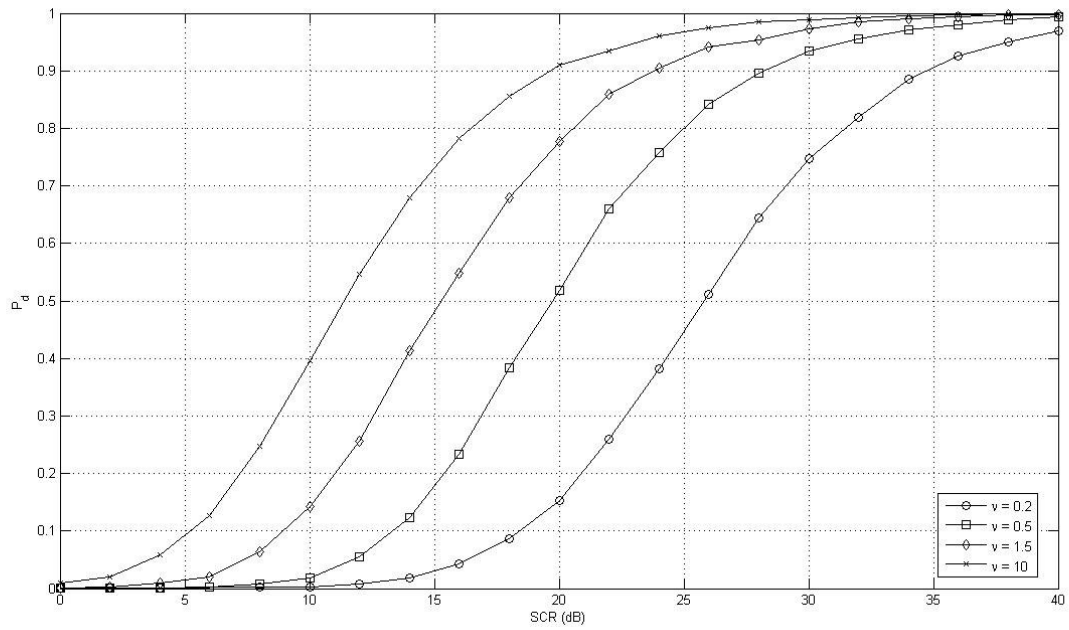


Figure 3-8 P_d vs. SCR for SU clutter, $P_{fa} = 10^{-4}$, SW-II target, $M = 16$ and $N = 1$

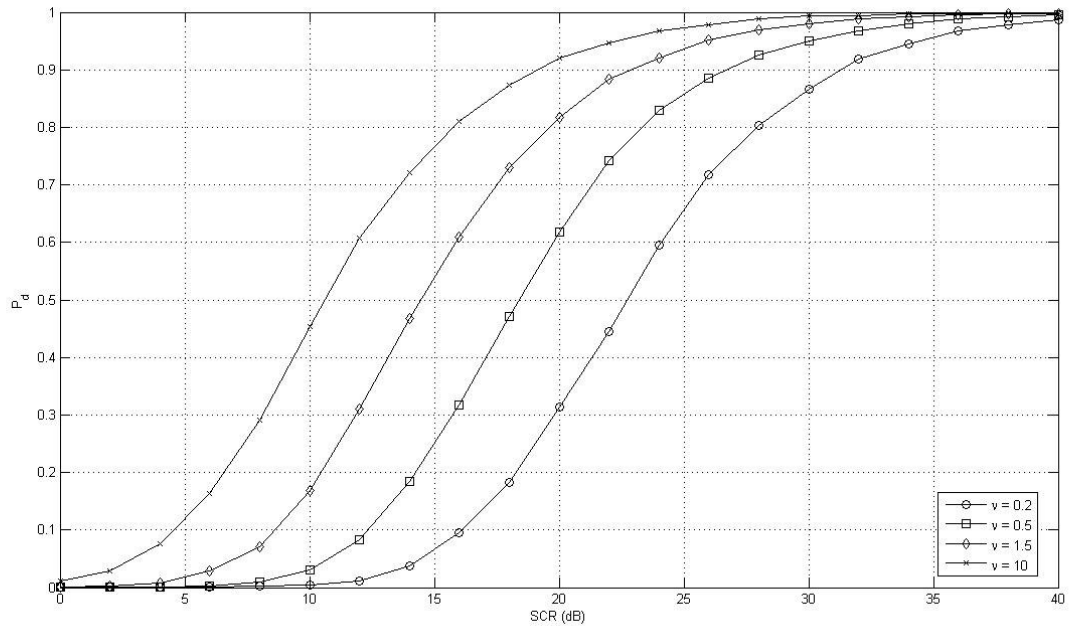


Figure 3-9 P_d vs. SCR for SU clutter, $P_{fa} = 10^{-4}$, SW-II target, $M = 32$ and $N = 1$

As explained in Section 2.3.3 the detection performance of CA-CFAR processors compared to fixed threshold detection can also be measured from the P_d versus SCR curves. This time, true CFAR loss calculation results are given from Figure 3-10 to Figure 3-13 for sample values of P_d (0.5 and 0.9), P_{fa} (10^{-3} and 10^{-4}), ν (0.2, 0.5, 1.5 and 10) and CA-CFAR window size, M (4, 8, 16 and 32).

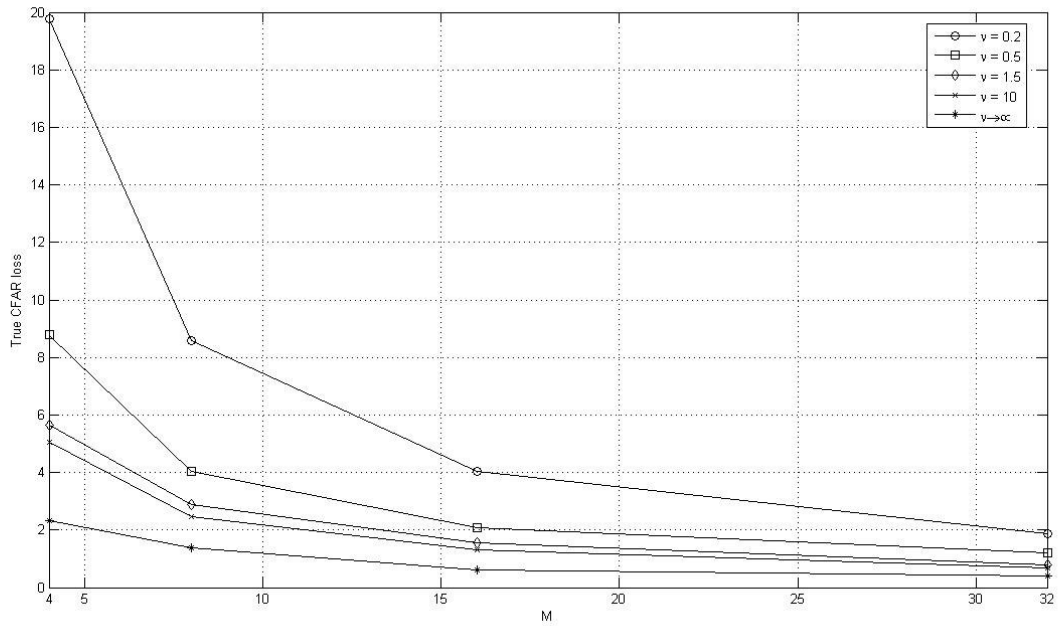


Figure 3-10 True CFAR loss vs. M for SU clutter, SW-II target, $P_{fa} = 10^{-3}$, $P_d = 0.5$ and $N = 1$

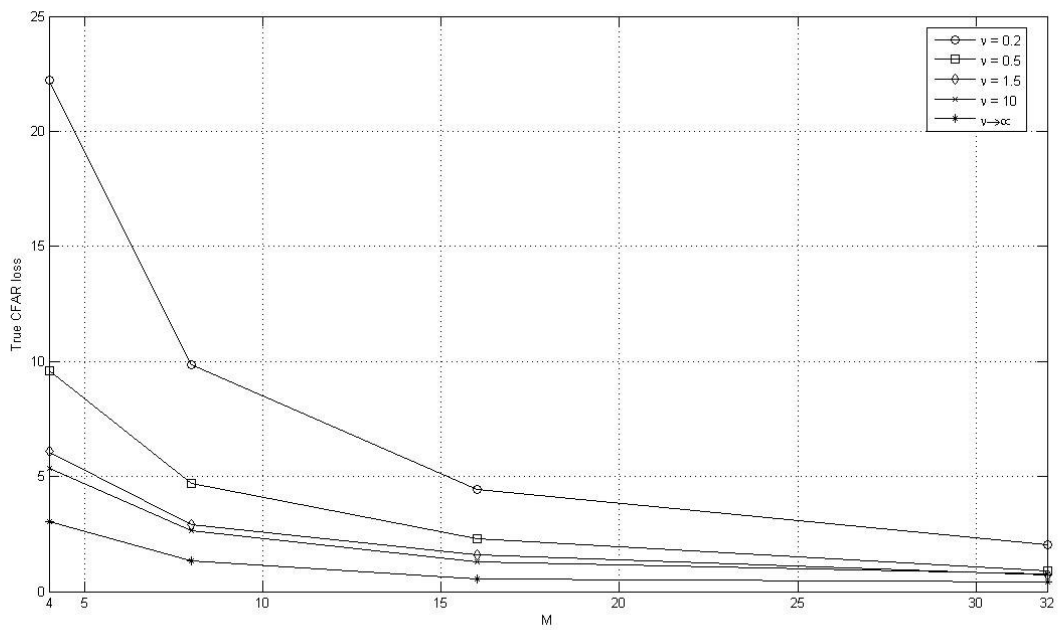


Figure 3-11 True CFAR loss vs. M for SU clutter, SW-II target, $P_{fa} = 10^{-3}$, $P_d = 0.9$ and $N = 1$

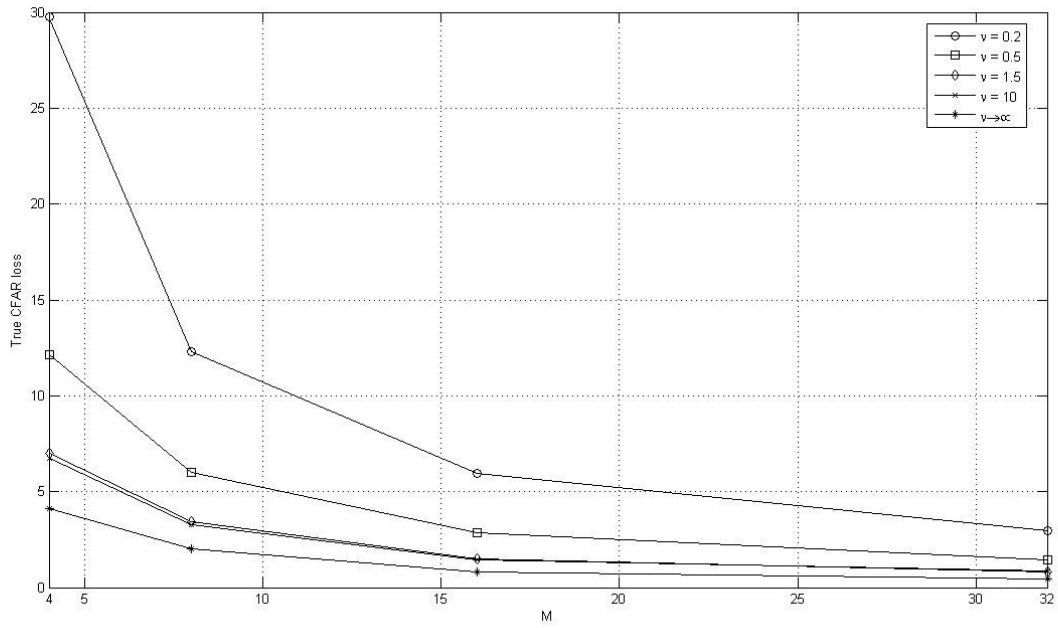


Figure 3-12 True CFAR loss vs. M for SU clutter, SW-II target, $P_{fa} = 10^{-4}$, $P_d = 0.5$ and $N = 1$

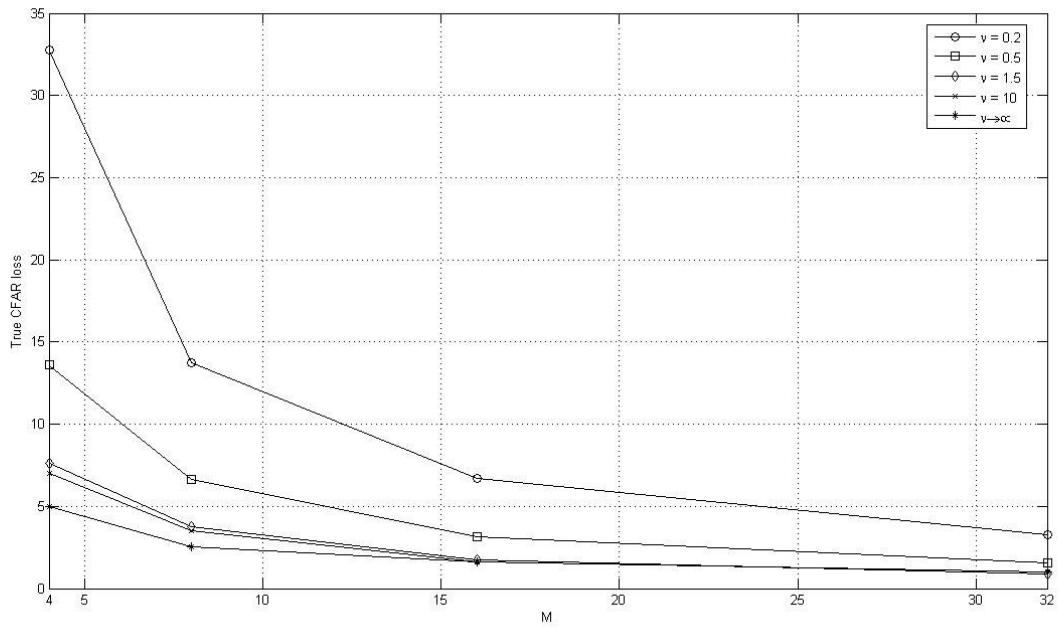


Figure 3-13 True CFAR loss vs. M for SU clutter, SW-II target, $P_{fa} = 10^{-4}$, $P_d = 0.9$ and $N = 1$

Similar conclusions made above for the results of CFAR loss using threshold multiplier method are also evident in figures from Figure 3-10 to Figure 3-13. To summarize, as the length of the window size increases, true CFAR loss decreases and in the figures it is also seen that true CFAR loss is also strongly dependent on ν and the desired P_{fa} . Moreover, the above curves gives the information about the relationship between the P_d and true CFAR loss. As the desired P_d increases from 0.5 to 0.9, the resulting true CFAR loss increases as expected. This increase in CFAR loss is at most ~ 3 dB for $\nu = 0.2$, $M = 4$ and $P_{fa} = 10^{-4}$ from Figure 3-12 and Figure 3-13. This difference reduces and becomes less noticeable as clutter gets less spiky and also CA-CFAR window size increases.

As mentioned in Section 2.3.3 there are two methods for measuring CFAR loss. One is named here as threshold multiplier method which gives approximate CFAR losses. Second method comes from the definition of CFAR loss which is named as true CFAR loss in this thesis. The loss curves of both methods are compared in the following graphs, Figure 3-14 and Figure 3-15 for $P_d = 0.5$, P_{fa} values of 10^{-3} and 10^{-4} and various ν values (0.2, 0.5, 1.5 and 10). In these figures solid lines refers to the true CFAR loss calculation and the results represented by the dashed dotted lines are obtained by the threshold multiplier method.

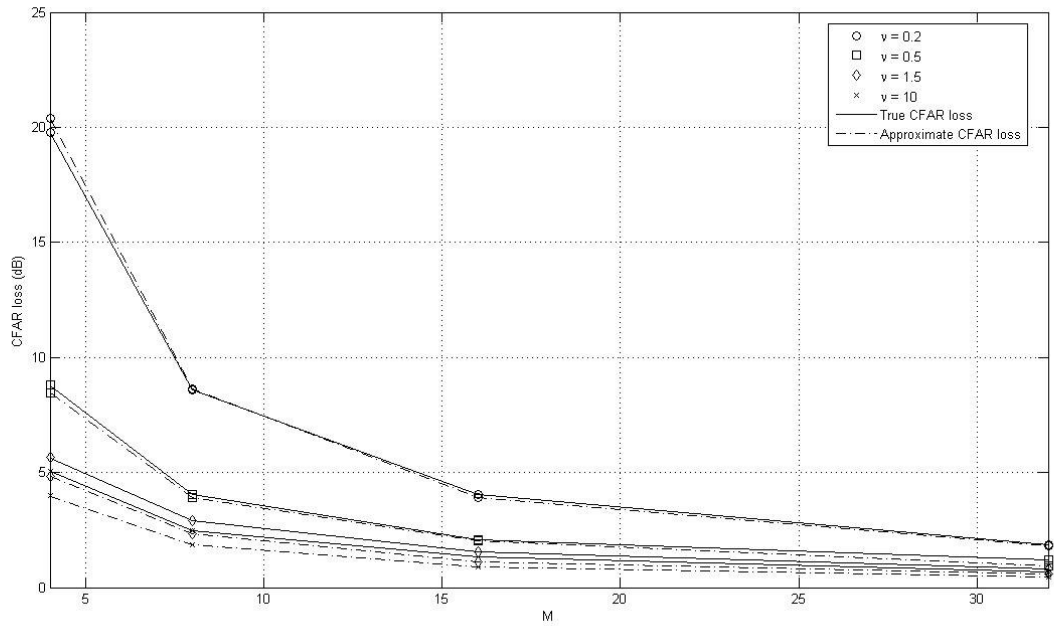


Figure 3-14 A comparison of CFAR loss methods for SU clutter, SW-II target,
 $P_{fa} = 10^{-3}$, $P_d = 0.5$ and $N = 1$

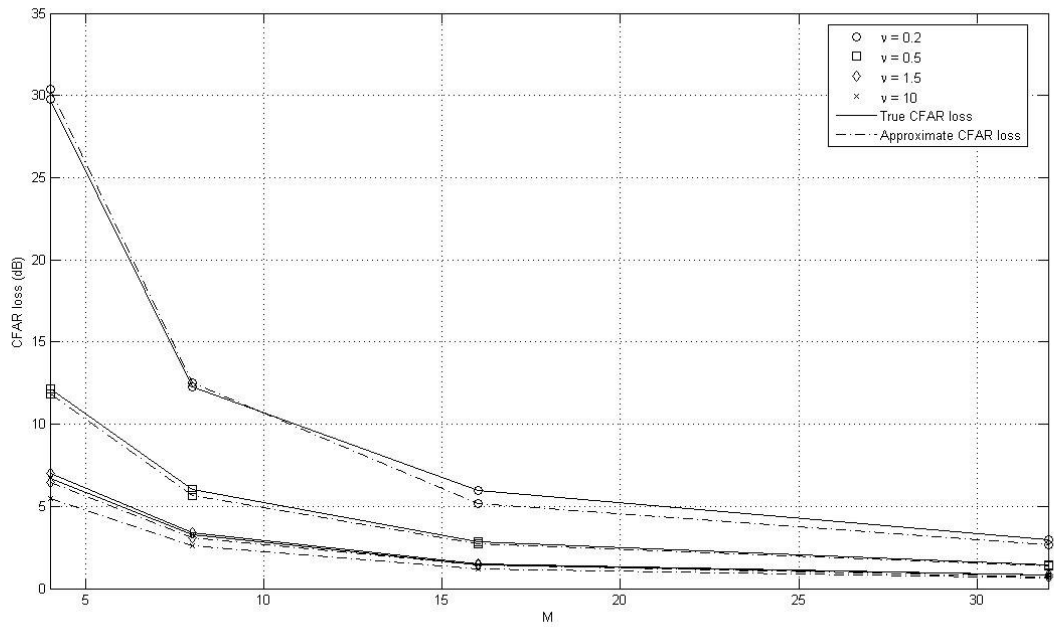


Figure 3-15 A comparison of CFAR loss methods for SU clutter, SW-II target,
 $P_{fa} = 10^{-4}$, $P_d = 0.5$ and $N = 1$

In Figure 3-14 and Figure 3-15 it is seen that threshold multiplier may be a good guide in understanding the general behaviour of CFAR loss. The difference in loss between the two methods is not more than ~ 1 dB. However when P_d is not equal to 0.5, the approximate CFAR loss method starts to underestimate the true CFAR loss. A sample case for $P_d = 0.9$ and $P_{fa} = 10^{-4}$ is given in Figure 3-16. As a result, for exact calculation the true CFAR loss method should be preferred.

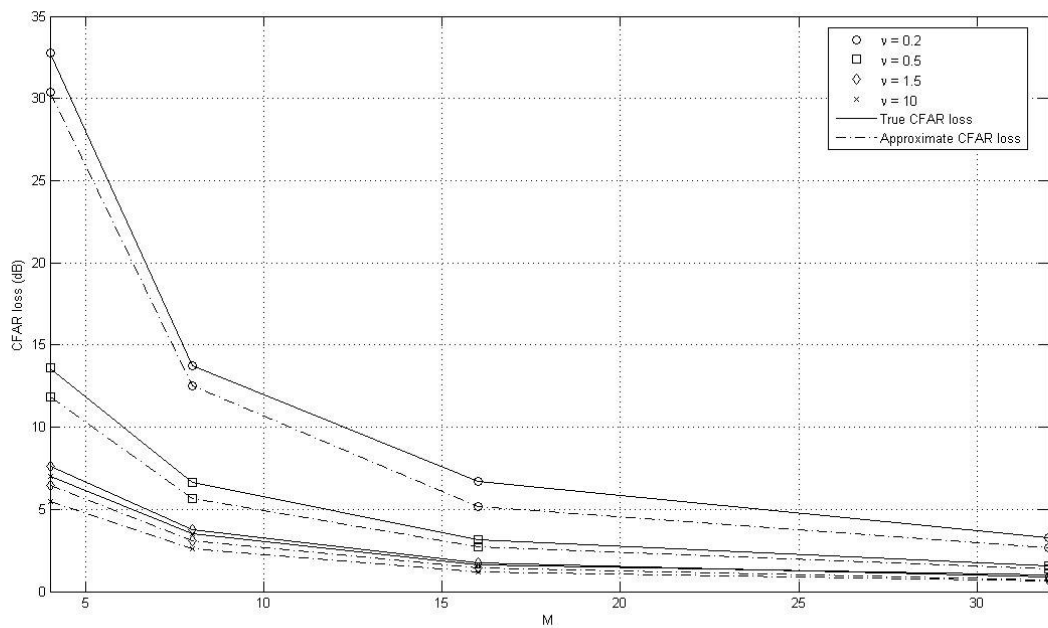


Figure 3-16 A comparison of CFAR loss methods for SU clutter, SW-II target, $P_{fa} = 10^{-4}$, $P_d = 0.9$ and $N = 1$

3.4.2. Multiple Pulse Detection

This section includes the effects of pulse to pulse integration prior to CA-CFAR processor. For this purpose 3, 10, 20 and 30 pulses are integrated non-coherently.

The values α for different P_{fa} values is first to be determined to set a threshold and decide the CFAR loss. In the following Figure 3-17 shows sample $\log_{10}(P_{fa})$ versus α curves if the radar integrated N (1, 3 and 10) successive pulses. Here ν is chosen to be 1.5 and the window size of CA-CFAR processor is 32. In Figure 3-17 fixed threshold detection curves are also shown for different values of N by dashed dotted lines.

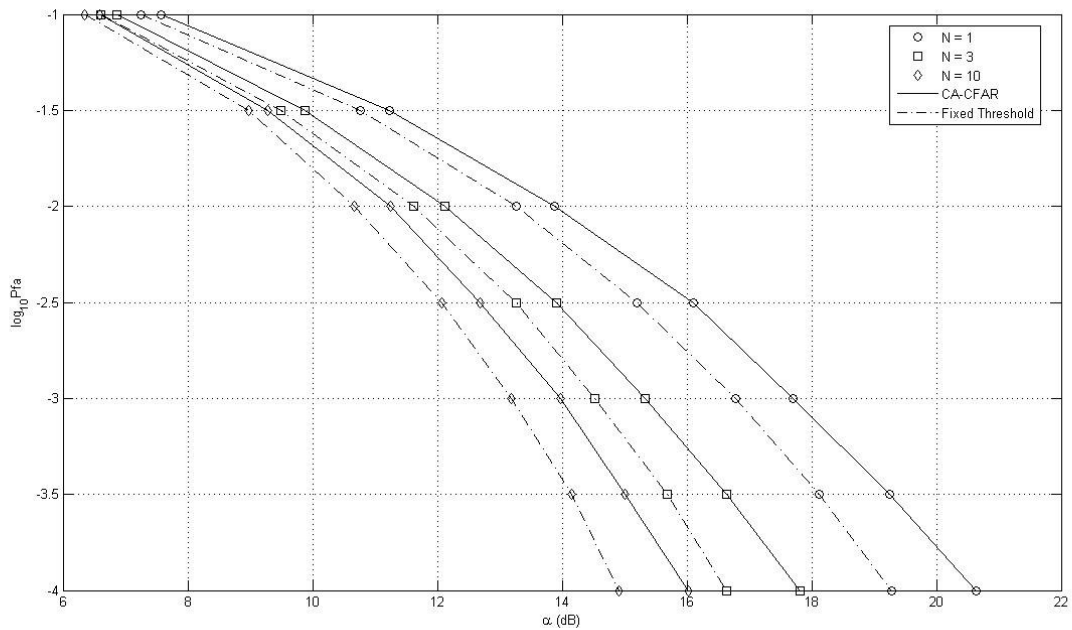


Figure 3-17 $\log_{10} P_{fa}$ vs. α for SU clutter with $\nu = 1.5$ and $M = 32$

The previous figure is given to indicate that as N increases for a given P_{fa} lower threshold multiplier results are obtained both for CA-CFAR detection curves and the fixed threshold detection curves by using which the approximate CFAR loss values are calculated. The same behaviour for different values of shape parameter and window size is also observed however the figures are not shown for brevity.

The values of threshold multiplier, α for different values of P_{fa} are obtained for

various ν , M and N by MC simulations. Then, as in previous section the approximate CFAR loss from threshold multiplier method is calculated. To find CFAR loss the fixed threshold curves are also simulated for multiple pulse integration. Hence, the CFAR loss versus N curves are shown in from Figure 3-18 to Figure 3-21 in order to evaluate performance when multiple pulse is integrated in uncorrelated K-distributed sea clutter.

The true CFAR loss is also calculated in a similar fashion explained in the previous section. The resulting true CFAR loss versus N graphs of various values of ν (0.2, 0.5, 1.5 and 10) are also given with dashed dotted lines in from Figure 3-18 to Figure 3-21. In these figures both CFAR losses are given as a function of the number of integrated pulses N (1, 3, 10, 20 and 30) for various values of ν (0.2, 0.5, 1.5 and 10). Here the results from single pulse detection are also given for comparison. The window size of CA-CFAR processor, M is 16 in Figure 3-18 and Figure 3-20; 32 in Figure 3-19 and Figure 3-21. The desired P_{fa} is 10^{-3} in Figure 3-18 and Figure 3-19 ; 10^{-4} in Figure 3-20 and Figure 3-21.

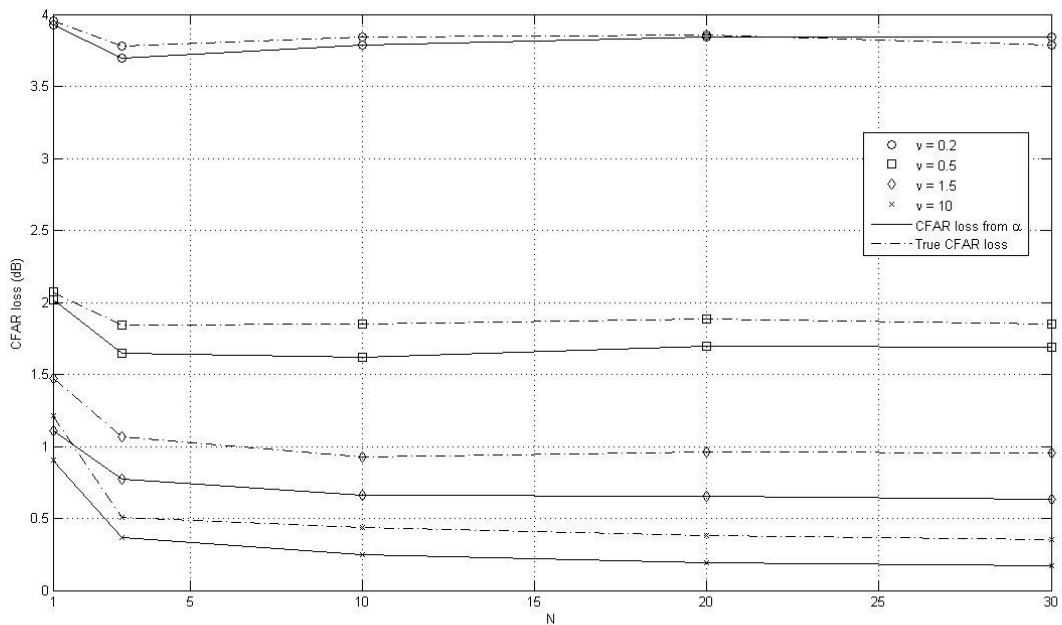


Figure 3-18 CFAR loss vs. N for SU clutter, SW-II target, $P_{fa} = 10^{-3}$ and $M = 16$

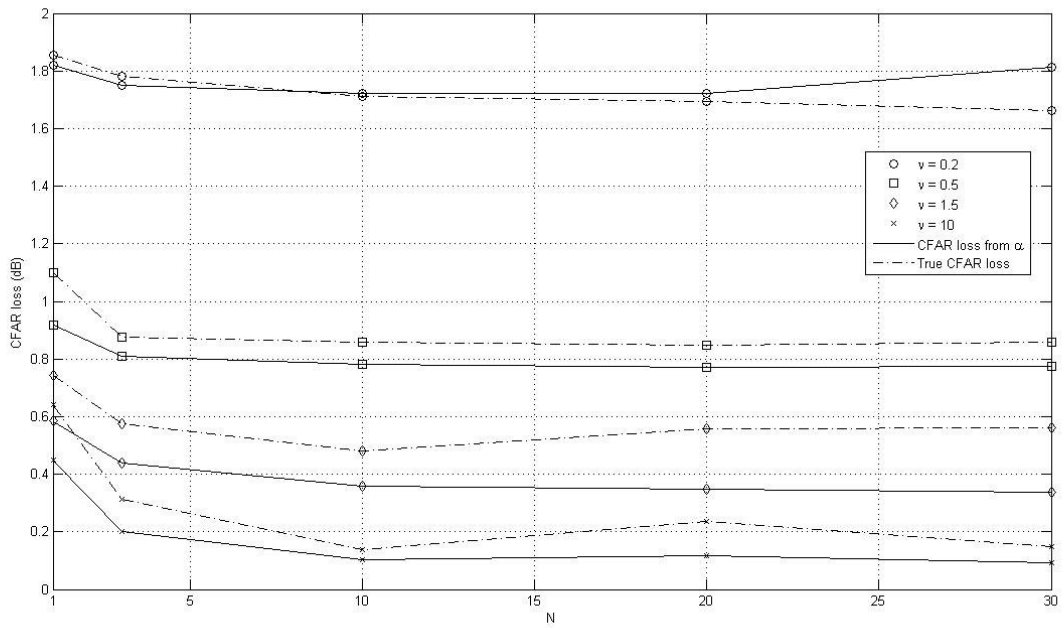


Figure 3-19 CFAR loss vs. N for SU clutter, SW-II target, $P_{fa} = 10^{-3}$ and $M = 32$

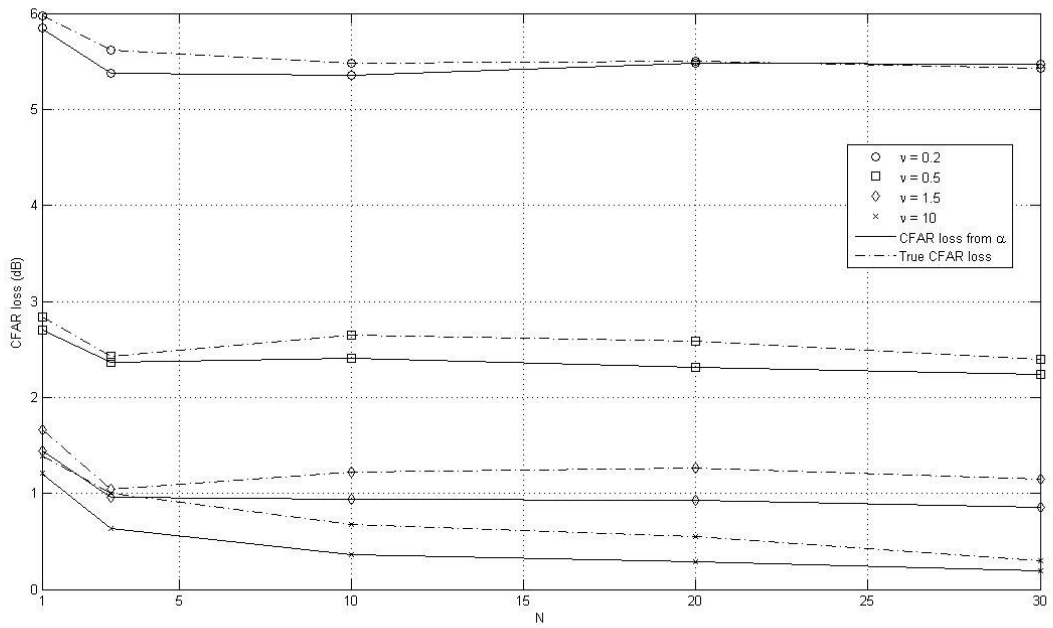


Figure 3-20 CFAR loss vs. N for SU clutter, SW-II target, $P_{fa} = 10^{-4}$ and $M = 16$

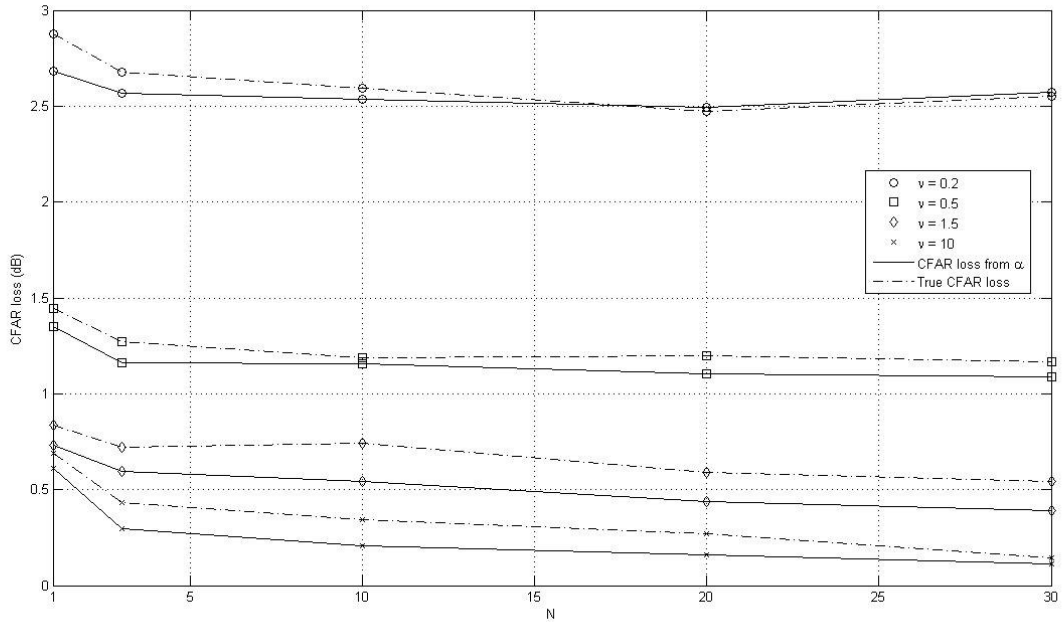


Figure 3-21 CFAR loss vs. N for SU clutter, SW-II target, $P_{fa} = 10^{-4}$ and $M = 32$

The previous figures result in a number of conclusions. First approximate CFAR loss values obtained by threshold multiplier method is analysed. The expectation for general behaviour of detection performance for increasing N is met. In other words with increasing N , the detection performance is also increases with the means of CFAR loss. Even though the pulse integration shows some improvement compared to single pulse detection, the improvement between 10, 20 and 30 pulses is not significant. For instance, in Figure 3-21 for $\nu = 0.2$ the CFAR loss shows a slight increase (less than ~ 0.1 dB) when number of integrated pulses, N increases from 16 to 32 pulses. Similar slight increases is also seen from Figure 3-18 to Figure 3-20 and do not exceed 0.15 dB. This is due to the sensitivity of the simulation. The difference between CFAR loss values for higher N becomes closer and the simulation is not capable of distinguishing this amount of difference. Hence the sensitivity of the simulation is not high enough to get the accurate results. However it is still possible to conclude that even though there is an obvious improvement in CFAR loss when compared to single pulse detection

case, using 10 or 20 or 30 pulses for integration does not make a considerable change in the value of CFAR loss.

Before proceeding to the conclusions of the true CFAR loss curves, P_d versus SCR curves for a sample case is analysed. A resulting graph with various N (1, 3, 10, 20 and 30) is given in Figure 3-22 for $\nu = 0.5$, $P_{fa} = 10^{-3}$ and $M = 32$ for SW-II target.

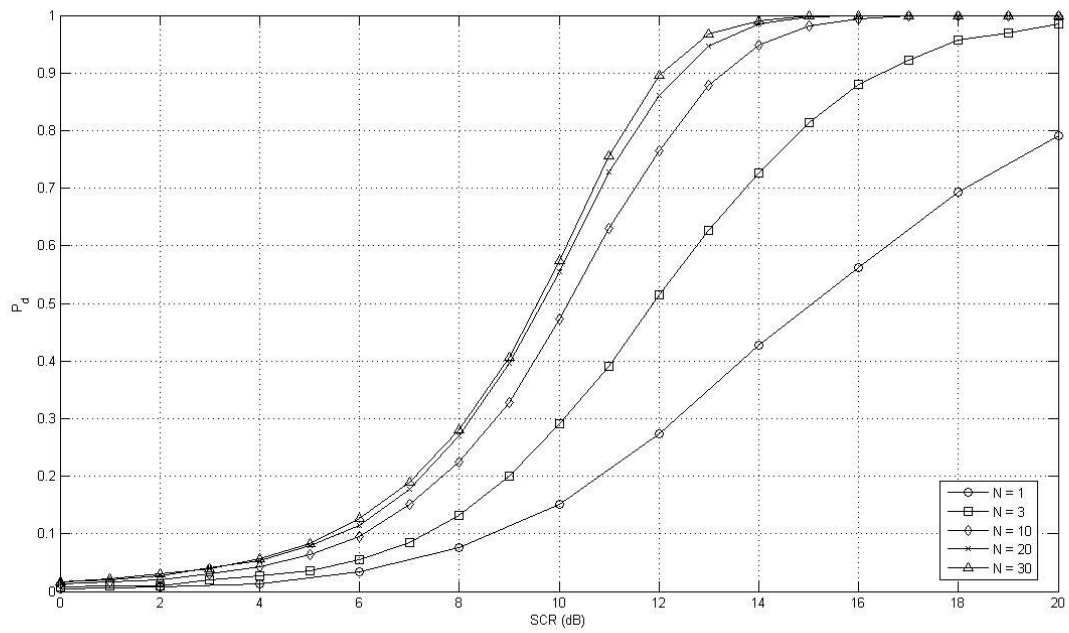


Figure 3-22 P_d vs. SCR curves for SU clutter with $\nu = 0.5$, SW-II target, $P_{fa} = 10^{-3}$ and $M = 32$

It is seen in Figure 3-22 that required SCR reduces with the increasing number of pulses integrated in order to reach a certain P_d .

True CFAR loss values, obtained by using P_d versus SCR curves like the ones in Figure 3-22, are shown in from Figure 3-18 to Figure 3-21 together with approximate CFAR loss values. The true CFAR loss and approximate CFAR loss

values are seen to be close to each other. The difference is at most ~ 0.4 dB. And if this amount of loss is negligible for a particular radar performance threshold multiplier method might be used to approximate the true CFAR losses.

More informative curves of SCR versus N are given in from Figure 3-23 to Figure 3-26 for different values of ν (0.2, 0.5, 1.5 and 10) and M (16 and 32). In these figures, P_{fa} takes the values of 10^{-3} and 10^{-4} , P_d takes the values of 0.5 and 0.9.

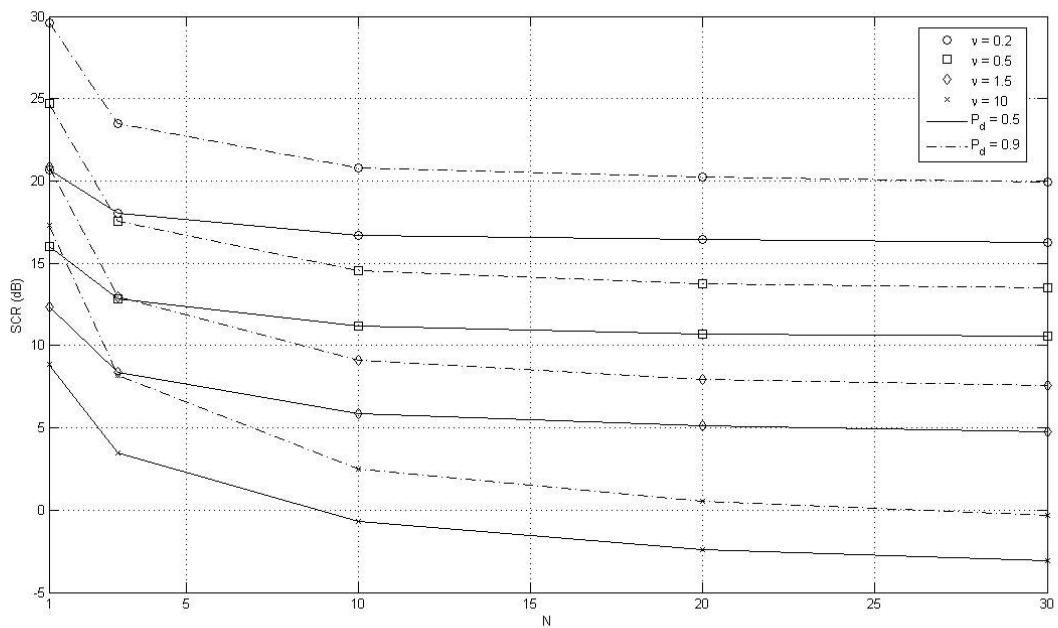


Figure 3-23 SCR vs. N curves for SU clutter, SW-II target, $P_{fa} = 10^{-3}$ and $M = 16$

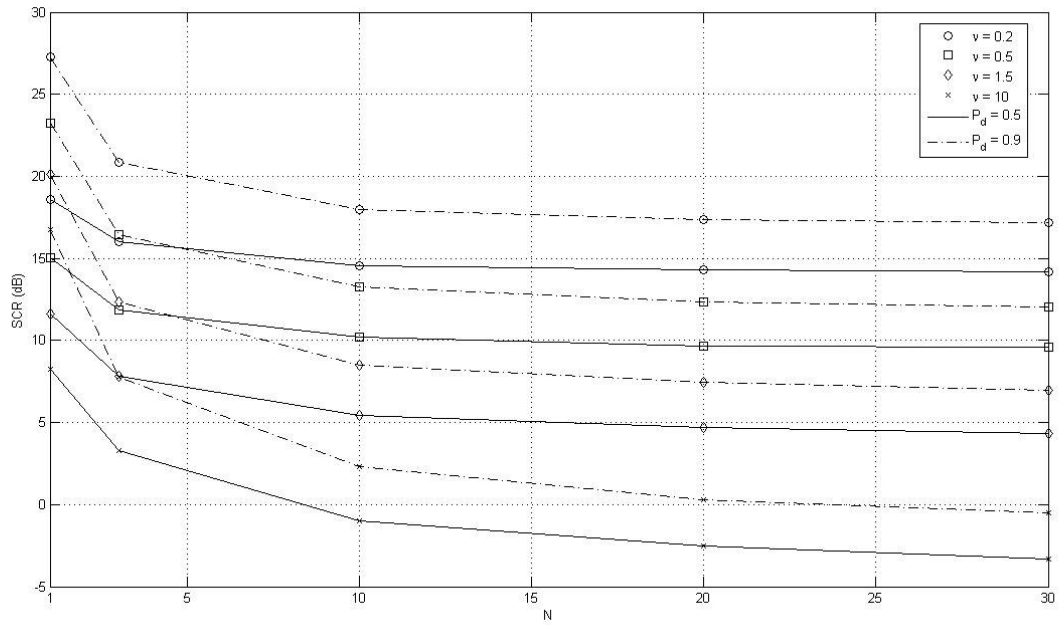


Figure 3-24 SCR vs. N curves for SU clutter, SW-II target, $P_{fa} = 10^{-3}$ and $M = 32$

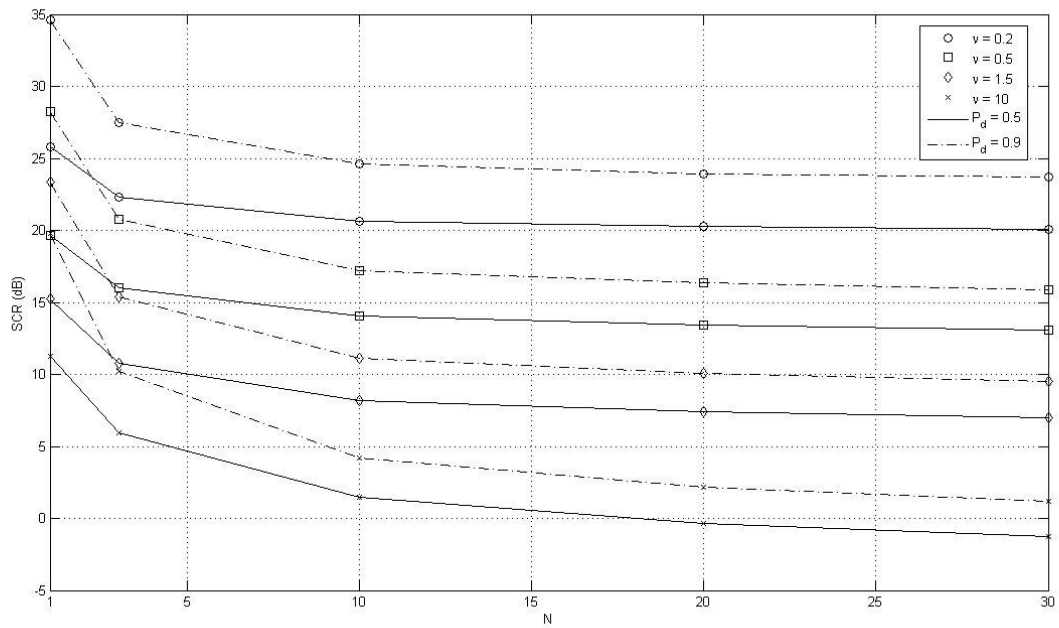


Figure 3-25 SCR vs. N curves for SU clutter, SW-II target, $P_{fa} = 10^{-4}$ and $M = 16$

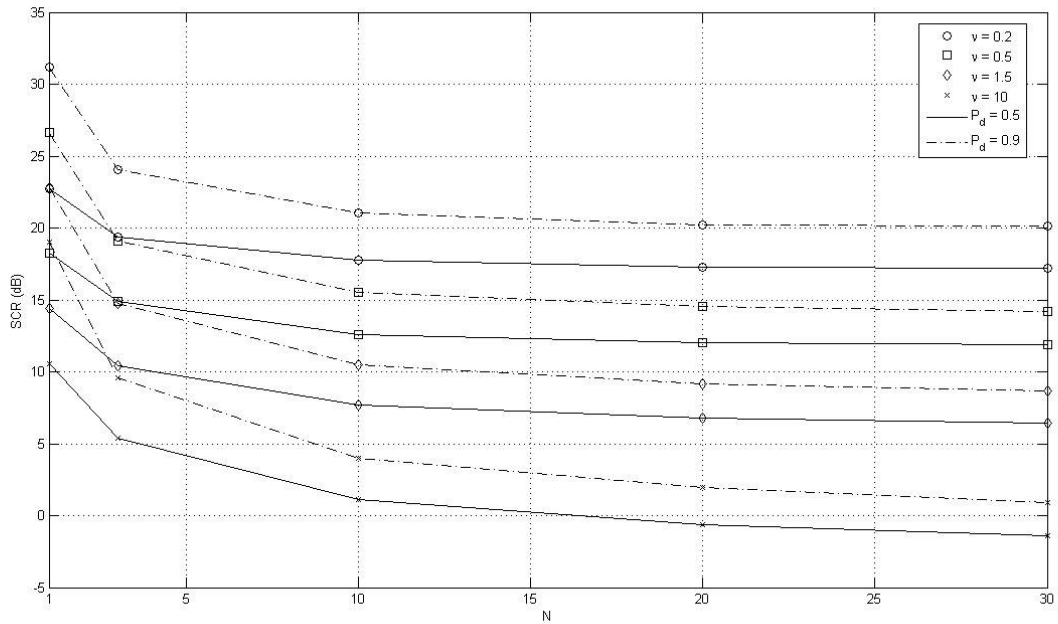


Figure 3-26 SCR vs. N curves for SU clutter, SW-II target, $P_{fa} = 10^{-4}$ and $M = 32$

As shown in from Figure 3-23 to Figure 3-26 as the number of pulses integrated increases the required SCR reduces. However the decrease in SCR slows down as the number of integrated pulses increases. For instance when $\nu = 0.5$, $P_{fa} = 10^{-4}$ and $M = 32$ (Figure 3-24) using 10 pulses instead of single pulse decreases the required SCR from ~ 15 dB to ~ 10.2 dB, whereas using 30 pulses decreases the required SCR ~ 9.6 dB which corresponds to only ~ 0.6 dB improvement. Moreover, the figures also shows as P_d increases from 0.5 to 0.9, significant amount of increase appears in the required SCR, as expected. On the other hand, the time to spend for detection decision is longer when multiple pulse is integrated than single pulse since the detection decision is made after the processing of N pulses.

3.5. CA-CFAR DETECTION IN SPATIALLY CORRELATED (SC) K-DISTRIBUTED CLUTTER

In the results presented so far, it has been assumed that the CA-CFAR uses independent samples of overall clutter distribution to estimate the local mean level. If the CUT is correlated with the surrounding data, a better estimate may be achieved in some circumstances. Now rather than a CFAR loss, it appears that there is a CFAR gain relative to the 'ideal' fixed threshold as will be shown later in this section. The correlated data samples used are obtained using the method explained in Section 2.2.4.

Figure 3-27 and Figure 3-28 show the approximate CFAR loss in K-distributed clutter of $\nu = 1.5$ as a function of window size M for spatial correlation lengths $R = 5, R = 10$ and $R = 30$. In these figures the values of approximate CFAR loss for clutter with no spatial correlation ($R = 0$) are also shown for comparison. The results in Figure 3-27 are for $P_{fa} = 10^{-3}$ and one in Figure 3-28 shows the CFAR loss results for $P_{fa} = 10^{-4}$. In both figures single pulse detection ($N = 1$) is shown by solid lines and 10 pulse detection is shown by dash-dotted lines. Again pulse returns are integrated prior to operation of the CA-CFAR. Here the threshold multiplier method is used to give a guide to CFAR loss.

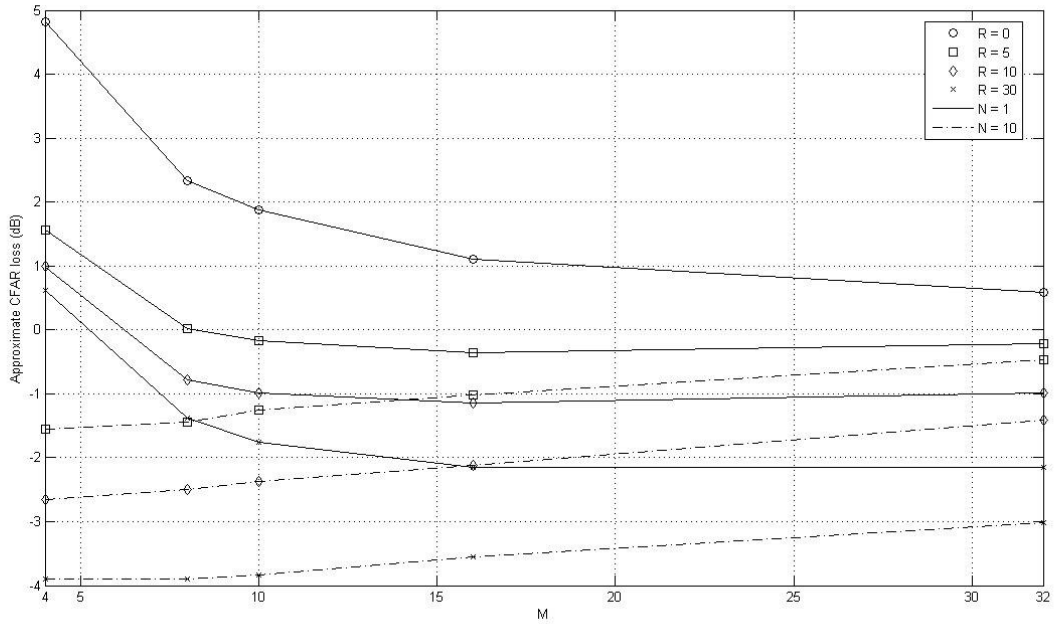


Figure 3-27 Approximate CFAR loss vs. M for SC clutter with $\nu = 1.5$,
 $N = 1$ & 10 and $P_{fa} = 10^{-3}$

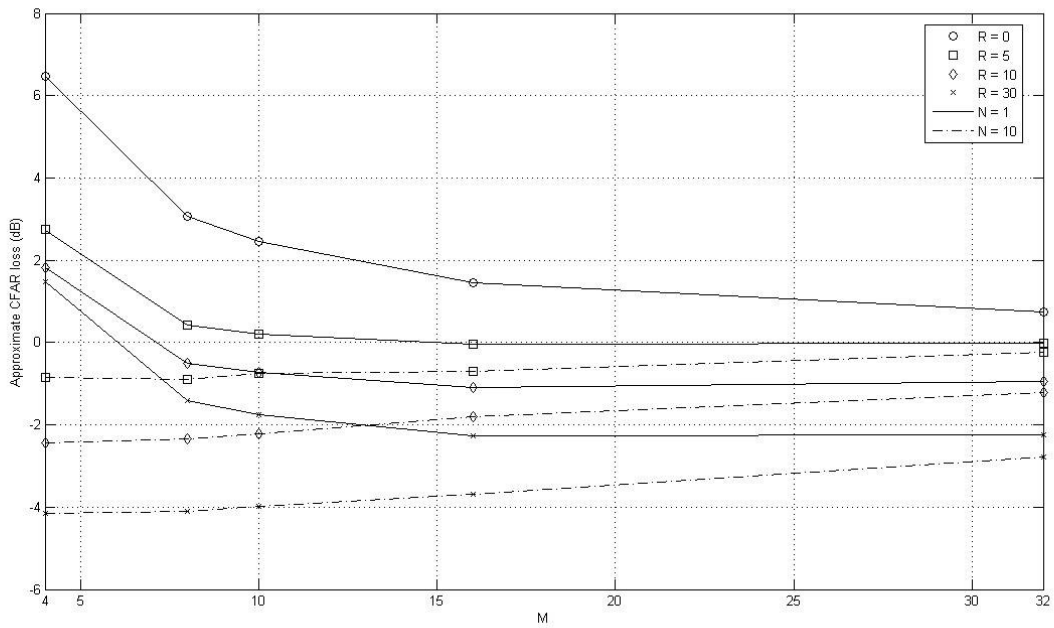


Figure 3-28 Approximate CFAR loss vs. M for SC clutter with $\nu = 1.5$,
 $N = 1$ & 10 and $P_{fa} = 10^{-4}$

When the shape parameter of K-distributed clutter is equal to 10, the CFAR loss versus M graphs are given in the following figures, Figure 3-29 and Figure 3-30. Here the $N = 1$ and $N = 10$ results are shown on the same plots again.

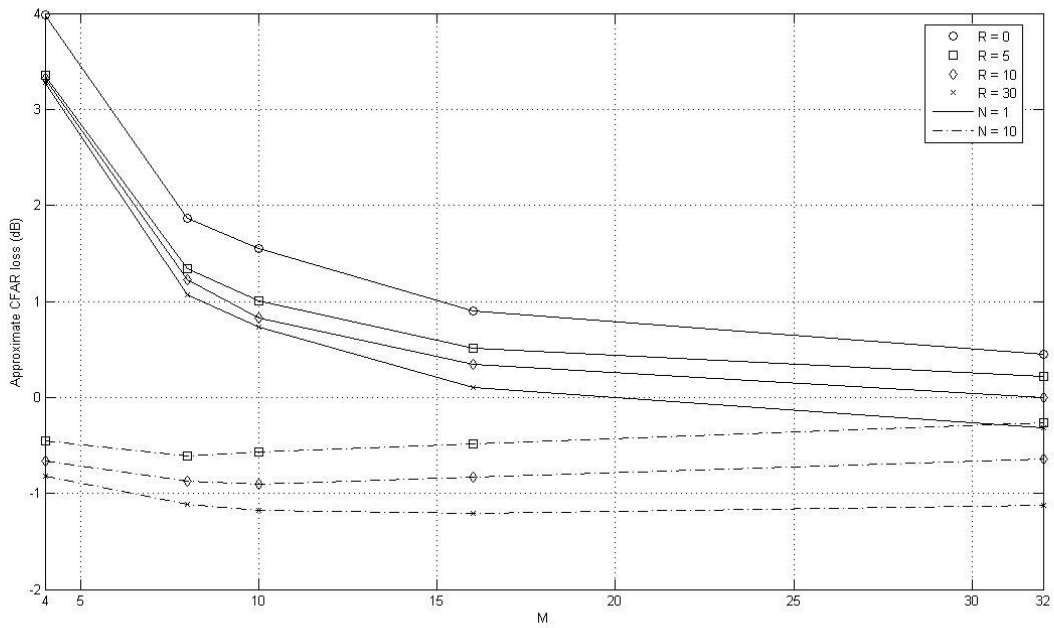
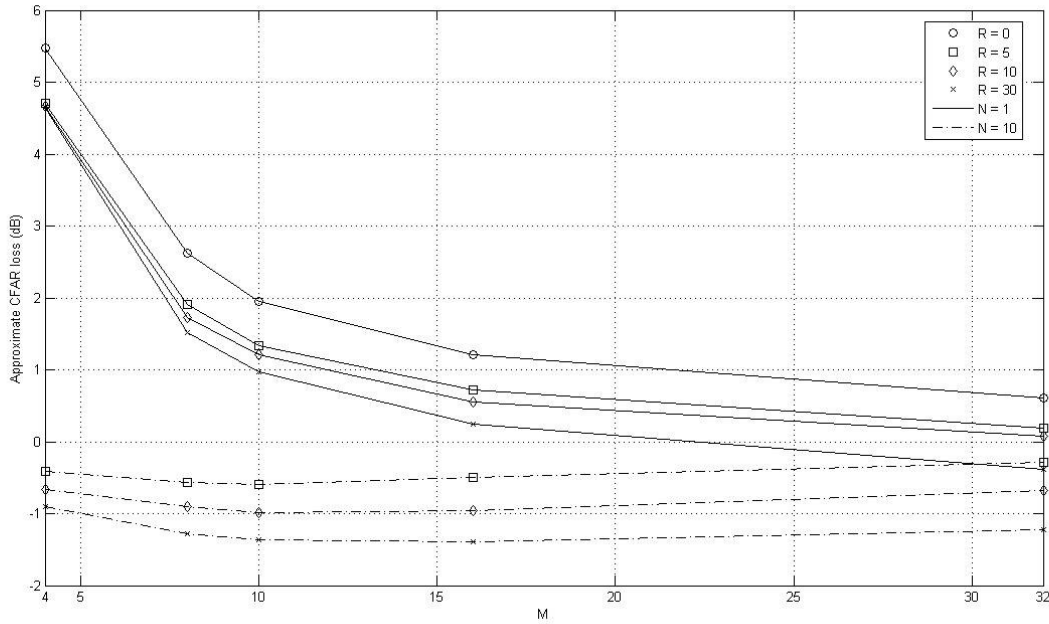


Figure 3-29 Approximate CFAR loss vs. M for SC clutter with $\nu = 10$,
 $N = 1$ & 10 and $P_{fa} = 10^{-3}$



**Figure 3-30 Approximate CFAR loss vs. M for SC clutter with $\nu = 10$,
 $N = 1$ & 10 and $P_{fa} = 10^{-4}$**

In the figures from Figure 3-27 to Figure 3-30 the effect of correlation is remarkable. As the sea clutter becomes more correlated (R increases), CFAR loss decreases and for higher correlation lengths even CFAR gain is obtained.

In these figures, it is seen that integration of 10 pulses results in lower CFAR loss values for all correlation lengths. Integration gives CFAR gain even though the single pulse detection results in CFAR losses.

When the shape parameter of K-distributed clutter is equal to spikier values 0.2 and 0.5, the approximate CFAR loss versus M graphs are given in the following figures from Figure 3-31 to Figure 3-34 similarly.

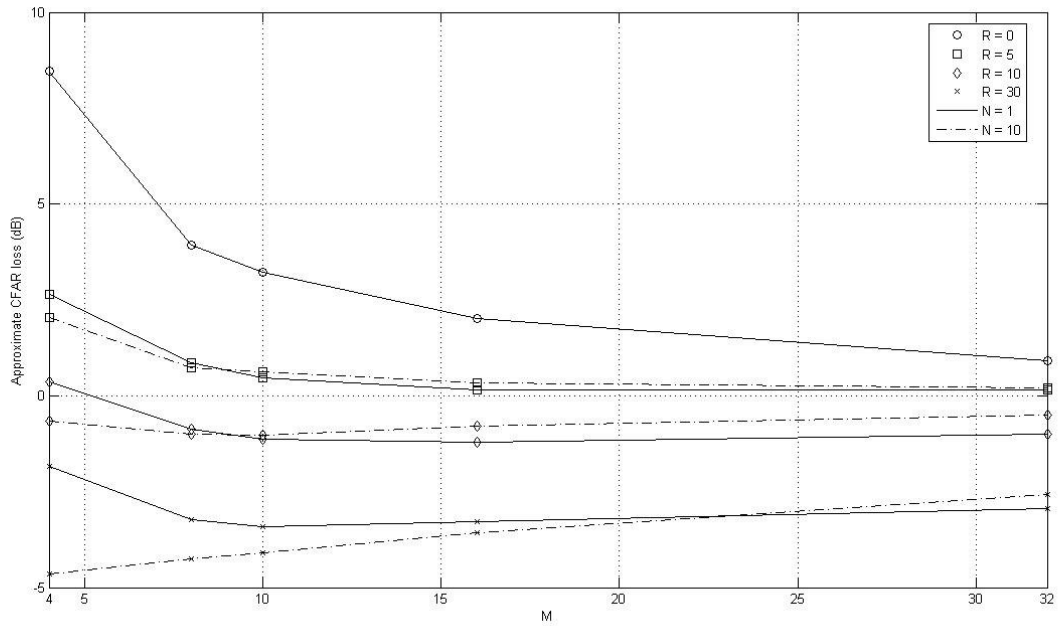


Figure 3-31 Approximate CFAR loss vs. M for SC clutter with $\nu = 0.5$,
 $N = 1$ & 10 and $P_{fa} = 10^{-3}$

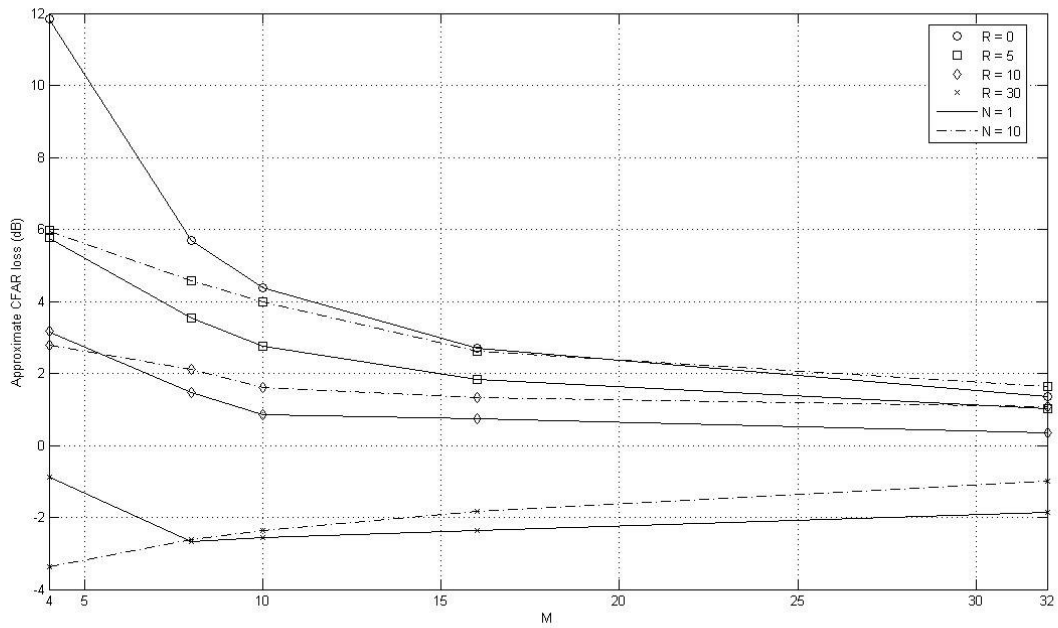


Figure 3-32 Approximate CFAR loss vs. M for SC clutter with $\nu = 0.5$,
 $N = 1$ & 10 and $P_{fa} = 10^{-4}$

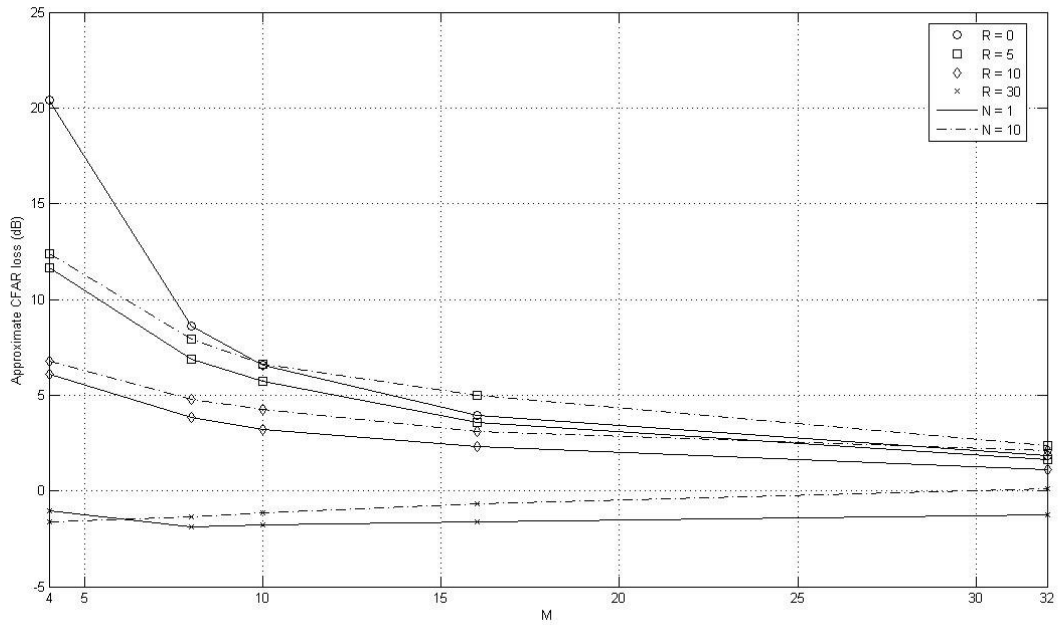


Figure 3-33 Approximate CFAR loss vs. M for SC clutter with $\nu = 0.2$,
 $N = 1$ & 10 and $P_{fa} = 10^{-3}$

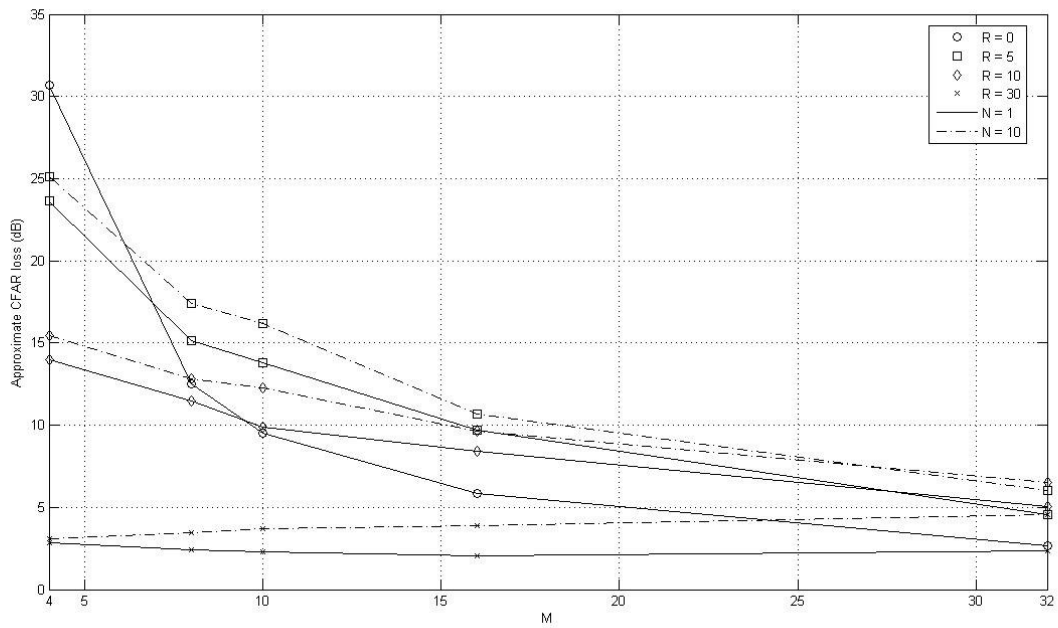


Figure 3-34 Approximate CFAR loss vs. M for SC clutter with $\nu = 0.2$,
 $N = 1$ & 10 and $P_{fa} = 10^{-4}$

Figure 3-31 and Figure 3-32 show that higher correlation lengths gives lower CFAR loss values and even CFAR gain for both single and 10 pulse detection. The higher correlation between the CA-CFAR output and the CUT results in lowest CFAR losses for short CA-CFAR window sizes. This significant result gives an optimum value of M where the maximum CFAR gain is achieved, i.e. the highest CFAR gain is achieved for a finite value of M . For instance, from Figure 3-31 it is seen that the optimum value $M \approx 10$ with $\nu = 0.5$, $R = 30$ and $P_{fa} = 10^{-3}$. Figure 3-32 also shows another optimum $M \approx 8$ with $\nu = 0.5$, $R = 30$ and $P_{fa} = 10^{-4}$. In these figures, 10 pulse integration does not give lower values of CFAR loss or higher values of CFAR gain compared to single pulse detection case especially for higher CA-CFAR window sizes. Similar behaviour is also reported in [16] for empirical sea clutter data.

Figure 3-33 and Figure 3-34 show the CFAR loss values for spikiest clutter example ($\nu = 0.2$). It is seen once again in these figures that for $R = 30$ an optimum value of CA-CFAR window size is present for single pulse detection. In Figure 3-34 correlated clutter of $R = 5$ and $R = 10$ gives higher CFAR loss values than uncorrelated case. As [16] indicates, short correlation length has the effect of reducing the number of independent samples in the CA-CFAR window when compared to uncorrelated case but leaving the CA-CFAR output decorrelated from CUT. The CFAR loss in this case is then greater than would be expected for totally uncorrelated clutter ($R = 0$) in CA-CFAR window. In other words for low values of correlation length R ($R = 5$ and $R = 10$ in this case), the CA-CFAR processor perform worse than a fixed threshold when compared to uncorrelated clutter in CA-CFAR window.

In the figures from Figure 3-27 to Figure 3-32 it is seen that as M becomes large, performance tends to the CFAR loss associated with clutter with no spatial correlation. It is also concluded in these figures as P_{fa} decreases from 10^{-3} to 10^{-4} the values of CFAR loss increases and CFAR gain decreases in general.

It has been showed that the highest values of CFAR gain are achieved with short CA-CFAR lengths in highly spatially correlated clutter. However such short CA-CFAR will also produce the highest CFAR loss in uncorrelated clutter. For this reason it is clear that a practical radar must be able to adapt its CA-CFAR window size according to the conditions if best performance is to be achieved [18].

The true CFAR loss graphs are also obtained as a function of M for single pulse detection and SW-II target. They are given in figures from Figure 3-35 to Figure 3-38 for various values of ν together with approximate CFAR loss values from threshold multiplier method.

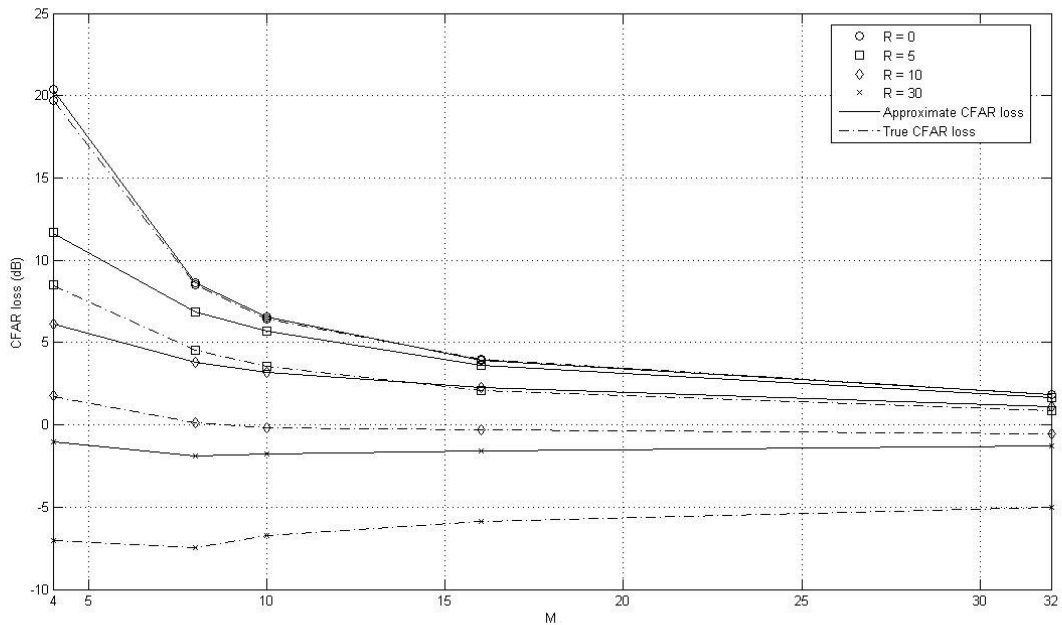


Figure 3-35 CFAR loss vs. M for SC clutter with $\nu = 0.2$, SW-II target, $N = 1$,

$$P_{fa} = 10^{-3} \text{ and } P_d = 0.5$$

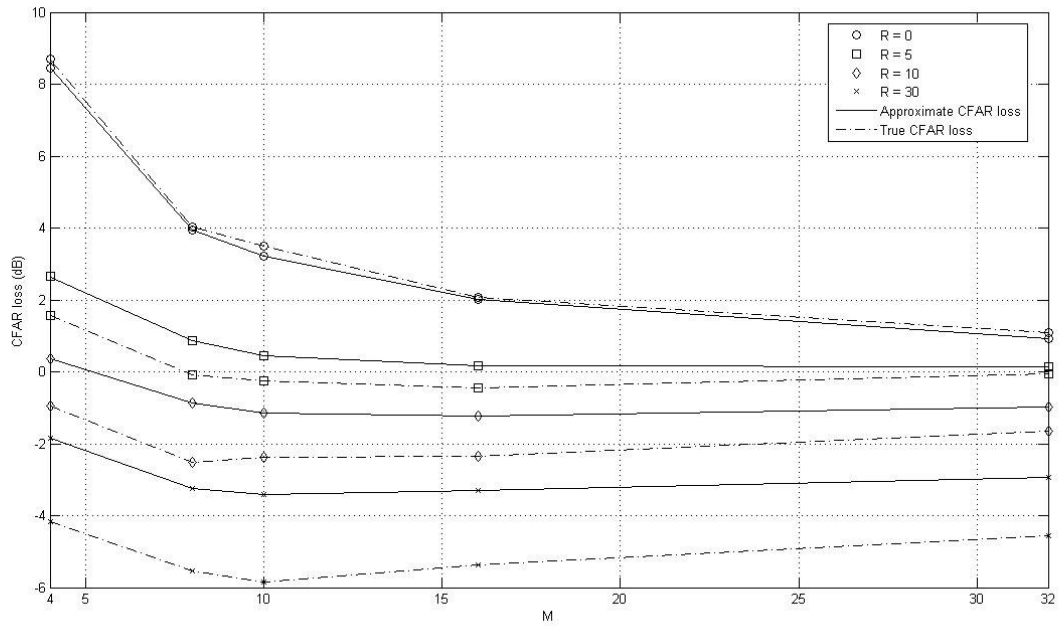


Figure 3-36 CFAR loss vs. M for SC clutter with $\nu = 0.5$, SW-II target, $N = 1$, $P_{fa} = 10^{-3}$ and $P_d = 0.5$

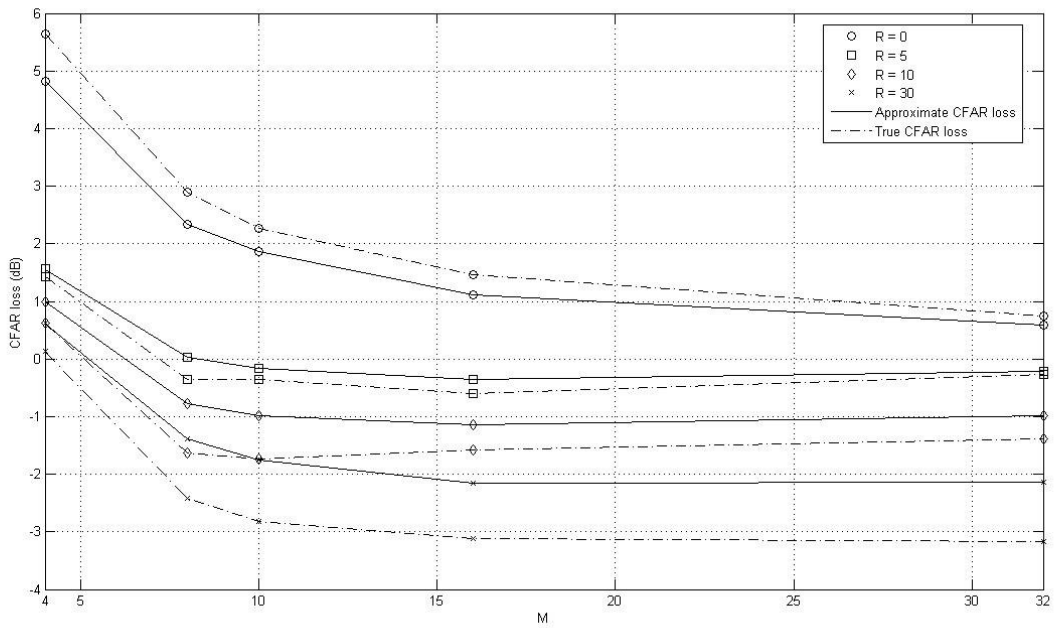


Figure 3-37 CFAR loss vs. M for SC clutter with $\nu = 1.5$, SW-II target, $N = 1$, $P_{fa} = 10^{-3}$ and $P_d = 0.5$

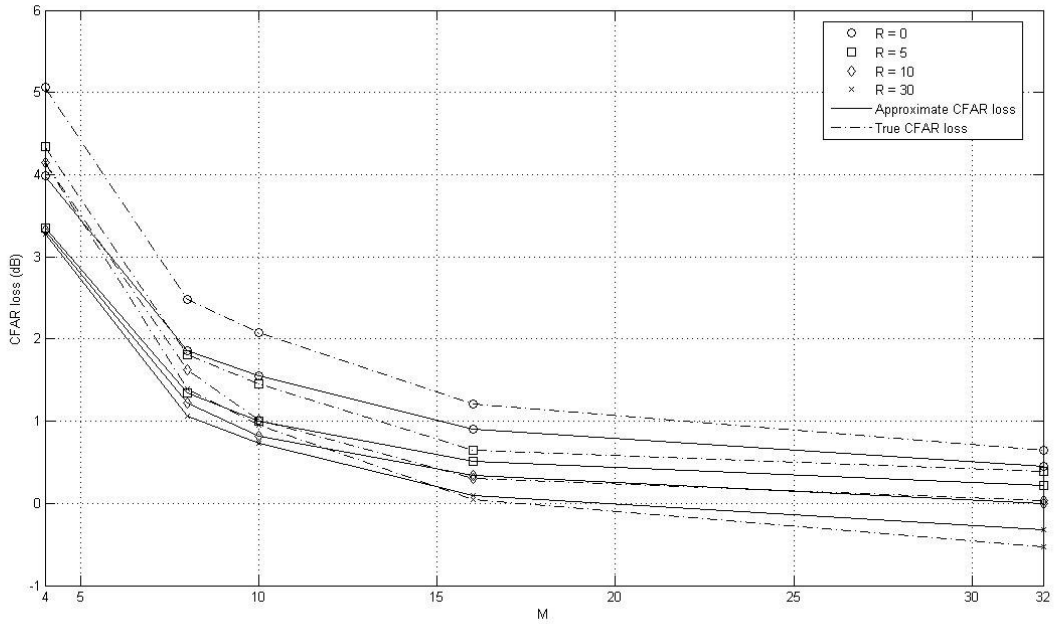


Figure 3-38 CFAR loss vs. M for SC clutter with $\nu = 10$, SW-II target, $P_{fa} = 10^{-3}$, $P_d = 0.5$ and $N = 1$

Same trends in CFAR loss versus M curves are also seen in the previous true CFAR loss curves. For low values of the shape parameter ($\nu = 0.2$ and $\nu = 0.5$) the best performance is nearly always achieved for a short CA-CFAR window size. When there is a little spatial correlation and for high values of the shape parameter ($\nu = 10$) the best performance will be obtained from a longer CA-CFAR window size.

The difference between approximate and true CFAR loss values is more apparent when correlation effect is included. For spikier clutter and also with higher correlation lengths this difference increases. For instance in Figure 3-35 the difference is ~ 5 dB for $\nu = 0.2$ and $R = 30$.

The following figures from Figure 3-39 to Figure 3-42 show true CFAR loss versus M curves together with approximate CFAR loss curves for 10 pulse detection and SW-II target.

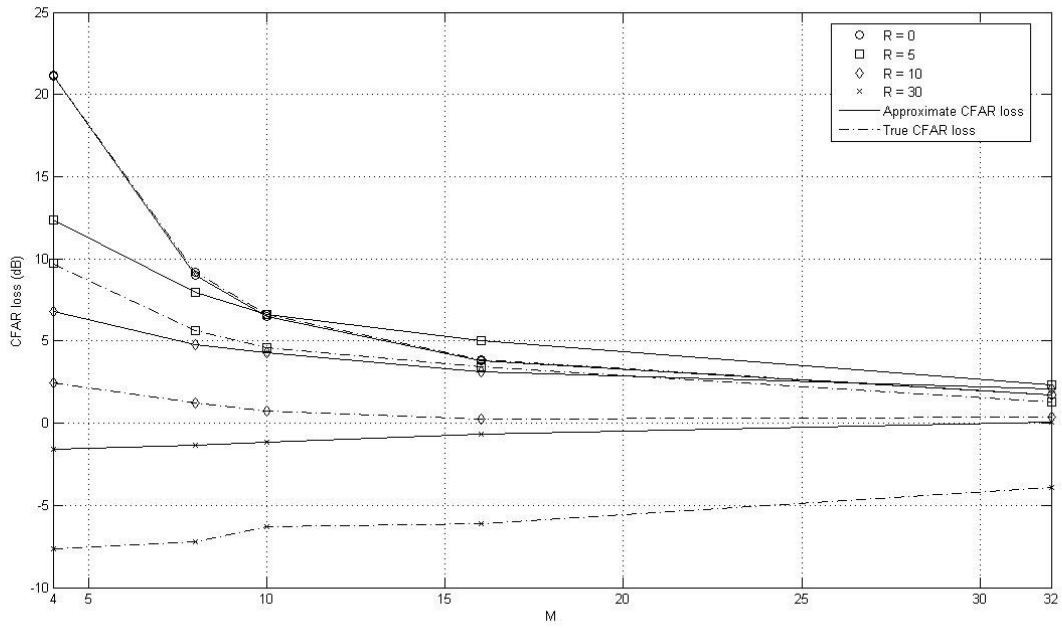


Figure 3-39 CFAR loss vs. M for SC clutter with $\nu = 0.2$, SW-II target, $P_{fa} = 10^{-3}$ and $N = 10$

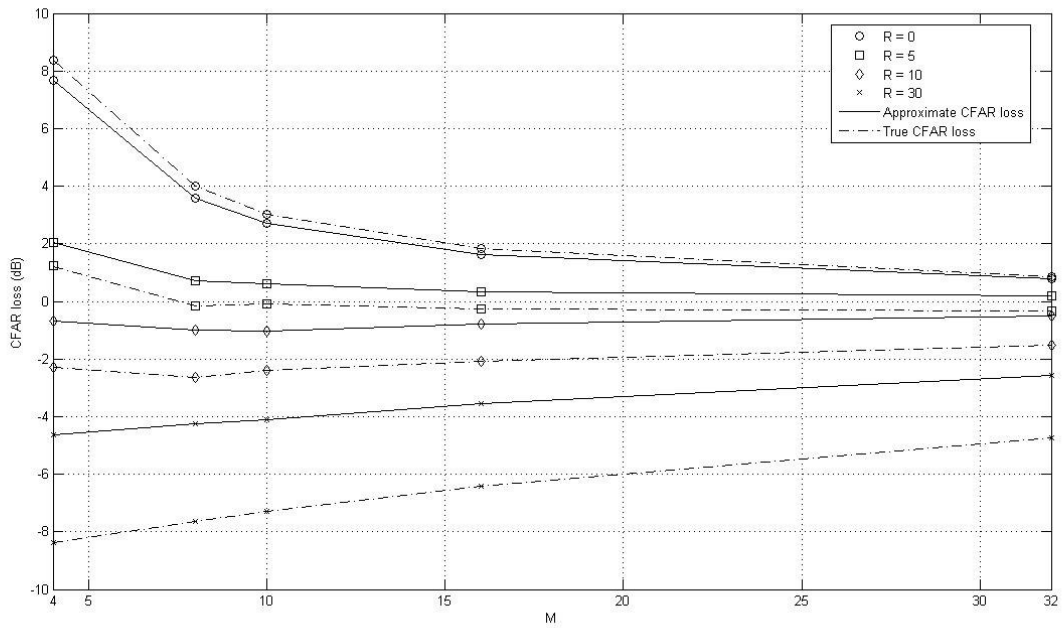


Figure 3-40 CFAR loss vs. M for SC clutter with $\nu = 0.5$, SW-II target and $P_{fa} = 10^{-3}$ and $N = 10$

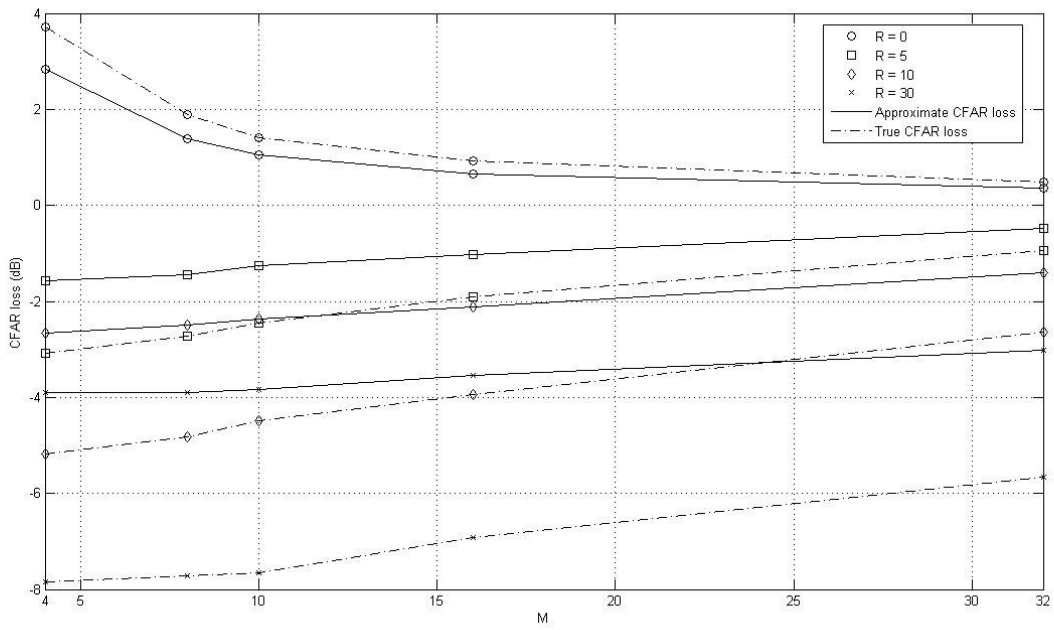


Figure 3-41 CFAR loss vs. M for SC clutter with $\nu = 1.5$, SW-II target, $P_{fa} = 10^{-3}$ and $N = 10$

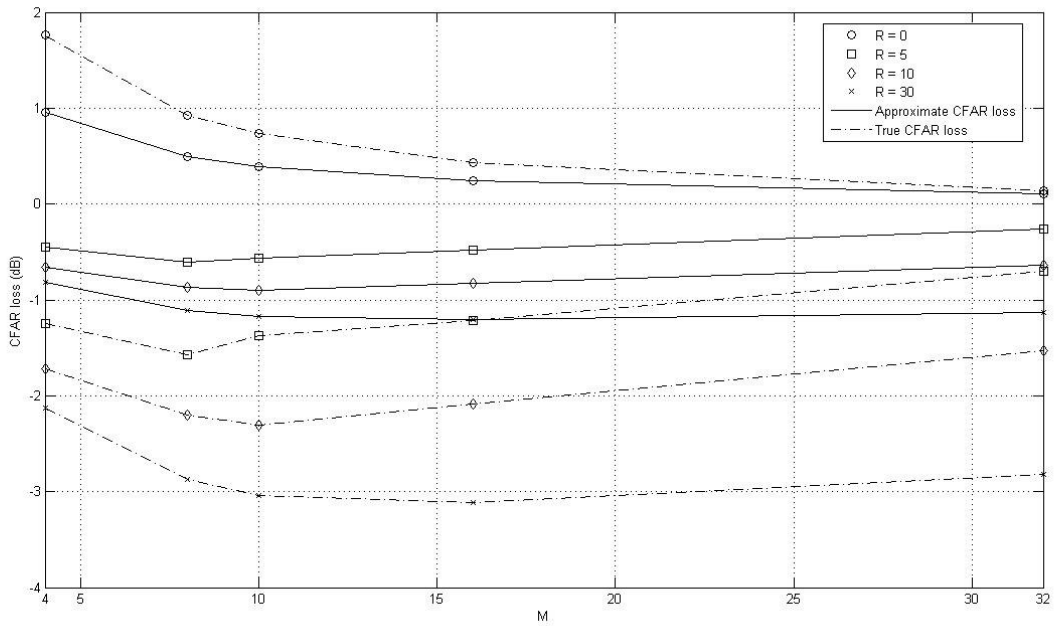


Figure 3-42 CFAR loss vs. M for SC clutter with $\nu = 10$, SW-II target, $P_{fa} = 10^{-3}$ and $N = 10$

The difference between approximate and true CFAR loss values for 10 pulse detection is again more remarkable when correlation effect is included. Similar to the single pulse detection, this difference increases with increasing clutter spikiness and also with higher correlation lengths. However this time even for low clutter spikiness this difference is remarkable. For instance, when $\nu = 10$, $R = 30$ and $M = 10$, in Figure 3-38 the difference is ~ 0.3 dB for single pulse detection whereas in Figure 3-42 the difference is ~ 2 dB for 10 pulse detection.

CHAPTER 4

PRACTICAL POINT OF VIEW

Most radars include a number of adaptive features, which are becoming more and more extensive and sophisticated [27]. Adaptation is always aimed at improving radar performance in some sense. One of the common example of adaptive operation of radars is CFAR. Here by introducing the spatial correlation concept, a better CA-CFAR performance is shown to be achieved. Moreover, as [19] emphasizes, if the effects of sea clutter are not modelled realistically in the design process, it is unlikely that a radar system will fully meet its operational requirements.

The results obtained in this thesis can be used to develop practical CA-CFAR detection configurations. It may be appropriate to use these CA-CFAR parameters or to offer choices of CA-CFAR schemes selectable by the radar operator or to adapt automatically according to the sea conditions.

In a practical radar application the following steps may be taken:

1. The required operational P_{fa} and P_d are decided by the radar designers.
2. During radar operation, the local clutter statistics are to be estimated. These are the shape parameter and spatial correlation properties of the K-distributed clutter. As [28] indicates the best approach in real clutter is to estimate local statistics directly and set a threshold accordingly.

3. Now, choices must be made amongst the many possible configurations. Given the required P_{fa} and P_d , by using the CFAR loss versus CA-CFAR window size graphs given in Section 3.5 an optimum value for CA-CFAR window size is decided.
4. Then, in order to run the CA-CFAR algorithm the threshold multiplier is to be determined. The graphs of P_{fa} versus threshold multiplier for the right sea clutter structure and processor configuration are used to find the threshold multiplier.

4.1. ESTIMATION OF THE K-DISTRIBUTION SHAPE PARAMETER

Estimating the parameters of a statistical distribution from measured sample values forms an essential part of radar signal processing tasks. In radar signal processing parameter estimation is required to characterize the statistical properties of noise and/or clutter background. Hence estimation is necessary for target detection algorithms.

A good method of estimating ν in the absence of added thermal noise is based on the estimates of the mean, $\hat{\mu}$ and the mean of the logarithm of the data,

$\langle \ln(x) \rangle = \frac{1}{M} \sum_{i=1}^M \ln(x_i)$. It is found that

$$\ln(\hat{\nu}) - \psi(\hat{\nu}) = \ln(\hat{\mu}) - \langle \ln(x) \rangle + \psi(N) - \ln(N) \quad (4.1)$$

where $\psi(\cdot)$ is the digamma function and $\hat{\nu}$ is the estimate of ν . The digamma function is defined as the logarithmic derivative of the gamma function:

$$\psi(x) = \frac{d}{dx} \ln \Gamma(x) = \frac{\Gamma'(x)}{\Gamma(x)} \quad (4.2)$$

The estimate in (4.1) is a close approximation to the maximum likelihood estimate and gives better results than matching to the first and second intensity moments [16]. As [29] concludes, the best overall performance is provided by this estimation scheme that uses the mean of the data and the mean of the log of data.

4.2. EFFECT OF INCORRECT ESTIMATION OF THE SHAPE PARAMETER

The preceding discussions in Chapter 3 have assumed that the value of the shape parameter ν is known exactly. However in practice ν is need to be estimated which may result in approximate values of ν . If the value of ν is to be changed, this affects mainly the value of the threshold multiplier α needed to achieve a specified P_{fa} . Thus, errors made in estimating ν result in an incorrect value of α which causes a degradation in detection performance. If the threshold is set too high (ν is estimated too low), the consequence will be increased CFAR loss; if the threshold is set too low (ν is estimated too high), the consequence will be increased P_{fa} [2].

The approximate magnitude of the loss associated with the incorrect estimation of ν is obtained simply from CFAR loss versus ν curves given in Figure 4-1 and Figure 4-2 for various values of P_{fa} (10^{-2} , 10^{-3} and 10^{-4}) and CA-CFAR window size, M of 16 and 32. The difference between the CFAR loss at the estimated value of ν and the true value of ν is the approximate additional loss due to incorrect estimation of ν .

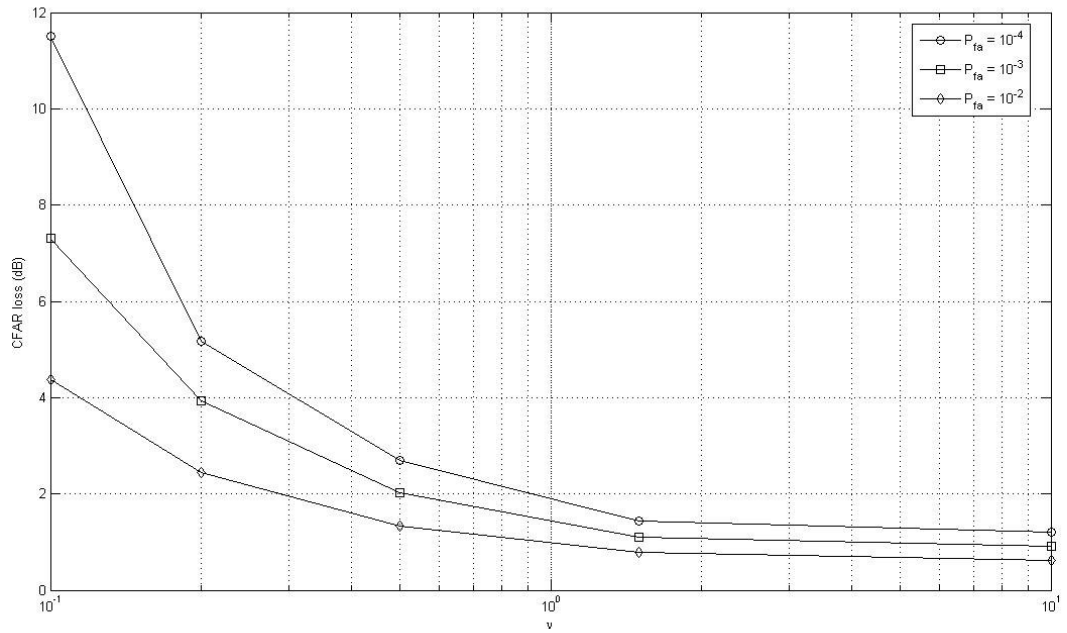


Figure 4-1 Approximate CFAR loss vs. ν for SU clutter, $N = 1$ and $M = 16$

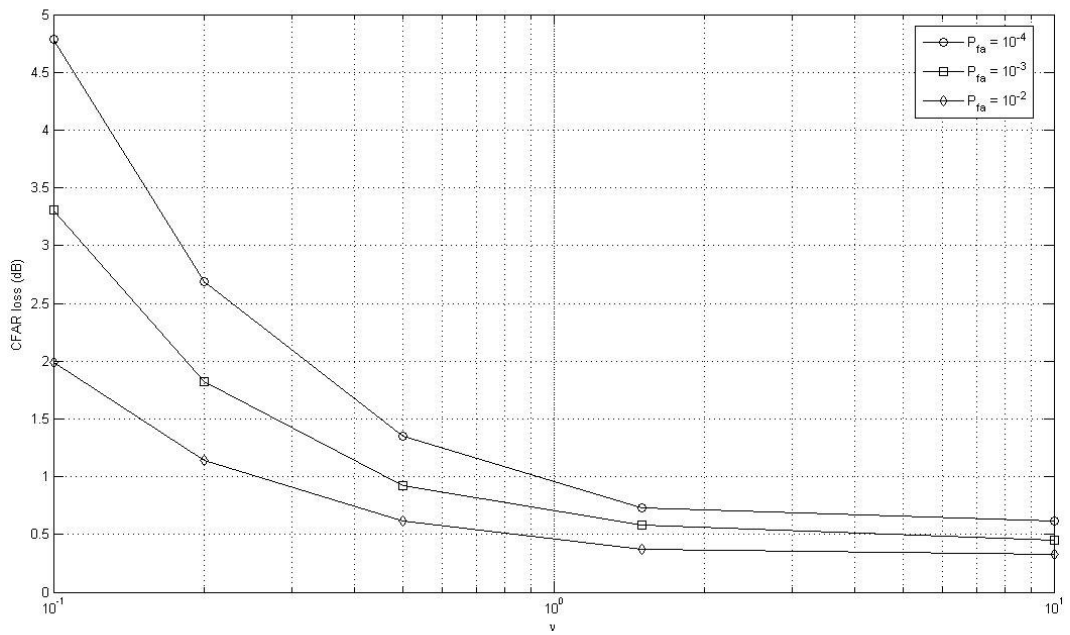


Figure 4-2 Approximate CFAR loss vs. ν for SU clutter, $N = 1$ and $M = 32$

According to [2], the performance degradation due to ν being estimated too high

will be more interest for most operating conditions since it may cause a notable increase in P_{fa} . P_{fa} is now evaluated as a function ν and threshold multiplier α in order to examine the severity of this increase in P_{fa} . The resulting graphs are given in Figure 4-3 and Figure 4-4 for different CA-CFAR cell sizes. To determine the increase in P_{fa} due to errors in estimating ν , the difference between P_{fa} at the estimated and true values of ν is taken.

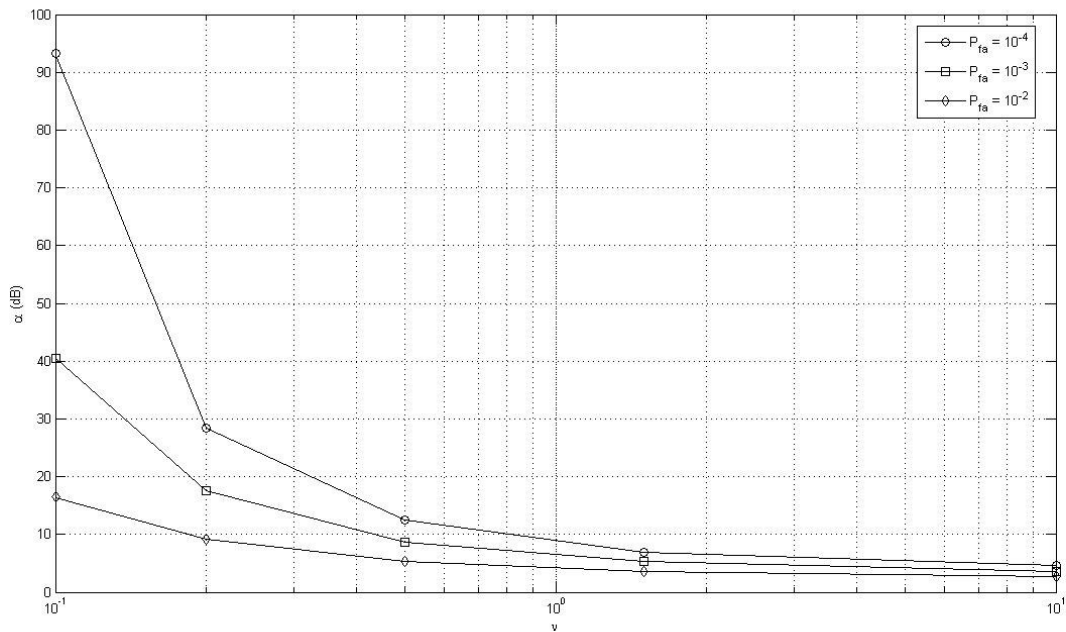


Figure 4-3 α vs. ν for SU clutter and $M = 16$

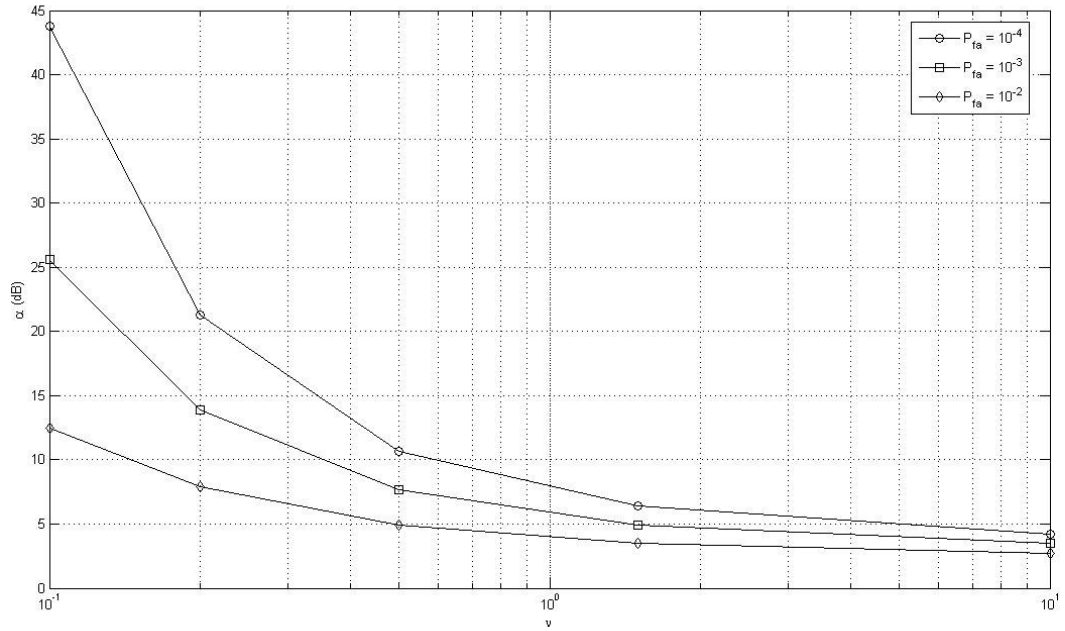


Figure 4-4 α vs. ν for SU clutter and $M = 32$

The examination of the graphs from Figure 4-1 to Figure 4-4 results in some conclusions about the reaction of CA-CFAR processor to incorrect estimation of ν . The CA-CFAR processor is more sensitive to errors in the estimated value of ν for small values of the clutter shape parameter than for large values. The effect of changing the number of CA-CFAR cells M does not significantly influence the sensitivity of the CFAR processors to errors in the estimated value of ν .

If the detector are designed for operation in Rayleigh clutter which is a special case of K-distribution with $\nu \rightarrow \infty$, but have to operate in a spiky K-distributed clutter, examination of the graphs of Figure 4-3 and Figure 4-4 indicates that α will be set too low when compared with the real K-distributed environment. Even though this low α corresponds to higher P_{fa} , much more worse P_{fa} is possible in even less spiky K-distributed clutter. This extreme condition illustrates the importance of estimating of correct shape parameter in the design of CA-CFAR processor.

CHAPTER 5

CONCLUSION

In this thesis amplitude distribution of sea clutter is modelled by compound K-distribution and CA-CFAR technique is used to detect SW-II targets. Radar detection performance analysis are made by several Monte Carlo (MC) simulations. Performance evaluations are quantified by CFAR loss. Performance evaluations show that sea clutter characteristics and CA-CFAR configuration can affect radar performance.

Since CFAR loss is used as a measure of performance evaluations, both CA-CFAR and fixed threshold detection curves are calculated by simulation. First of all, spatially uncorrelated K-distributed clutter is modelled. Then correlation is introduced into the sea clutter model. All performance evaluations are made both for single pulse and multiple pulse detection. Moreover, detection performance is examined for various values of sea clutter spikiness, CA-CFAR window size, P_{fa} and P_d . There are two different methods that may be employed to measure the CFAR loss; one using only CA-CFAR threshold multiplier, named threshold multiplier method and gives approximate CFAR loss values; the other one using P_d and gives true CFAR loss values. In this thesis both methods are also modelled, analysed and compared.

The results presented concentrate on two main issues, namely the CFAR loss suffered by CA-CFAR processor compared to fixed threshold detector and the

effects on CFAR loss of various conditions of spatial correlation of the K-distributed clutter.

Detection in uncorrelated sea clutter by CA-CFAR also results in a number of conclusions listed below:

- CFAR loss is strongly dependent on the shape parameter of K-distribution, ν . As clutter gets more spiky (ν decreases), CFAR loss increases.
- CFAR loss is also fairly strongly dependent on the size of CA-CFAR window. The use of large window size is required to decrease CFAR loss.
- CFAR loss increases with decreasing P_{fa} values for which CFAR loss becomes more sensitive to increasing clutter spikiness.
- As the desired P_d increases, the resulting true CFAR loss increases as expected. However this increase becomes less noticeable as clutter gets less spiky and also when large window sizes are used.
- In general as the number of non-coherently integrated pulses, N , increases the detection performance is also increases by means of decreasing CFAR loss. Even though the simulation is not sensitive enough to distinguish small amounts of decrease in CFAR loss for higher number of pulses integrated, it is still possible to conclude that there is an obvious improvement in CFAR loss when compared to single pulse detection case, however using 10 or 20 or 30 pulses for integration does not make a considerable change in the value of CFAR loss for higher window sizes.
- Threshold multiplier method may be a good guide in understanding the general behaviour of CFAR loss. However there is still some amount of difference in CFAR loss when compared to true CFAR loss values. When P_d is higher than 0.5, the approximate CFAR loss method starts to underestimate the true CFAR loss. For more accurate CFAR loss calculation true CFAR loss method should be preferred.

- As the number of pulses integrated increases, the required SCR reduces. However the decrease in SCR slows down as the number of integrated pulses increases. Besides, as P_d increases, the required SCR also increases.
- The time to spend for detection decision is longer when multiple pulse is integrated than single pulse since the detection decision is made after the processing of N pulses.

The spatial variation of clutter characteristics can have a significant effect on the performance of radar detection processing. The results presented here showed that a remarkable CFAR gain may be achieved under some circumstances as opposed to the more conventional expectation of a CFAR loss. The following conclusions are made when spatial correlation effect is included:

- For longer correlation lengths, the CA-CFAR output and CUT are highly correlated especially for short CA-CFAR window sizes. The CFAR loss in this case gives negative values, hence a CFAR gain is obtained. This means that the CA-CFAR performance is better than fixed threshold detection. The upper bound of CFAR gain can be achieved by ideal CFAR, where the threshold follows underlying mean level of K-distributed clutter exactly.
- Shorter correlation lengths have the effect of increasing the number of independent samples in the CA-CFAR cells but the CA-CFAR output may still be left decorrelated from the CUT. The CFAR loss in this case may be greater than would be expected for totally uncorrelated clutter samples in the CA-CFAR.
- For all correlation lengths, as the CA-CFAR window size becomes large, performance tends to the CFAR loss associated with clutter having no spatial correlation.
- There may be optimum values of M where the CFAR gain is maximum for some sea clutter spikiness. Increasing CA-CFAR window size beyond this value does improve the CFAR gain.

- For low values of the shape parameter ($\nu=0.2$ and $\nu=0.5$) the best performance is nearly always achieved for a short CA-CFAR window size. When there is a little spatial correlation and for high values of the shape parameter ($\nu=10$) the best performance will be obtained from a longer CA-CFAR window size.
- Another drawback of increasing CA-CFAR window size is that the sea clutter structure may change in the CA-CFAR window range, since the window range is the multiplication of range resolution and window size. Thus the CUT may not be representative of the local area. Decreasing range resolution may not be an appropriate solution since this may make the clutter more spiky.
- Non-coherent integration of spatially correlated pulses generally reduces the CFAR loss. However for spikier sea clutter pulse integration may result in higher CFAR losses especially for higher CA-CFAR window sizes.
- The difference between approximate and true CFAR losses is more remarkable when correlation effect is introduced. Moreover, this difference increases when pulse integration of correlated clutter is made especially for higher values shape parameter of K-distribution.

CFAR calculations so far are based on the exact calculation of the shape parameter. The effects of incorrect estimation of the shape parameter of K-distributed sea clutter are also investigated by using the curves for CFAR loss to the spikiness of clutter. Hence remarkable performance degradation may result if a wrong estimation is made. The following conclusions are also made when shape parameter is wrongly estimated;

- The CA-CFAR processor is more sensitive to errors in the estimated values of ν for small values of the clutter shape parameter than for large values.
- The effect of changing the number of CA-CFAR cells M does not significantly influence the sensitivity of the CFAR processors to errors in

the estimated value of ν .

Finally, in this thesis it is shown that the performance can vary widely and is a function of the CA-CFAR configuration, sea clutter structure, given P_{fa} and P_d . Furthermore, the analysis made in this thesis provides the radar system designer an understanding of the behaviour of sea clutter in order to develop suitable signal processing strategies and predict performance of radar under different clutter conditions.

5.1. FUTURE WORK

The analysis in this thesis has concentrated on targets of Swerling type II, i.e. target fluctuation rate is pulse to pulse and target RCS obeys Rayleigh-power distribution law. As mentioned in Chapter 1, there are other Swerling types for different RCS statistics and fluctuations rate. The target type is insignificant for performance evaluations made in terms of approximate CFAR loss since P_{fa} versus threshold multiplier curves are independent of P_d . However, the true CFAR loss also depends on target fluctuation characteristics via P_d . Hence, the performance evaluations in terms of true CFAR loss might be extended to other Swerling target types.

The lowest P_{fa} analysed in this thesis is 10^{-4} . This number is limited to the MC simulation number. In other words lower P_{fa} values can be obtained by increasing the MC simulation number. As indicated in Sections 3.1 and 3.3, in this thesis 10^6 MC simulation is made in order to get reliable PFAs (minimum 10^{-4}). Increasing the MC simulation number will result in lower P_{fa} values however lengthens the simulation time spent. As a result, MC simulation number might be increased to get performance evaluations for lower P_{fa} values.

REFERENCES

- [1]. Skolnik M. I., "Introduction to Radar Systems", Mc Graw Hill, 3. Edition, 2001.
- [2]. Armstrong B. C., Griffiths H. D., "CFAR Detection of Fluctuating Targets in Spatially Correlated K-Distributed Clutter", IEE Proceedings-F, Vol. 138, No.2, April 1991.
- [3]. Ward K. D., Baker C.J., Watts S., "Maritime Surveillance Radar Part 1: Radar Scattering from the Ocean Surface", IEE Proc., Vol. 137, Pt. F, No. 2, pp. 51-62, April 1990.
- [4]. Trunk, G. V., "Radar Properties of Non-Rayleigh Sea Clutter", IEEE Trans., AES-8, (2), pp. 196-204.
- [5]. Fay, F. A., Clarke, J., Peters, R. S., "The Weibull Distribution Applied to Sea Clutter", Radar-77, IEE Conf. Publ. 155, pp. 101-103, 1977.
- [6]. Ward K. D., "Compound Representation of High resolution Sea Clutter", Electron. Lett., Vol. 17, pp.561-563, 1981.
- [7]. Jakeman E., Pusey P.N., "A Model for Non-Rayleigh Sea Echo", IEEE Trans., AP-24, (6), pp. 806-814, May 1983.
- [8]. Chan H. C., "Radar Sea Clutter at Low Grazing Angles", IEE Proc. F, Radar & Signal Process., 137, (2), pp. 102-112, April 1990.
- [9]. Oliver C. J., "A Model For Non-Rayleigh Scattering Statistics", Opt. Acta, 31, (6), pp. 701-722, 1984.
- [10]. Lewinski, D. J., "Non-stationary Probabilistic Target And Clutter Scattering

- Models”, IEEE Trans., AP-31, (3), pp. 490-498, November 1976.
- [11]. Hair T., Lee T., Baker C. J., “Statistical properties of multifrequency high range resolution sea reflections”, IEE Proceedings, Vol. 138, Part F, pp. 75-79, April 1991.
- [12]. Watts S., “Radar Detection Prediction in Sea Clutter Using the Compound K Distribution Model”, Proc. IEE, Vol. 132, Part F, No. 7, pp. 613-620, December 1985.
- [13]. Watts, S., “Radar Detection Prediction in K-Distributed Sea Clutter and Thermal Noise”, IEEE Trans., AES-23, (1), pp. 40-45, January 1987.
- [14]. Barton D. K., Leonov S. A., “Radar Technology Encyclopedia”, Artech House, 1997.
- [15]. Finn M. M., Johnson R. S., “Adaptive Detection Mode With Threshold Control As a Function Of Spatially Sampled Clutter level Estimates”, RCA Rev., 1968, vol. 30, pp. 414-465.
- [16]. Watts S., “The Performance of Cell-Averaging CFAR Systems in Sea Clutter”, IEEE International Radar Conference, 2000.
- [17]. Ward K. D., Baker C.J., Watts S., “Maritime Surveillance Radar Part 2: Detection Performance Prediction In Sea Clutter”, IEE Proc., Vol. 137, Pt. F, No. 2, April 1990.
- [18]. Watts S., “Cell-Averaging CFAR Gain In Spatially Correlated K-Distributed Clutter”, IEE Proc. Radar, Sonar Navig., Vol. 143, No.5, October 1996.
- [19]. Ward K. D., Tough R. J. A., Watts S., “Sea Clutter: Scattering, the K Distribution and Radar Performance”, IET Radar, Sonar, Navigation and Avionics Series 20, 2006.
- [20]. Watts S., “A Practical Approach to the Prediction and Assessment of Radar Performance in Sea Clutter”, IEEE International Radar Conference, 1995.
- [21]. Gradshteyn I. S., Ryzhik I. M., “Table of Integrals, Series and Products ”,

Academic Press, 7th Edition, 2007.

- [22]. Ward K. D., “A radar sea clutter model and its application to performance assessment”, IEE Conf. Publ. 216, Radar 82, pp. 204-207, 1982.
- [23]. Tough R. J. A., Ward K. D., “The Correlation Properties of Gamma and Other Non-Gaussian Processes by Memoryless Nonlinear Transformation”, J. Phys. D: Appl. Phys. 32, 3075-3084, 1999.
- [24]. Gandhi P. P., Kassam S. A., “Analysis of CFAR Processors in Nonhomogeneous Background”, IEEE Transactions on Aerospace and Electronic Systems, Vol. 24, No. 4, July 1988.
- [25]. Raghavan R. S., “Analysis of CA-CFAR Processors for Linear-Law Detection”, IEEE Transactions on Aerospace and Electronic Systems, Vol. 28, No. 3, July 1992.
- [26]. DiFranco J. V., Rubin W. L., “Radar Detection”, Scitech Publishing, 2004.
- [27]. Watts, S., Griffiths H. D., Holloway J. R., Kinghorn A.M., Money D. G., Price D. J., Whitehead A. M., Moore A. R., Wood M. A., Bannister D. J., “The Specification and Measurement of Radar Performance”, IEE, 2002.
- [28]. Watts S., “Adaptation to the Clutter Environment by Airborne Maritime Surveillance Radars”, International Conference, Radar 99, Brest, Session 2.6, 17-21 May 1999.
- [29]. Blacknell D., “Comparison of Parameter Estimators for K-Distribution”, IEE Proc.-Radar, Sonar Navig., Vol. 141, No.1, February 1994.
- [30]. Peebles P.Z., Jr., “Probability, Random Variables and Random Signal Processing”, 4th Edition, McGraw-Hill, 2001.

APPENDIX A

CHANGE OF VARIABLES AND JACOBIAN CALCULATION

As [26] says, a problem often encountered is the determination of the PDF of a set of random variables that are related to an old set (with known density function) by one to one mapping. The Jacobian calculation appears when for this transformation is necessary.

Assume a change of variable $y = \phi(x)$ and it is a differential mapping on the interval $T = [c \ d]$ and T' is the interval $[a \ b]$ with $\phi(c) = a$ and $\phi(d) = b$. In one dimension, the explicit statement of the change of variables theorem for f a continuous function of y is

$$\int_T f(\phi(x)) \frac{d\phi}{dx} dx = \int_{T'} f(y) dy \quad (\text{A.1})$$

In two dimensions, $x = x(u, v)$ and $y = y(u, v)$ are assumed. Suppose that the region S' in the uv -plane is transformed to a region S in the xy -plane under this transformation. Define the Jacobian of the transformation as

$$J(u, v) = \begin{bmatrix} \frac{\partial x}{\partial u} & \frac{\partial x}{\partial v} \\ \frac{\partial y}{\partial u} & \frac{\partial y}{\partial v} \end{bmatrix} \quad (\text{A.2})$$

It turns out that this describes the relationship between the element of area $dxdy$ and the corresponding area element $dudv$. With this definition, the change of variable formula becomes

$$\iint_S f(x, y)dxdy = \iint_{S'} f(x(u, v), y(u, v))|J(u, v)|dudv \quad (\text{A.3})$$

Change of variables theorem and also the Jacobian determinant $|J(u, v)|$, often called Jacobian as well, are used in order to change the random variables.

A.1. Obtaining Rayleigh Distributed Envelope from Two Complex Gaussian Component

If \tilde{X} is a complex Gaussian variable with in-phase and quadrature components x_I and x_Q , the envelope of which is given in (A.4).

$$|\tilde{X}| = s = \sqrt{x_I^2 + x_Q^2} \quad (\text{A.4})$$

The inphase and quadrature components can be changed as

$$\begin{aligned} x_I &= s \cos(\phi) \\ x_Q &= s \sin(\phi) \end{aligned} \quad (\text{A.5})$$

By using the Jacobian calculation $f_{s,\phi}(s, \phi)$ is given by

$$f_{s,\phi}(a, \phi) = |J(I, Q)| f_{x_I, x_Q}(s \cos(\phi), s \sin(\phi)) \quad (\text{A.6})$$

In (A.7) the Jacobian $|J(I, Q)|$ is calculated by using (A.2).

$$\begin{aligned} |J(I, Q)| &= \begin{vmatrix} \frac{\partial x_I}{\partial s} & \frac{\partial x_I}{\partial \phi} \\ \frac{\partial x_Q}{\partial s} & \frac{\partial x_Q}{\partial \phi} \end{vmatrix} \\ &= \begin{vmatrix} \cos(\phi) & -s \sin(\phi) \\ \sin(\phi) & s \cos(\phi) \end{vmatrix} = s \end{aligned} \quad (\text{A.7})$$

Since x_I and x_Q are independent, their joint density function $f_{x_I, x_Q}(x_I, x_Q)$ becomes

$$f_{x_I, x_Q}(x_I, x_Q) = \frac{1}{2\pi\sigma^2} \exp\left(-\frac{x_I^2 + x_Q^2}{2\sigma^2}\right) \quad (\text{A.8})$$

The resulting compound PDF is given in (A.9) where the individual PDFs are given in (A.10).

$$f_{s,\phi}(s, \phi) = \frac{1}{2\pi} \frac{s}{\sigma^2} \exp\left(-\frac{s^2}{2}\right) \quad (\text{A.9})$$

Finally the envelope of complex Gaussian distributed variables has a Rayleigh distributed PDF $f_s(s)$ as given in in (A.10).

$$\begin{aligned} f_s(s) &= \frac{s}{\sigma^2} \exp\left(-\frac{s^2}{2\sigma^2}\right) \\ f_\phi(\phi) &= \frac{1}{2\pi} \end{aligned} \quad (\text{A.10})$$

A.2. Generalised Distributed Voltage to Gamma Distributed Power

The generalised Chi distribution has the form given in (A.11).

$$f_Y(y) = \frac{2b^{2\nu}}{\Gamma(\nu)} y^{2\nu-1} \exp(-b^2 y^2) \quad (\text{A.11})$$

If the variable y is changed by z^2 , the expression of $f_Z(z)$ will be as in (A.12) by using (A.1).

$$f_Z(z) = \frac{1}{\left| \frac{\partial z}{\partial y} \right|} f_Y(\sqrt{y}) \quad (\text{A.12})$$

After solving (A.12), the resulting PDF $f_R(r)$ will be found as in (A.13).

$$f_Z(z) = \frac{b^{2\nu}}{\Gamma(\nu)} z^{\nu-1} \exp(-b^2 z) \quad (\text{A.13})$$

Finally, $f_z(z)$ has the form of gamma distribution.

A.3. Rayleigh Distributed Voltage to Exponentially Distributed Power

Rayleigh distributed variable s 's PDF is as given in (A.14), with parameter σ .

$$f_S(s) = \frac{s}{\sigma^2} \exp\left(-\frac{s^2}{2\sigma^2}\right) \quad (\text{A.14})$$

If the variable r is represented as s^2 , the relationship between the resulting PDFs of $f_R(r)$ and $f_S(s)$ will be as in (A.15) by using (A.1).

$$f_R(r) = \frac{1}{\left| \frac{\partial r}{\partial s} \right|} f_S(\sqrt{r}) \quad (\text{A.15})$$

After solving (A.15), the resulting PDF $f_R(r)$ will be found as in (A.16).

$$f_R(r) = \frac{1}{2\sigma^2} \exp\left(-\frac{r}{2\sigma^2}\right) \quad (\text{A.16})$$

Here $f_R(r)$ has the exponential distribution shape with mean $2\sigma^2$.

APPENDIX B

CHARACTERISTIC FUNCTIONS OF RANDOM VARIABLES

Suppose that κ is a random variable on sample space K and $f_{\kappa}(\cdot)$ is the probability density function of κ . The characteristic function of K , denoted $C_{\kappa}(\cdot)$ is defined as in if κ is a continuous random variable,

$$\begin{aligned} C_{\kappa}(t) &\triangleq E\langle \exp(jt\kappa) \rangle \\ &= \int_{-\infty}^{\infty} \exp(jtx) f_{\kappa}(x) dx \end{aligned} \quad (\text{B. 1})$$

In (B. 1), $C_{\kappa}(t)$ is seen to be the Fourier transform (with the sign reversed). Because of this fact if $C_{\kappa}(t)$ is known, $f_{\kappa}(x)$ can be found from inverse Fourier transform [30]. Given the characteristic function of a random variable κ , it can be shown that the PDF of κ can be obtained from the inverse formula

$$f_{\kappa}(x) = \frac{1}{2\pi} \int_{-\infty}^{\infty} \exp(-jtx) C_{\kappa}(t) dt \quad (\text{B. 2})$$

.The characteristic function is used in calculating the PDF for the sum of n

independent random variables. For instance, suppose that $\kappa_1, \kappa_2, \dots, \kappa_n$ are n independent random variables on a sample space with corresponding PDFs: $f_{\kappa_1}, f_{\kappa_2}, \dots, f_{\kappa_n}$. Further suppose that another random variable on the space, ξ is defined as

$$\xi = \kappa_1 + \kappa_2 + \dots + \kappa_n \quad (\text{B. 3})$$

Given expressions for PDFs: $f_{\kappa_1}, f_{\kappa_2}, \dots, f_{\kappa_n}$, the PDF f_ξ can be obtained from them by use of characteristic functions. Since,

$$\begin{aligned} C_\kappa(t) &\triangleq E\langle \exp(jt\kappa) \rangle \\ &= \int_{-\infty}^{\infty} \int_{-\infty}^{\infty} \dots \int_{-\infty}^{\infty} \exp(jt(\kappa_1 + \kappa_2 + \dots + \kappa_n)) f_{\kappa_1, \kappa_2, \dots, \kappa_n}(\kappa_1, \kappa_2, \dots, \kappa_n) d\kappa_1 d\kappa_2 \dots d\kappa_n \quad (\text{B. 4}) \\ &= C_{\kappa_1}(t) C_{\kappa_2}(t) \dots C_{\kappa_n}(t) \end{aligned}$$

If the characteristic function of each κ_i can be calculated from (B. 1) and (B. 4) is applied to obtain expression for C_ξ in terms of the individual characteristic functions. Then, the PDF of ξ , f_ξ can be obtained from (B. 5).

$$f_\xi(x) = \frac{1}{2\pi} \int_{-\infty}^{\infty} \exp(-jtx) C_\xi(t) dt \quad (\text{B. 5})$$